Investigation of Negative Moment Reinforcing in Bridge Decks

BRIDGE ENGINEERING CENTER

Final Report
September 2015

IOWA STATE UNIVERSITY
Institute for Transportation

Sponsored by
Iowa Highway Research Board
(IHRB Project TR-660)
Iowa Department of Transportation
(InTrans Project 13-469)

About the BEC

The mission of the Bridge Engineering Center is to conduct research on bridge technologies to help bridge designers/owners design, build, and maintain long-lasting bridges.

Disclaimer Notice

The contents of this report reflect the views of the authors, who are responsible for the facts and the accuracy of the information presented herein. The opinions, findings and conclusions expressed in this publication are those of the authors and not necessarily those of the sponsors.

The sponsors assume no liability for the contents or use of the information contained in this document. This report does not constitute a standard, specification, or regulation.

The sponsors do not endorse products or manufacturers. Trademarks or manufacturers' names appear in this report only because they are considered essential to the objective of the document.

Non-Discrimination Statement

Iowa State University does not discriminate on the basis of race, color, age, ethnicity, religion, national origin, pregnancy, sexual orientation, gender identity, genetic information, sex, marital status, disability, or status as a U.S. veteran. Inquiries regarding non-discrimination policies may be directed to Office of Equal Opportunity, Title IX/ADA Coordinator, and Affirmative Action Officer, 3350 Beardshear Hall, Ames, Iowa 50011, 515-294-7612, email eooffice@iastate.edu.

Iowa Department of Transportation Statements

Federal and state laws prohibit employment and/or public accommodation discrimination on the basis of age, color, creed, disability, gender identity, national origin, pregnancy, race, religion, sex, sexual orientation or veteran's status. If you believe you have been discriminated against, please contact the Iowa Civil Rights Commission at 800-457-4416 or Iowa Department of Transportation's affirmative action officer. If you need accommodations because of a disability to access the Iowa Department of Transportation's services, contact the agency's affirmative action officer at 800-262-0003.

The preparation of this report was financed in part through funds provided by the Iowa Department of Transportation through its "Second Revised Agreement for the Management of Research Conducted by Iowa State University for the Iowa Department of Transportation" and its amendments.

The opinions, findings, and conclusions expressed in this publication are those of the authors and not necessarily those of the Iowa Department of Transportation.

Technical Report Documentation Page

1. Report No. IHRB Project TR-660	**2. Government Accession No.**	**3. Recipient's Catalog No.**	
4. Title and Subtitle Investigation of Negative Moment Reinforcing in Bridge Decks		**5. Report Date** September 2015	
		6. Performing Organization Code	
7. Author(s) Brent M. Phares, Sameera Jayathilaka, and Lowell Greimann		**8. Performing Organization Report No.** InTrans Project 13-469	
9. Performing Organization Name and Address Bridge Engineering Center Iowa State University 2711 South Loop Drive, Suite 4700 Ames, IA 50010-8664		**10. Work Unit No. (TRAIS)**	
		11. Contract or Grant No.	
12. Sponsoring Organization Name and Address Iowa Highway Research Board Iowa Department of Transportation 800 Lincoln Way Ames, IA 50010		**13. Type of Report and Period Covered** Final Report	
		14. Sponsoring Agency Code IHRB Project TR-660	
15. Supplementary Notes Visit www.intrans.iastate.edu for color pdfs of this and other research reports.			

16. Abstract

Multi-span pre-tensioned pre-stressed concrete beam (PPCB) bridges made continuous usually experience a negative live load moment region over the intermediate supports. Conventional thinking dictates that sufficient reinforcement must be provided in this region to satisfy the strength and serviceability requirements associated with the tensile stresses in the deck. The American Association of State Highway and Transportation Officials (AASHTO) Load and Resistance Factor Design (LRFD) Bridge Design Specifications recommend the negative moment reinforcement (b2 reinforcement) be extended beyond the inflection point. Based upon satisfactory previous performance and judgment, the Iowa Department of Transportation (DOT) Office of Bridges and Structures (OBS) currently terminates b2 reinforcement at 1/8 of the span length. Although the Iowa DOT policy results in approximately 50% shorter b2 reinforcement than the AASHTO LRFD specifications, the Iowa DOT has not experienced any significant deck cracking over the intermediate supports.

The primary objective of this project was to investigate the Iowa DOT OBS policy regarding the required amount of b2 reinforcement to provide the continuity over bridge decks. Other parameters, such as termination length, termination pattern, and effects of the secondary moments, were also studied. Live load tests were carried out on five bridges. The data were used to calibrate three-dimensional finite element models of two bridges. Parametric studies were conducted on the bridges with an uncracked deck, a cracked deck, and a cracked deck with a cracked pier diaphragm for live load and shrinkage load. The general conclusions were as follows:

- The parametric study results show that an increased area of the b2 reinforcement slightly reduces the strain over the pier, whereas an increased length and staggered reinforcement pattern slightly reduce the strains of the deck at 1/8 of the span length.
- Finite element modeling results suggest that the transverse field cracks over the pier and at 1/8 of the span length are mainly due to deck shrinkage.
- Bridges with larger skew angles have lower strains over the intermediate supports.
- Secondary moments affect the behavior in the negative moment region. The impact may be significant enough such that no tensile stresses in the deck may be experienced.

17. Key Words calibration—continuous deck—field test—finite element model—negative moment reinforcement—parametric study—transverse cracks		**18. Distribution Statement** No restrictions.	
19. Security Classification (of this report) Unclassified.	**20. Security Classification (of this page)** Unclassified.	**21. No. of Pages** 110	**22. Price** NA

Form DOT F 1700.7 (8-72) **Reproduction of completed page authorized**

INVESTIGATION OF NEGATIVE MOMENT REINFORCING IN BRIDGE DECKS

Final Report
September 2015

Principal Investigator
Brent Phares
Director
Bridge Engineering Center, Iowa State University

Co-Principal Investigator
Lowell Greimann
Bridge Engineer
Bridge Engineering Center, Iowa State University

Research Assistant
Sameera Jayathilaka

Authors
Brent Phares, Sameera Jayathilaka, and Lowell Greimann

Sponsored by
the Iowa Highway Research Board and
the Iowa Department of Transportation
(IHRB Project TR-660)

Preparation of this report was financed in part
through funds provided by the Iowa Department of Transportation
through its Research Management Agreement with the
Institute for Transportation
(InTrans Project 13-469)

A report from
Bridge Engineering Center
Iowa State University
2711 South Loop Drive, Suite 4700
Ames, IA 50010-8664
Phone: 515-294-8103
Fax: 515-294-0467
www.bec.iastate.edu

TABLE OF CONTENTS

ACKNOWLEDGMENTS xi

EXECUTIVE SUMMARY xiii

Recommendations xiv

1 INTRODUCTION 1

1.1 Background 1
1.2 Objectives of the Research 2
1.3 Research Plan 2
Task 1 – Information Gathering 2
Task 2 – Field Test and Inspection 2
Task 3 – Analytical Modeling 3
Task 4 – Reporting the Recommendations 3

2 LITERATURE REVIEW AND SURVEY 4

2.1 Introduction to Transverse Cracks on Bridge Decks 4
2.1.1 Material and Mix Design 4
2.1.2 Construction Practices and Environmental Conditions 5
2.1.3 Structural Design Factors 6
2.2 Transverse Cracks at the Intermediate Supports of PPCB Bridges 6
2.2.1 Design of the Reinforcement at the Bottom of the Continuity Connection 7
2.2.2 Design of the Reinforcement at the Top of the Continuity Connection 7
2.3 State of the Practice on Negative Moment Reinforcement Design 8

3 FIELD TESTS 10

3.1 Introduction 10
3.2 Instrumentation 10
3.3 Bridge Loading 13
3.4 Deck Gauge Longitudinal Strain Profiles 13
3.5 Girder Gauge Longitudinal Strain Profiles 14
3.6 Rosette Longitudinal Strain Profiles 15

4 FINITE ELEMENT MODELS OF TWO BRIDGES 19

4.1 Introduction 19
4.2 Bridge A Finite Element Model 19
4.2.1 Element Type Selection 19
4.2.2 Element Properties 19
4.2.3 Material Properties 20
4.2.4 Finite Element Model 20
4.2.5 Finite Element Model Support Conditions 23
4.2.6 Loading Conditions 25
4.2.7 Model Calibration from Field Test Results 25
4.2.8 Comparison of Cracking Strain with Field Cracks 37
4.3 Finite Element Model of Bridge B 43
4.3.1 Calibration of Bridge B 45

5 PARAMETRIC STUDIES 50
5.1 Model Configuration 50
5.1.1 Model 1 - Uncracked Deck 50
5.1.2 Model 2 - Cracked Deck 50
5.1.3 Model 3 - Cracked Deck with Cracked Pier Diaphragm 53
5.2 Parametric Studies of Bridge A 53
5.2.1 Live Load 54
5.2.2 Shrinkage Load 57
5.2.3 Summary 59
5.3 Parametric Studies of Bridge B 59
5.3.1 Live Load 60
5.3.2 Shrinkage Load 62
5.3.3 Summary 64
6 EVALUATION OF SECONDARY MOMENTS OF BRIDGE A 65
6.1 Introduction 65
6.2 Calculation of Secondary Moments 66
6.2.1 Portland Cement Association (PCA) Method 66
6.2.2 Construction Technology Laboratory (CTL) Method 66
6.2.3 P-Method 67
6.2.4 RMCalc Program 67
6.2.5 RESTRAINT Program 67
6.2.6 mRESTRAINT Program by Chebole 67
6.2.7 mRESTRAINT Program by Ghinire 68
6.3 Comparison of Secondary Moment of Bridge A 68
6.4 Live Load Moment 69
6.4.1 Summary 70
7 CONCLUSIONS AND RECOMMENDATIONS 71
7.1 Summary 71
7.1.1 Literature Review 71
7.1.2 Field Testing 71
7.1.3 Calibration 72
7.1.4 Parametric Studies 73
7.1.5 Secondary Moment 73
7.2 Conclusions 74
7.3 Recommendations 74
REFERENCES 75
APPENDIX: FIELD TEST RESULTS FOR EACH BRIDGE 77
A.1 Bridge 1: On County Road C50 over US 218 77
A.2 Bridge 2: On I-80 over US 65 81
A.3 Bridge 3: On Meredith Drive over I-35/I-80 85
A.4 Bridge 4: On Mt. Pleasant Bypass over Big Creek 89
A.5 Bridge 5: On US 20 over Big Whiskey Creek 92

LIST OF FIGURES

Figure 1. Longitudinal reinforcement arrangement in the deck of a PPCB bridge 1
Figure 2. Force diagram at continuity connection 8
Figure 3. Typical deck gauge installation plan 11
Figure 4. Strain gauges end of the b2 bar 11
Figure 5. Cover plates prevent damage.....11
Figure 6. Rosette near b2 reinforcement.....12
Figure 7. Typical girder gauge locations 12
Figure 8. Details of the loading truck 13
Figure 9. Typical deck gauge strain variations 14
Figure 10. Typical girder gauge strain variations 15
Figure 11. 45° rectangular strain gauge rosettes.....15
Figure 12. Typical principal strain variations for two-span bridges with wheel paths close to the rosettes 16
Figure 13. Typical principal strain variations for two-span bridges with wheel paths away from the rosettes.....17
Figure 14. Typical principal strain variations for three-span bridges with wheel paths close to the rosettes 17
Figure 15. Typical principal strain variations for three-span bridges with wheel paths away from the rosettes.....18
Figure 16. Bridge A finite element model plan view.....21
Figure 17. Cross-section A-A 21
Figure 18. Actual deck, girder, and b2 reinforcement 22
Figure 19. Idealized deck, girder, and b2 reinforcement 22
Figure 20. Finite element model of the abutment 23
Figure 21. Support condition at the pier diaphragm 24
Figure 22. Support conditions at the abutment 24
Figure 23. Bridge A instrumentation plan of deck gauges 25
Figure 24. Strain variation of deck gauges (G1 and G11) close to the wheel path, (LC1).....26
Figure 25. Strain variation of deck gauges (G2 and G12) close to the wheel path, (LC1).....26
Figure 26. Strain variation of deck gauges (G5 and G15) away from the wheel path, (LC1).....27
Figure 27. Bridge A instrumentation plan of girder gauges 27
Figure 28. Strain variation of girder gauges (G1 and G15) close to the wheel path, (LC1).....28
Figure 29. Strain variation of girder gauges (G8 and G22) close to the wheel path, (LC1).....29
Figure 30. Strain variation of girder gauges (G9 and G23) close to the wheel path, (LC1).....29
Figure 31. Strain variation of girder gauge G8 with different girder fc' 30
Figure 32. Strain variation of girder gauge G22 with different girder fc′.....30
Figure 33. Strain variation of deck gauge G1 with different girder fc' 31
Figure 34. Strain variation of deck gauge G11 with different girder fc' 31
Figure 35. Variation of average % difference with the girder strength 32
Figure 36. Strain variation of girder gauge G8 with abutment boundary conditions girder $fc' = 12ksi$ 32
Figure 37. Strain variation of girder gauge G22 with abutment boundary conditions girder $fc' = 12ksi$ 33

Figure 38. Strain variation of deck gauge G1 with abutment boundary conditions girder $fc' = 12ksi$ 34
Figure 39. Strain variation of deck gauge G11 with abutment boundary conditions girder $fc' = 12ksi$ 34
Figure 40. Bridge A instrumentation plan of rosettes....35
Figure 41. Variation of principal strains of rosette R5 for LC1....36
Figure 42. Variation of principal strains of rosette R6 for LC1....36
Figure 43. Crack map....37
Figure 44. Details of the HS20 truck loading....38
Figure 45. Typical variation of ε_1 strain for truck in Lane1, end of the b2 reinforcement....39
Figure 46. Typical variation of ε_1 strain for truck in Lane1, at the pier....39
Figure 47. Strain (ε_Z) due to equivalent eight HS20 truck loads....40
Figure 48. Major principal strain magnitude and direction around Region P, equivalent UDL....41
Figure 49. Major principal strain magnitude and direction around Region P due to cold weather....42
Figure 50. Major principal strain magnitude and direction around Region P due to shrinkage after 56 days....43
Figure 51. Finite element model of the Bridge B: Plan view....44
Figure 52. Bridge B instrument plan of deck gauges....45
Figure 53. Strain variation of deck gauges (G1 and G15) closer to axles, (LC1)....45
Figure 54. Strain variation of deck gauges (G5 and G19) away from axles, (LC1)....46
Figure 55. Bridge B instrument plan of girder gauges....46
Figure 56. Strain variation of girder gauges (G9 and G25) closer to axles, (LC1)....47
Figure 57. Strain variation of girder gauges (G12 and G28) away from axles, (LC1)....47
Figure 58. Bridge B instrument plan of rosettes....48
Figure 59. Variation of principal strains of rosette R2 for LC1....48
Figure 60. Strain variation of girder gauge G1 with different calibration types....49
Figure 61. Cracked deck condition....51
Figure 62. Method to determine cracked section of Model 2....51
Figure 63. Negative moment region over pier....52
Figure 64. Uncracked deck condition....53
Figure 65. Parametric study region....54
Figure 66. Major principal strain magnitude and direction of Bridge A of Model 1, Load = Equivalent UDL....55
Figure 67. Major principal strain magnitude and direction of Bridge A of Model 1, Load = Shrinkage (56 days)....58
Figure 68. Major principal strain magnitude and direction of Bridge B of Model 1, Load = Equivalent UDL....61
Figure 69. Major principal strain magnitude and direction of Bridge B of Model 1, Load = Shrinkage (56 days)....63
Figure 70. Construction sequence and development of secondary moments in a two-span continuous bridge....65
Figure 71. Restraint moments from laboratory tests, PCA, CTL and P-Methods....67
Figure 72. Secondary moment values versus age of girder....68

Figure 73. Variation of secondary moments with girder age at the continuity connection construction 69
Figure 74. Simplified model of Bridge A used to calculate live load negative moment 70
Figure A.1.1. Bridge 1 plan view 77
Figure A.1.2. Bridge 1 deck gauge instrumentation plan 77
Figure A.1.3. Bridge 1 typical deck gauge longitudinal strain variations close to the wheel path (LC1) 78
Figure A.1.4. Bridge 1 typical deck gauge longitudinal strain variations away from the wheel path (LC1) 78
Figure A.1.5. Bridge 1 girder gauge instrumentation plan 79
Figure A.1.6. Bridge 1 typical girder gauge strain variations (LC1) 79
Figure A.1.7. Bridge 1 rosette instrumentation plan 80
Figure A.1.8. Bridge 1 typical principal strain variations of rosettes (R7) close to wheel path (LC4) 80
Figure A.1.9. Bridge 1 typical principal strain variations of rosettes (R7) away from wheel path (LC1) 81
Figure A.2.1. Bridge 2 plan view 81
Figure A.2.2. Bridge 2 deck gauge instrumentation plan 81
Figure A.2.3. Bridge 2 typical deck gauge longitudinal strain variations close to the wheel path (LC1) 82
Figure A.2.4. Bridge 2 typical deck gauge longitudinal strain variations away from the wheel path (LC1) 82
Figure A.2.5. Bridge 2 girder gauge instrumentation plan 83
Figure A.2.6. Bridge 2 typical girder gauge strain variations (LC1) 83
Figure A.2.7. Bridge 2 rosette instrumentation plan 84
Figure A.2.8. Bridge 2 typical principal strain variations of rosettes (R4) close to wheel path (LC1) 84
Figure A.2.9. Bridge 2 typical principal strain variations of rosettes (R4) away from wheel path (LC6) 84
Figure A.3.1. Bridge 3 plan view 85
Figure A.3.2. Bridge 3 deck gauge instrumentation plan 85
Figure A.3.3. Bridge 3 typical deck gauge longitudinal strain variations close to the wheel path (LC1) 85
Figure A.3.4. Bridge 3 typical deck gauge longitudinal strain variations away from the wheel path (LC1) 86
Figure A.3.5. Bridge 3 girder gauge instrumentation plan 86
Figure A.3.6. Bridge 3 typical girder gauge strain variations (LC1) 87
Figure A.3.7. Bridge 3 rosette instrumentation plan 87
Figure A.3.8. Bridge 3 typical principal strain variations of rosettes (R6) close to wheel path (LC4) 88
Figure A.3.9. Bridge 3 typical principal strain variations of rosettes (R6) away from wheel path (LC1) 88
Figure A.4.1. Bridge 4 plan view 89
Figure A.4.2. Bridge 4 deck gauge instrumentation plan 89
Figure A.4.3. Bridge 4 typical deck gauge longitudinal strain variations close to the wheel path (LC1) 89

Figure A.4.4. Bridge 4 typical deck gauge longitudinal strain variations away from the wheel path (LC1) 90
Figure A.4.5. Bridge 4 girder gauge instrumentation plan 90
Figure A.4.6. Bridge 4 typical girder gauge strain variations (LC1) 91
Figure A.4.7. Bridge 4 rosette instrumentation plan 91
Figure A.4.8. Bridge 4 typical principal strain variations of rosettes (R8) close to wheel path (LC4) 92
Figure A.4.9. Bridge 4 typical principal strain variations of rosettes (R8) away from wheel path (LC1) 92
Figure A.5.1. Bridge 5 plan view 92
Figure A.5.2. Bridge 5 deck gauge instrumentation plan 93
Figure A.5.3. Bridge 5 typical deck gauge longitudinal strain variations close to the wheel path (LC1) 93
Figure A.5.4. Bridge 5 typical deck gauge longitudinal strain variations away from the wheel path 94
Figure A.5.5. Bridge 5 girder gauge instrumentation plan 94
Figure A.5.6. Bridge 5 typical girder gauge strain variations (LC1) 95
Figure A.5.7. Bridge 5 rosette instrumentation plan 95
Figure A.5.8. Bridge 5 typical principal strain variations of rosettes (R9) close to wheel path (LC4) 96
Figure A.5.9. Bridge 5 typical principal strain variations of rosettes (R9) away from wheel path (LC1) 96

LIST OF TABLES

Table 1. Cause of transverse cracks on bridge decks 4
Table 2. Bridge characteristics 10
Table 3. Summary of gauges 13
Table 4. Types of elements used in the analysis 19
Table 5. Summary of calibration results 35
Table 6. Comparisons of the properties of Bridge A and Bridge B 44
Table 7. Calibration types of Bridge B 49
Table 8. Average longitudinal strain (με) of Bridge A due to the live load 56
Table 9. Average longitudinal strain (με) of Bridge A due to 56-day shrinkage load 59
Table 10. Average longitudinal strain (με) of Bridge B due to the live load 62
Table 11. Average longitudinal strain (με) of Bridge B due to 56-day shrinkage load 64

ACKNOWLEDGMENTS

The authors would like to thank the Iowa Highway Research Board (IHRB) and the Iowa Department of Transportation (DOT) for providing the funds for this project. Special thanks to the Iowa DOT Office of Bridges and Structures staff who provided feedback and direction on multiple aspects of the project.

EXECUTIVE SUMMARY

For design, multi-span pre-tensioned pre-stressed concrete beam (PPCB) bridges are usually assumed to experience two different stages of behavior. During the first stage, the PPCB girders are placed on supports and are assumed to behave as a simply-supported span to resist the self-weight of the structure.

After the concrete deck is placed and fully cured, the bridge moves to the second stage, during which it behaves like a fully continuous structure over the intermediate support to resist live loads and superimposed dead loads that occur after the deck has cured. During the second stage, the structure will experience negative moments over the intermediate supports.

Conventional thinking dictates that sufficient reinforcement must be provided in this region to satisfy the strength and serviceability requirements associated with the tensile stresses in the deck. The American Association of State Highway and Transportation Officials (AASHTO) Load and Resistance Factor Design (LRFD) Bridge Design Specifications recommend the negative moment reinforcement (b2 reinforcement) be extended beyond the inflection point.

However, based upon satisfactory previous performance and judgment, the Iowa Department of Transportation (DOT) Office of Bridges and Structures (OBS) currently terminates b2 reinforcement at 1/8 of the span length. Although the Iowa DOT policy results in approximately 50% shorter b2 reinforcement than the AASHTO LRFD specifications, the Iowa DOT has not experienced any significant deck cracking over the intermediate supports.

The primary objective of this project was to investigate the Iowa DOT OBS policy regarding the required amount of b2 reinforcement to provide the continuity over bridge deck. Other parameters, such as termination length, termination pattern, and effects of the secondary moments, were also studied.

Live load tests were carried out on five bridges. The data were used to calibrate three-dimensional finite element models of two bridges. Parametric studies were conducted on the bridges with an uncracked deck, a cracked deck, and a cracked deck with a cracked pier diaphragm for live load and shrinkage load testing.

The general conclusions were as follows:

- The parametric study results show that an increased area of the b2 reinforcement slightly reduces the strain over the pier. Whereas, an increased length and staggered reinforcement pattern slightly reduce the strains of the deck at 1/8 of the span length.

- Finite element modeling results suggest that the transverse field cracks over the pier and at 1/8 of the span length are mainly due to deck shrinkage.

- Bridges with larger skew angles have lower strains over the intermediate supports.

- Secondary moments affect the behavior in the negative moment region. The impact may be significant enough such that no tensile stresses in the deck may be experienced.

Recommendations

- Based on the finite element results, termination of b2 reinforcement at 1/8 of the span length is acceptable.

- Secondary moments may reduce the amount and length of the b2 reinforcement required.

Due to uncertainties associated with these secondary moments, further field tests and laboratory tests are recommended.to gain more confidence in considering them. This research would include a broad experimental program coupled with a detailed analytical evaluation and should result in the development and recommendation of design tools for considering secondary moments in PPCB design and detailing.

1 INTRODUCTION

1.1 Background

For design, multi-span pre-tensioned pre-stressed concrete beam (PPCB) bridges are usually assumed to experience two different stages of behavior. During the first stage, the PPCB girders are placed on supports and are assumed to behave as a simply-supported span to resist the self-weight of the structure. After the concrete deck is placed and fully cured, the bridge moves to the second stage, during which it behaves like a fully continuous structure over the intermediate support to resist live loads and superimposed dead loads that occur after the deck has cured.

During the second stage, the structure will experience negative moments over the intermediate supports, and, as a result, reinforcement must be provided to satisfy the strength and serviceability requirements. According to the Iowa Department of Transportation (DOT) Office of Bridges and Structures (OBS) bridge design manual, continuous longitudinal reinforcement (b1 reinforcement) is provided over the top and bottom of the entire deck. In addition to the b1 reinforcement, negative moment reinforcement (b2 reinforcement) is provided for strength over the intermediate supports and to control the cracks due to negative moments (Figure 1).

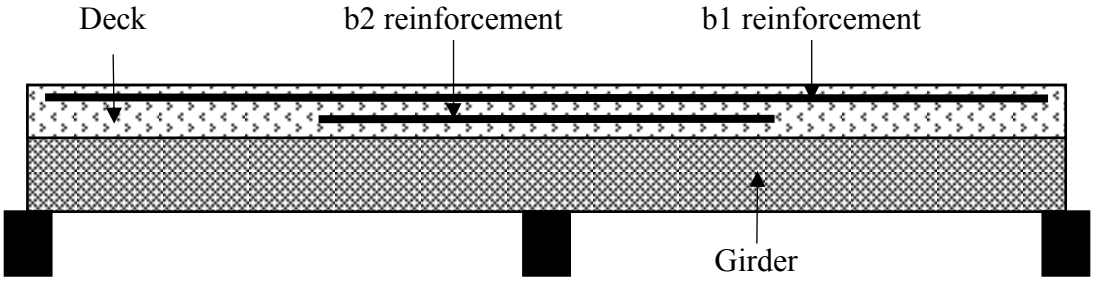

Figure 1. Longitudinal reinforcement arrangement in the deck of a PPCB bridge

The amount of b2 reinforcement is designed based on the negative moments occurring at the intermediate supports due to the live loads and the superimposed dead loads. However, current OBS policy regarding the termination of the b2 reinforcement is, in many cases, based upon anecdotal evidence of satisfactory previous performance. As per Iowa DOT OBS bridge design manual 5.4.2.4.1.7, the b2 reinforcement is terminated at 1/8 of the span length, which, perhaps not coincidentally, is also generally the location of allowable deck construction joints. However, the Association of State Highway and Transportation Officials (AASHTO) Load and Resistance Factor Design (LRFD) Specifications (2004) section5.14.1.4.8 states that “longitudinal reinforcement used for the negative moment connection over an interior pier shall be anchored in regions of the slab that are in compression at strength limit state and shall satisfy the requirements of AASHTO 5.11.1.2.3. The termination of this reinforcement shall be staggered” (AASHTO 2004). AASHTO 5.11.1.2.3 further describes the development length of b2 reinforcement as follows: “at least one third of the total reinforcement provided for the negative moment at a support shall have an embedment length beyond the point of inflection not less than

(1) The effective depth of the member, (2) 12.0 times the nominal diameter of the bar, (3) 0.0625 times the clear span" (AASHTO 2004).

The distance to the inflection point of a two-span continuous beam under uniformly distributed load is about 1/4 of the span, which is about twice the length prescribed by the Iowa DOT. Although the Iowa DOT policy may result in shorter b2 reinforcement than the AASHTO LRFD Specifications, the Iowa DOT has not experienced any significant deck cracking in the negative moment regions of PPCB bridges.

1.2 Objectives of the Research

Because the Iowa DOT OBS has observed satisfactory historical performance of its PPCB bridges, there is a desire to provide research evidence as to the appropriateness of current OBS policy. If necessary, the current OBS policy should be modified. The objectives of this work were as follows:

- Investigate the OBS policy regarding the required amount of b2 reinforcement
- Investigate the OBS policy regarding the termination length of b2 reinforcement
- Investigate the impact of the b2 reinforcement termination pattern
- Investigate the effect of secondary moments on the performance of PPCB bridges

1.3 Research Plan

To achieve the research objectives, four tasks were undertaken. Each task was developed based on lessons learned from each previous task.

Task 1 – Information Gathering

A literature search was conducted to collect information on the design of negative moment reinforcement for PPCB bridges. The current domestic state of the practice with regard to continuity and the associated design of b2 reinforcement and termination were also collected through a web-based survey.

Task 2 – Field Test and Inspection

Field tests and inspections were conducted on five bridges with diverse geometric properties (width, length, skew angle, girder type, number of spans, and number of girders) to study the actual behavior of typical PPCBs. Strain gauges were installed on the decks and girders at several transverse sections. A known truck then crossed the bridges along several longitudinal paths, generating longitudinal strain profiles. Strain profiles were used to study general bridge performance and, later, to calibrate analytical models.

Task 3 – Analytical Modeling

Based on the field test observations, two bridges were selected for finite element modeling. Finite element models were highly discretized in such a way that the behavior of an individual b2 reinforcement could be evaluated. Finite element models calibrated from the live load testing completed in Task 2 were then used to conduct parametric studies. In addition, one bridge was selected to study the significance of secondary moment at the intermediate supports.

Task 4 – Reporting the Recommendations

A final report was developed to present all the observations, conclusions, and recommendations on the design of negative bending moment b2 reinforcement of multi-span continuous PPCB bridges.

2 LITERATURE REVIEW AND SURVEY

2.1 Introduction to Transverse Cracks on Bridge Decks

Most concrete bridge decks develop transverse cracks at an early stage. According to the literature, the predominant mode of deck cracking is transverse cracking, which usually occurs over the transverse reinforcement. It has been estimated that more than 100,000 bridges in the US have transverse cracks on their decks (Hadidi and Saadeghvaziri 2005). These cracks can accelerate the corrosion of the reinforcement, especially where deicing chemicals are applied, and thus reduce the service life of the structure while increasing the maintenance costs. Freeze-thaw cycles when water is present inside the cracks can also reduce the service life of the structure.

Although transverse cracks in bridge decks are a concern among designers and researchers, the effects of numerous contributing factors and mitigation procedures are not yet fully understood. The material and mix design, construction practices, environmental conditions, and structural design factors are the primary causes of the transverse cracks. Additional factors are listed in Table 1 (Hadidi and Saadeghvaziri 2005).

Table 1. Cause of transverse cracks on bridge decks

Material and mix design	Construction practices and environmental conditions	Structural design factors
Aggregates	Weather condition and concrete temperature	Girder type, boundary conditions, and spacing
Water content	Curing	Shear studs configuration and properties
Cement type	Pour length and sequence	Concrete cover
Cement content	Time of casting	Deck thickness
Water/Cement ratio	Finishing	Reinforcement type, spacing, size, and distribution
Concrete strength	Vibration of fresh concrete	Section stiffness
Slump	Construction loads	Vibration and impact characteristics
Air content	Form type	Traffic

Source: Hadidi and Saadeghvaziri 2005

2.1.1 Material and Mix Design

Most research related to understanding bridge deck cracking has been conducted on material and mix design to determine why transverse cracks occur on bridge decks. Several researchers found that the type of aggregates used in the concrete is correlated with deck cracking (Babaei and

Purvis 1994). Suggestions have shown that larger aggregates with high specific gravity and low shrinkage aggregates may minimize deck cracking.

Babaei and Purvis (1994) suggested that the maximum water content be 12 lb/ft^3. Higher cement content induces higher temperatures throughout the hydration processes and leads to drying shrinkage and thereby cracks in the concrete deck. French et al. (2007) and Babaei and Purvis (1994) provided an acceptable cement content range of 22 lb/ft^3 to 28 lb/ft^3 to minimize concrete deck cracking. Schmitt and Darwin (1995) found that an increase in water content increases deck cracking and recommended to not exceed 27% of both water and cement content of the total concrete volume. Reducing the water/cement ratio reduces the shrinkage. Schmitt and Darwin (1995) suggested a water/cement ratio of 0.40 to 0.48 to minimize deck cracking.

The compressive strength of the concrete is another factor that is thought to affect deck cracking. However, there is no general consensus among researchers on this factor. Schmitt and Darwin (1995) observed an increase in deck cracking due to an increase in compressive strength. Krauss and Rogalla (1996) proposed that low early strength concrete be used to minimize deck cracking. The slump of a concrete mix is also a factor that leads to concrete cracking. Most researchers have noticed that the higher the slump level, the more deck cracks that are observed (Issa 1999).

Cheng and Johnson (1985) and Schmitt and Darwin (1995) observed that deck cracking can be reduced by increasing the air content of the concrete. Schmitt and Darwin (1995) proposed that at least 6% air content be used. Similarly, Babaei and Purvis (1994) proposed 5.5% to 6.0% air content to minimize cracking.

2.1.2 Construction Practices and Environmental Conditions

The temperature of the concrete is an important factor that affects cracking. After concrete placement, the temperature of the deck increases due to hydration. However, the temperature of the girders remains almost unchanged. The larger the temperature difference between the deck and the girders, the greater the chance for deck cracking. French et al. (2007) suggested 40°F as the minimum temperature and 90°F as the maximum temperature for concrete deck placement. Babaei and Purvis (1994) recommended that the temperature difference between the deck and girders be maintained below 22°F for at least 24 hours to minimize the chance of deck cracking.

High temperature with low humidity and high wind speed increase the evaporation of water from the concrete, which can lead to the formation of plastic shrinkage cracks. Several researchers recommended that special attention be given when the evaporation rate exceeds 0.2 lb/ft^2/hr for normal concrete and 0.1 lb/ft^2/hr for concrete with low water/cement ratios (Krauss and Rogalla 1996).

Several studies showed that concrete placement length and sequence may have some effect on deck cracking. Kochanski et al. (1990) suggested that concrete pour rates greater than 0.6 span length/hour minimize the cracking of the concrete deck. Based on an analytical study, Issa

(1999) concluded that placing concrete first in the positive moment region will reduce deck cracking. Ramey et al. (1997) recommended a detailed procedure to minimize cracking.

Some studies illustrate the effect of form type on deck cracking. Frosch et al. (2002) showed that stay-in-place forms increase deck cracking and suggested other form types for deck construction.

Research has shown that the vibration and impact characteristics of the live loads on the superstructure affect deck cracking. Babaei and Purvis (1994) suggested the use of vibrations with low amplitude and frequency to compact the concrete to minimize deck cracking. Mckeel (1985) observed that bridges carrying a large number of trucks at high speeds experience more deck cracking.

2.1.3 Structural Design Factors

Very little research has been carried out on the effects of structural design factors such as girder type, shear studs configuration, deck thickness, reinforcement size and type, and vibrations on deck cracking.

Concrete has a lower thermal conductivity than steel. Therefore, bridges with steel girders experience more deck cracking than concrete girder bridges due to the higher temperature gradients (Krauss and Rogalla 1996). Composite action is achieved through shear studs between the deck and the girders. However, these shear studs restrain the shrinkage of the concrete deck, which leads to cracking of the concrete deck. Although Krauss and Rogalla (1996) did not give any recommendations, they stated that the girder restraint and shear stud type can cause a significant amount of cracking. French et al. (2007) recommended fewer studs with smaller row lengths, but specific guidelines were not given.

Higher deck thicknesses decreases transverse cracking. This may be due to the increased deck/girder stiffness ratio (Hadidi and Saadeghvaziri 2005). Kochanski et al. (1990) recommended that 8.5 in. to 9 in. decks be used, whereas French et al. (2007) suggested that deck thicknesses greater than 6.25 in. generally perform well.

Several researchers have observed that reinforcement size, type, and distribution affect deck concrete cracking. As bar size increases, cracking increases. Several researchers suggested the use of No. 5 reinforcement as the maximum reinforcement size for the longitudinal reinforcement (Kochanski et al. 1990, Ramey et al. 1997). However, Krauss and Rogalla (1996) recommended the use of No. 4 bars as the largest reinforcement with a 6 in. spacing to minimize deck cracking. Ramey et al. (1997) gave detailed guidelines for reinforcement to decrease cracking tendency.

2.2 Transverse Cracks at the Intermediate Supports of PPCB Bridges

According to the literature, two primary concepts can be found related to the design of the reinforcement at the intermediate supports of PPCB bridges: design of continuity reinforcement

at the bottom of the connection and design of continuity reinforcement at the top of the connection.

2.2.1 Design of the Reinforcement at the Bottom of the Continuity Connection

According to McDonagh and Hinkley (2003), time-dependent (secondary) moments due to creep of the girders and differential shrinkage between the deck and the girders play an important role in the design of the reinforcement at the bottom of the continuity connection. Creep of the girders induces a positive secondary moment, whereas differential shrinkage generates a negative secondary moment at the bottom of the continuity connection. A Portland Cement Association (PCA) report (Freyermuth 1969) showed that the positive secondary moments are often greater than the negative secondary moments. Further, based on an experimental and analytical study of the behavior of jointless integral abutment bridges, Oesterle et al. (2004) concluded that the negative moment induced by the live load can be significantly reduced by the time-dependent load effects.

Unfortunately, the time-dependent secondary moments mentioned above cannot be calculated reliably. Several methods have been proposed to calculate these secondary moments. The PCA method (Freyermuth 1969) is the most popular method. The Construction Technology Laboratory (CTL) method, NCHRP Report 322 guidelines, and RMCalc software (McDonagh and Hinkley 2003) from the Washington State DOT (WSDOT) are also available to estimate the secondary moments.

The positive moment continuity connection varies from state to state (Hastak et al. 2003) conducted research to study the different types of positive moment connections used around the country and also to identify the potential problems associated with those connections. Newhouse (2005) conducted research that involved a comparison of different methods used to calculate the secondary moments. The results were used to develop three different types of continuity connection details at the bottom of the intermediate support. Recently, Chebole (2011) conducted research to investigate the accuracy of the calculation methods for secondary moments, and a program was developed to enhance the estimation accuracy of the secondary moments. Kwak and Seo (2002) developed an analytical model to simulate the time-dependent effects of creep, shrinkage, and concrete cracking of PPCB bridges. The model was calibrated experimentally. The researchers concluded that the positive reinforcing steel at the support has no significant effect on the resulting negative moment.

2.2.2 Design of the Reinforcement at the Top of the Continuity Connection

No research was found that addressed the design of reinforcement at the top of the continuity connection (b2 reinforcement). If fact, no guidelines on the design of reinforcement at the top of the continuity connection are given in the AASHTO LRFD design speciation. Iowa DOT designs the reinforcement by assuming a fully cracked section, as shown in Figure 2. Wassef et al. (2003) used a similar design procedure to calculate the required negative moment reinforcement.

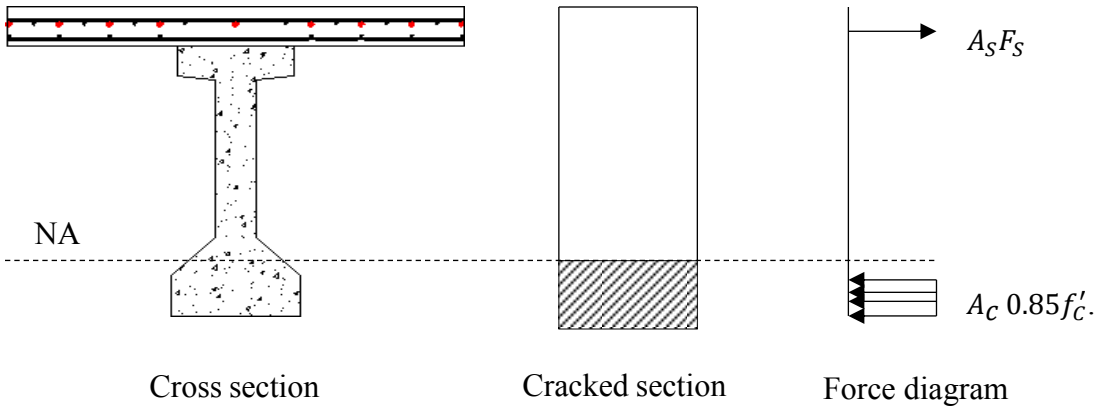

Figure 2. Force diagram at continuity connection

As mentioned in the Chapter 1, guidance is given in the AASHTO LRFD specification regarding the termination point and pattern of the b2 reinforcement. However, the Iowa DOT uses reinforcement approximately 50% shorter than the recommended length, without experiencing significant cracks. In their detailed design example, Wassef et al. (2003) do not provide any details regarding the termination of the b2 reinforcement.

2.3 State of the Practice on Negative Moment Reinforcement Design

The Iowa State University Bridge Engineering Center (BEC) in cooperation with the Iowa DOT OBS conducted a web-based survey to identify the state of the practice on continuity considerations and negative moment reinforcement (b2 reinforcement, Figure 1), with an emphasis on the design policies and practices associated with designing multi-span PPCB bridges.

To summarize, about 45% of the respondents assumed that adjacent spans act as simple spans for dead loads (girder and deck self-weight) and as continuous for superimposed dead (wearing surface, parapets) and live loads on the composite structure. Simple span for all dead loads and continuous for all live loads was assumed by 30% of the respondents. Furthermore, 20% of the respondents assumed simple spans for all loads.

Extension of the bottom pre-stressing strands with the girder end embedded into the diaphragm plus additional negative moment reinforcement in the deck were the most commonly used continuity connection details. Different DOTs use various practices to terminate the b2 reinforcement.

For example, in addition to the embedment length, the North Carolina DOT uses 1/3 of the span for termination of the b2 reinforcement, whereas the Kansas DOT uses 1/4 of the span, both near the point of inflection. The Delaware DOT, Nevada DOT, and several other DOTs follow the AASHTO LRFD guidelines to terminate the b2 reinforcement (Chapter 1). The New Mexico DOT uses the lengths as per the CONSPAN bridge design software. The Michigan DOT and

Pennsylvania DOT use a staggered b2 reinforcement pattern to minimize any transverse cracking.

3 FIELD TESTS

3.1 Introduction

Five bridges with different characteristics (see Appendix) were selected for field testing. Table 2 shows the general bridge characteristics for these five bridges.

Table 2. Bridge characteristics

Bridge #		1	2	3	4	5
	On	County Road C50	I-80	Meredith Drive	Mt. Pleasant Bypass	US 20
Location	Over	US 218	US 65	I-35/I-80	Big Creek	Whiskey Creek
Spans		2	2	2	3	3
Length (ft)		277	316	270	215	203
Width (ft)		47.2	76.5	82	42.5	43.2
Skew (degrees)		24	42	5	36	0
No. of girders		6	11	11	6	6
Type of girders		BTE	BTE	BTD	DM	LXD
Length of b2 (ft)		35	39	36	30	29

BTE – Bulb-tee Type E
BTD – Bulb-tee Type D
DM – US 34 over Big Creek drawing, Sheet 31
LXD – LXD – US 20 over Big Whiskey creek drawing, Sheet 30

The bridges were selected because they have differing numbers of spans, span lengths, widths, skew angles, numbers of girders, and girder types. However, the length of the negative moment b2 reinforcement (Figure 3) is approximately the same. As a result, it was anticipated that the field testing program would allow the research team to investigate the effects of bridge characteristics on the negative bending behavior. It is also worth noting that, in addition to allowing side-by-side comparisons, the field test results will be used to calibrate the subsequently described finite element models.

3.2 Instrumentation

During testing, strain gauges were installed at two general locations: on the top surface of the bridge deck in the negative bending region and on the girders. To study the effects of the b2 reinforcement and to generally aid in understanding bridge deck behavior, a set of deck strain gauges was placed 1 ft beyond the end of the b2 reinforcement and another set was placed 1 ft within the b2 reinforcement towards the pier. Another set of deck strain gauges was located over the pier (Figure 3, Figure 4, and Figure 5).

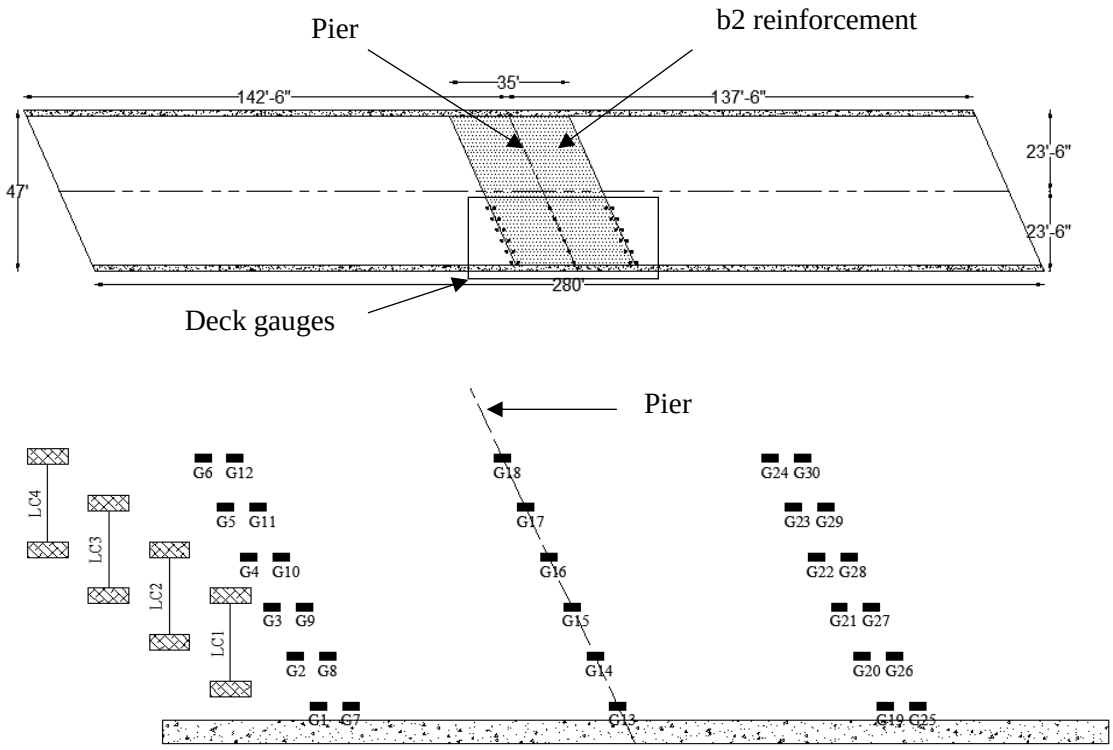

Figure 3. Typical deck gauge installation plan

Figure 4. Strain gauges end of the b2 bar

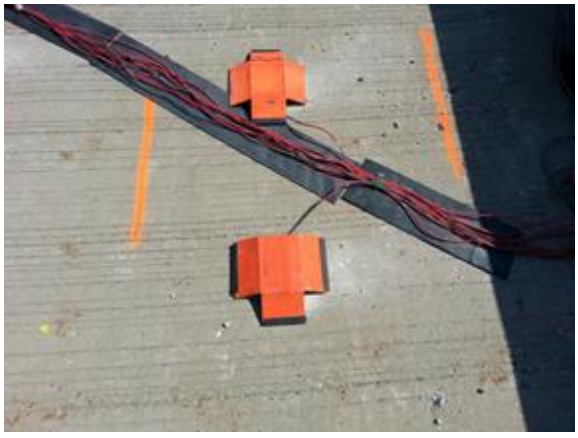

Figure 5. Cover plates prevent damage

To investigate the behavior of the principal strains, several rosettes (Figure 6) were also installed at the end of the b2 reinforcement; as with the single gauge placements, the rosettes were similarly placed 1 ft towards the pier and 1 ft away from the pier at the termination of the b2 bar.

Figure 6. Rosette near b2 reinforcement

In addition to the sensors placed on the deck, several gauges were attached to the girders at the mid-span location and near one of the piers. As shown in Figure 7, the gauges were attached to both the top and bottom flanges.

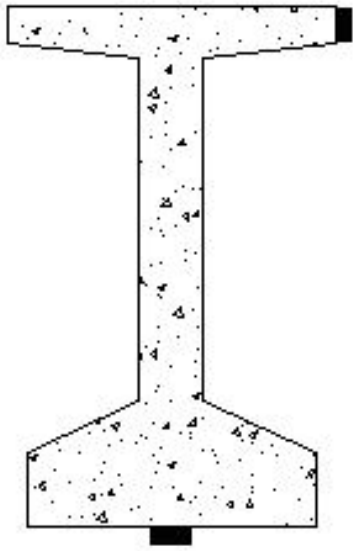

Figure 7. Typical girder gauge locations

A summary of the number of deck gauges, girder gauges, and rosettes used in field tests on each bridge is given in Table 3. Further, details regarding the gauge locations for each bridge is shown in the Appendix.

Table 3. Summary of gauges

Bridge #	Total gauges attached		Rosettes
	On deck	On girders	
1	46	16	8
2	43	32	4
3	37	28	6
4	46	20	8
5	55	20	10

3.3 Bridge Loading

Once all the strain gauges were installed, a standard snooper truck provided by the Iowa DOT (Figure 8) crossed the bridge along multiple transverse paths at a crawl speed. Details of the load cases (LC) for each bridge tested are given in the Appendix.

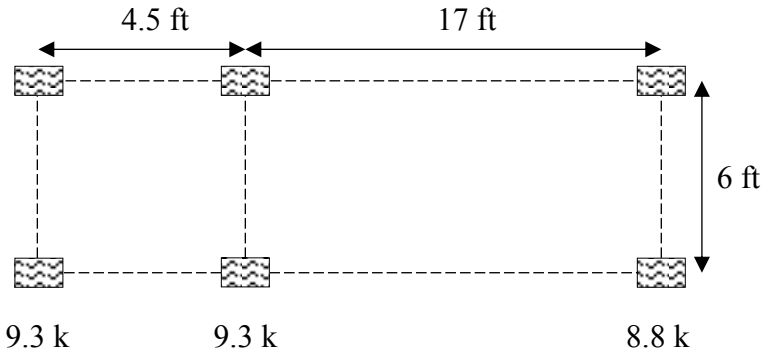

Figure 8. Details of the loading truck

3.4 Deck Gauge Longitudinal Strain Profiles

According to the strain profiles of the deck gauges (see the Appendix), almost every gauge on the bridge deck showed an expected tension/compression behavior of the bridge due to the truck load in the strain variation (Figure 9).

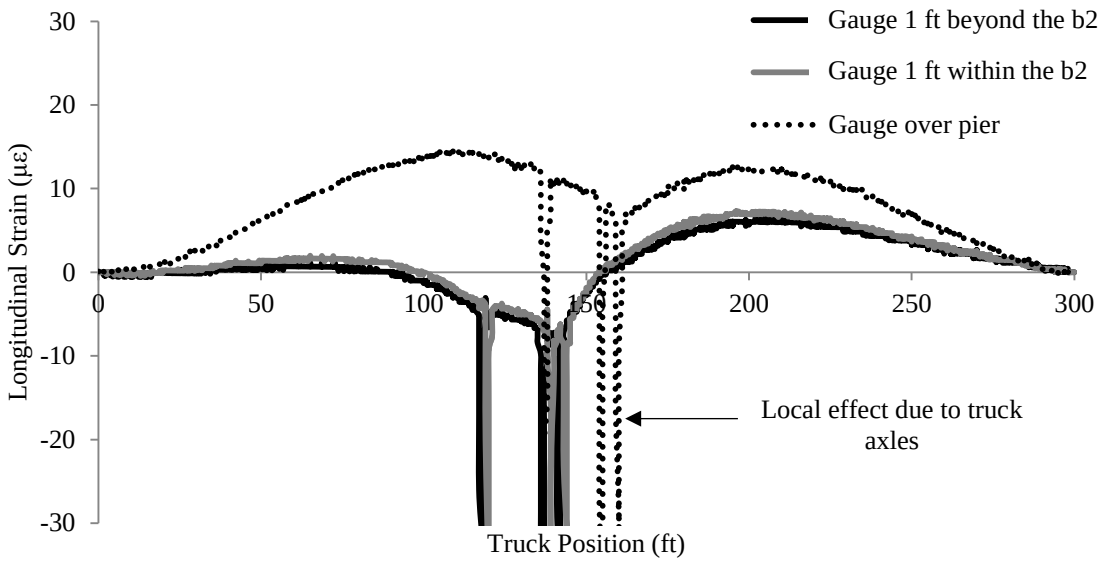

Figure 9. Typical deck gauge strain variations

It was found that the strain gauges beyond the end of the b2 reinforcement showed a slightly higher magnitude than the strain magnitude of the gauges within the end of the b2 reinforcement. Even though the field tests involved five bridges with different properties, the strain profiles of the deck gauges look similar in terms of pattern and sometimes magnitude. This loosely suggests that the negative moment b2 reinforcement may not be significantly affected by the gross geometric properties of the bridge, such as the number of spans, span lengths, widths, skew angles, number of girders, and girder types.

3.5 Girder Gauge Longitudinal Strain Profiles

In terms of patterns, and sometimes magnitudes, the strain variation of the girder gauges on all five bridges showed an expected tension/compression behavior of the bridge due to the truck load (see Figure 10 and the Appendix).

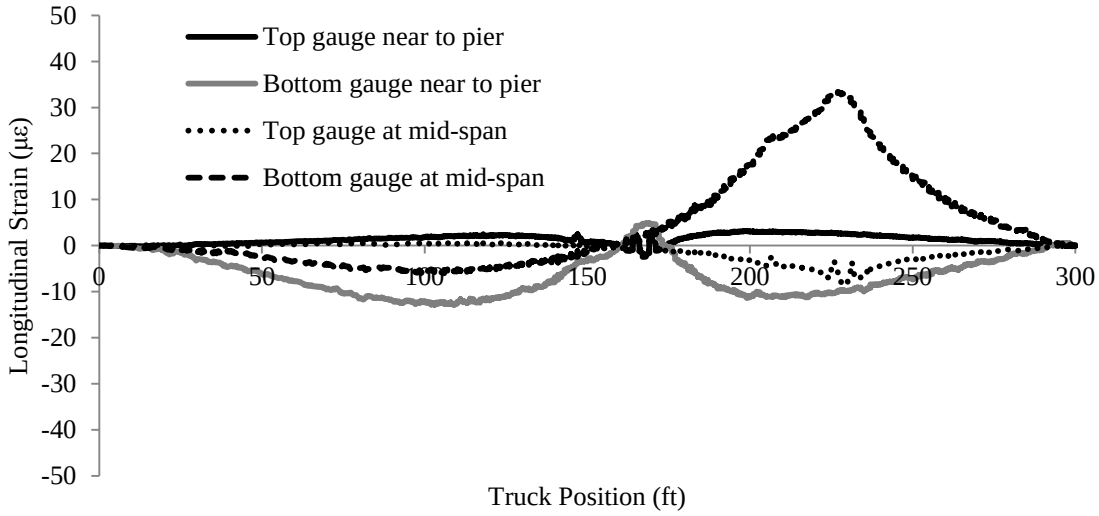

Figure 10. Typical girder gauge strain variations

3.6 Rosette Longitudinal Strain Profiles

In the absence of knowing the principal strain directions when designing an experiment, one needs three independent strain measurements to calculate the principal strains at a particular location. A strain gauge rosette is an arrangement of multiple closely placed gauges, which can be used to obtain those independent strain measurements. During the field tests, 45°rectangular strain gauge rosettes were used to determine the principal strains in the bridge deck (Figure 11).

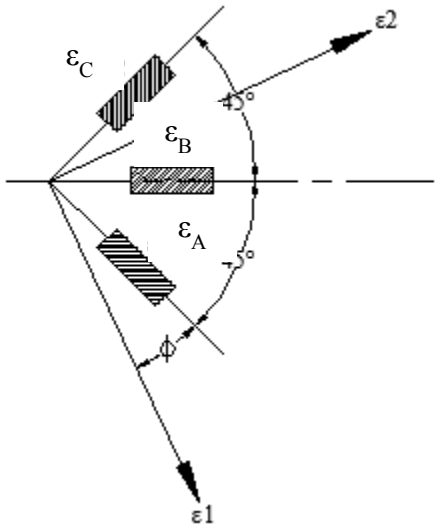

Figure 11. 45° rectangular strain gauge rosettes

The magnitude and the direction of the principal strains at the rosette's location are calculated as follows (Vishay Precision Group 2010):

$$\epsilon_{1,2} = \frac{\epsilon_A + \epsilon_B}{2} \pm \frac{1}{\sqrt{2}}\sqrt{(\epsilon_A - \epsilon_B)^2 + (\epsilon_B + \epsilon_C)^2} \quad (1)$$

$$\phi = \frac{1}{2}\tan^{-1}\left(\frac{\epsilon_A - 2\epsilon_B + \epsilon_C}{\epsilon_A - \epsilon_C}\right) \quad (2)$$

Where:
$\epsilon_A, \epsilon_B, \epsilon_C$ = Strain gauge data of the rosettes
ϵ_1 = Major principal strain
ϵ_2 = Minor principal strain
ϕ = Angle to the major principal strain

Based on the principal strain profiles, no significant difference was observed between the rosettes, which are beyond and within the end of the b2 reinforcement, indicating that the b2 reinforcement didn't influence the gross behavior significantly. However, in the two-span bridges, when the truck wheel paths were in the vicinity of the rosettes, a strain variation was observed as shown in Figure 12.

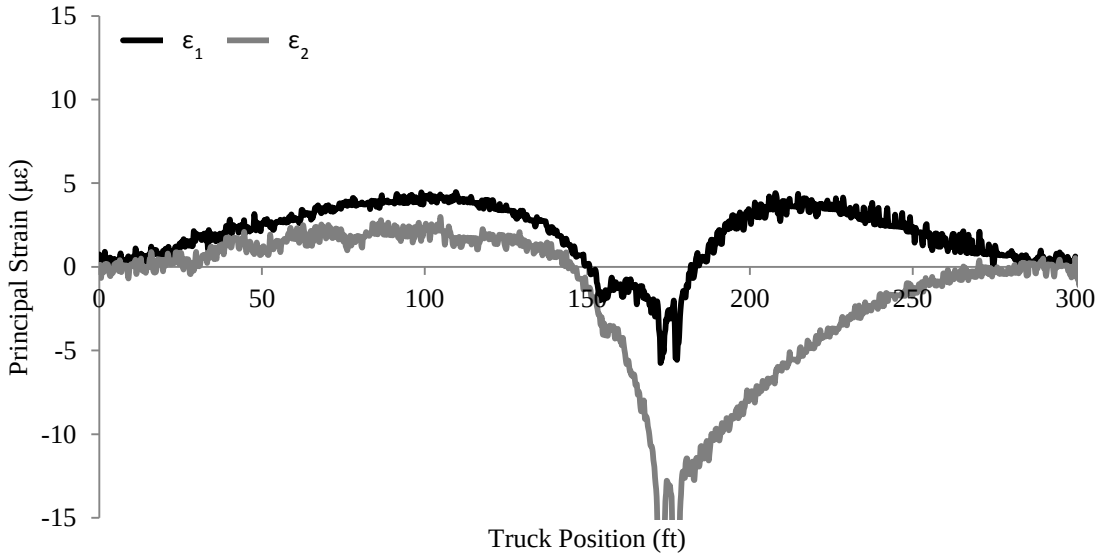

Figure 12. Typical principal strain variations for two-span bridges with wheel paths close to the rosettes

When the truck wheel paths were away from the rosettes, major (ε_1) and minor (ε_2) principal strains of approximately the same magnitudes with opposite signs were observed (Figure 13).

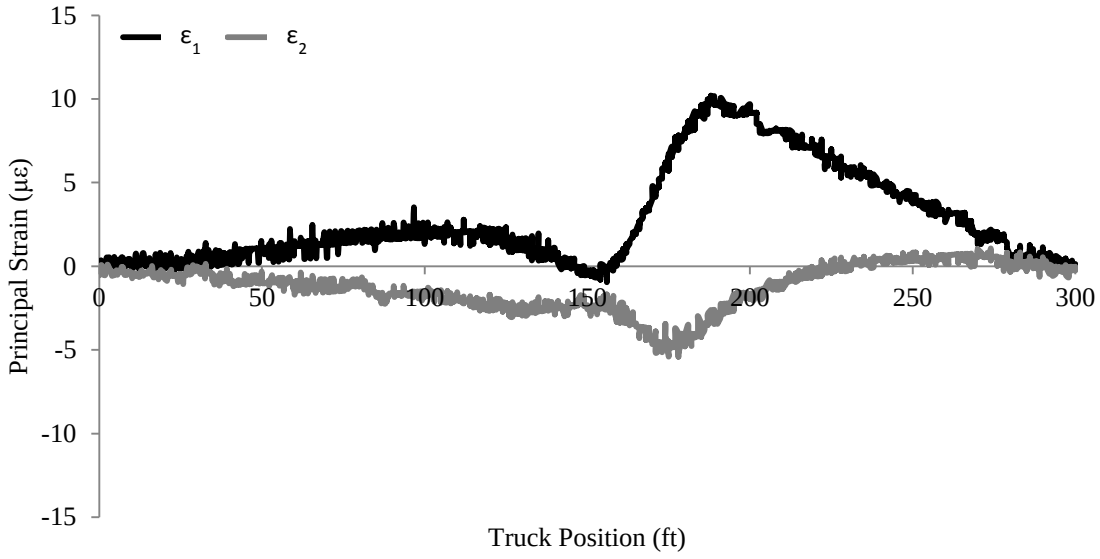

Figure 13. Typical principal strain variations for two-span bridges with wheel paths away from the rosettes

In the three-span bridges, approximately the same principal strain magnitudes with opposite signs were observed (Figure 14 and Figure 15).

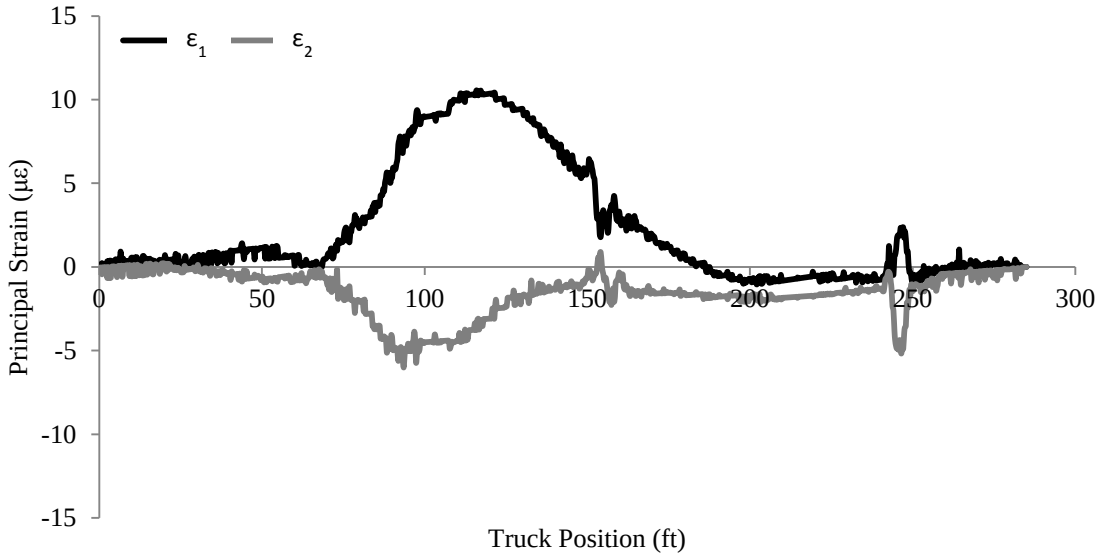

Figure 14. Typical principal strain variations for three-span bridges with wheel paths close to the rosettes

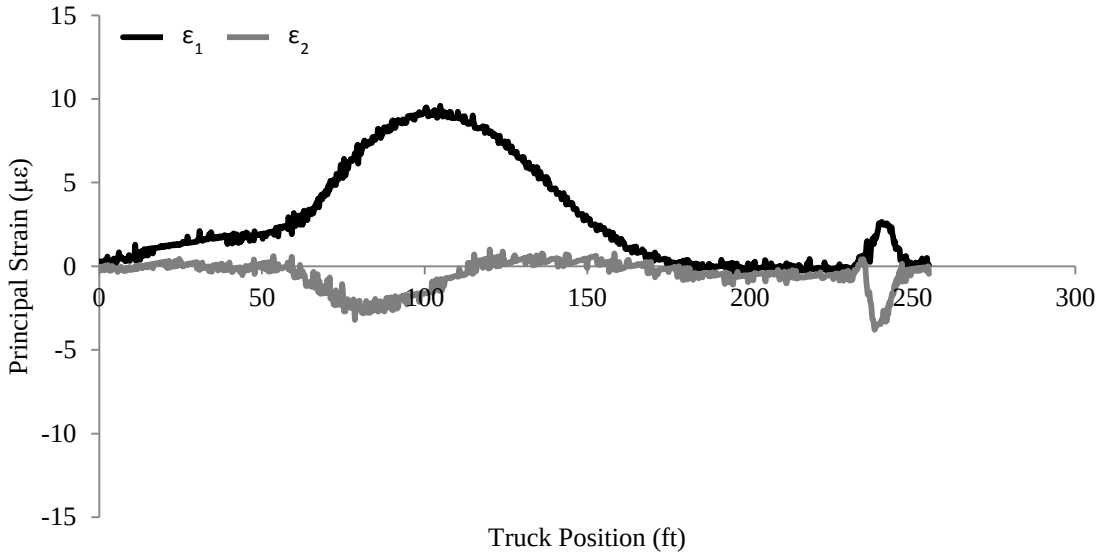

Figure 15. Typical principal strain variations for three-span bridges with wheel paths away from the rosettes

4 FINITE ELEMENT MODELS OF TWO BRIDGES

4.1 Introduction

A significant amount of effort during this research was aimed at investigating the effects of the b2 reinforcement on both skewed and non-skewed bridges with bulb-tee girders. Bridge 3 (Bridge A) and Bridge 2 (Bridge B) have similar characteristics (Table 2), except that Bridge A has a 5-degree skew angle, whereas Bridge B has a 42-degree skew angle. Based on input from the project advisory committee, Bridge A and Bridge B were used to investigate the role of skew angle on the negative bending behavior of PPCB bridges as well as to study the influence of the b2 reinforcing details.

ANSYS Mechanical APDL 14.5, a general purpose finite element package, was used to develop the three-dimensional finite element models of Bridge A and Bridge B. Chapter 4 describes the construction and calibration of the finite element model for Bridge A and Bridge B. The analysis results for Bridge A and Bridge B are discussed in Chapter 5.

4.2 Bridge A Finite Element Model

4.2.1 Element Type Selection

Bridge A consists of a continuous concrete deck, b2 reinforcement, barrier rails, precast pre-stressed girders, pier diaphragm, pier cap, pier columns, footings, piles, abutments, and wing walls. Of these components, the pier cap, pier columns, footings, piles, and wing walls were not discretely modeled, but were approximated within the boundary condition parameters. The elements used to model the components of Bridge A are listed in Table 4.

Table 4. Types of elements used in the analysis

Shell 181 element	Beam 188 element
Deck	Girder top flange
Pier diaphragm	Girder bottom flange
Abutment	Intermediate diaphragm
Barrier rails	b2 reinforcement
Girder web	

4.2.2 Element Properties

Shell 181 Element (ANSYS 2011)

The Shell 181 element is a structural element with four nodes in three-dimensional (3D) space, with each node having six degrees of freedom. This element is suitable for the analysis of thin to moderately thick shell structures. It can be used in linear and nonlinear applications that involve

large rotations and large strains. The Shell 181 element has the capacity to model layered applications, such as composite shells and sandwich constructions.

Beam 188 Element (ANSYS 2011)

The Beam 188 element is a structural beam element with two nodes in 3D space. Each node has six degrees of freedom and one optional degree of freedom to provide warping freedom. This element can be used to analyze slender to moderately thick beam structures. The Beam 188 element is based on Timoshenko beam theory; hence, this element can deal with shear deformation effects. This element is suitable for linear and nonlinear applications that involve large rotations and strains.

4.2.3 Material Properties

According to the structural drawings, Bridge A consists of pre-stressed girders with a specified compressive strength (f'_C) of 9 ksi. The specified compressive strength of the deck concrete is 4 ksi. Reinforcing steel with a 60 ksi yield strength was used for all mild steel reinforcement. An ultimate strength of 270 ksi was used for all high-strength strands specified in the pre-stressed girders.

Reinforcement in each component of the bridge, except the b2 reinforcement, was smeared into the associated finite element with an effective modulus of elasticity determined by the following:

$$E_{eff} = \frac{A_C E_C + A_S E_S}{A_C + A_S} \quad (3)$$

Where:
E_{eff} = Effective modulus of elasticity
A_C = Area of concrete
A_S = Area of steel
E_C = Modulus of elasticity of concrete
E_S = Modulus of elasticity of steel

4.2.4 Finite Element Model

Figure 16 shows a plan view of the finite element model of Bridge A. The bridge deck was meshed with 6-in. (Z direction) by 9-in. (X direction) shell elements.

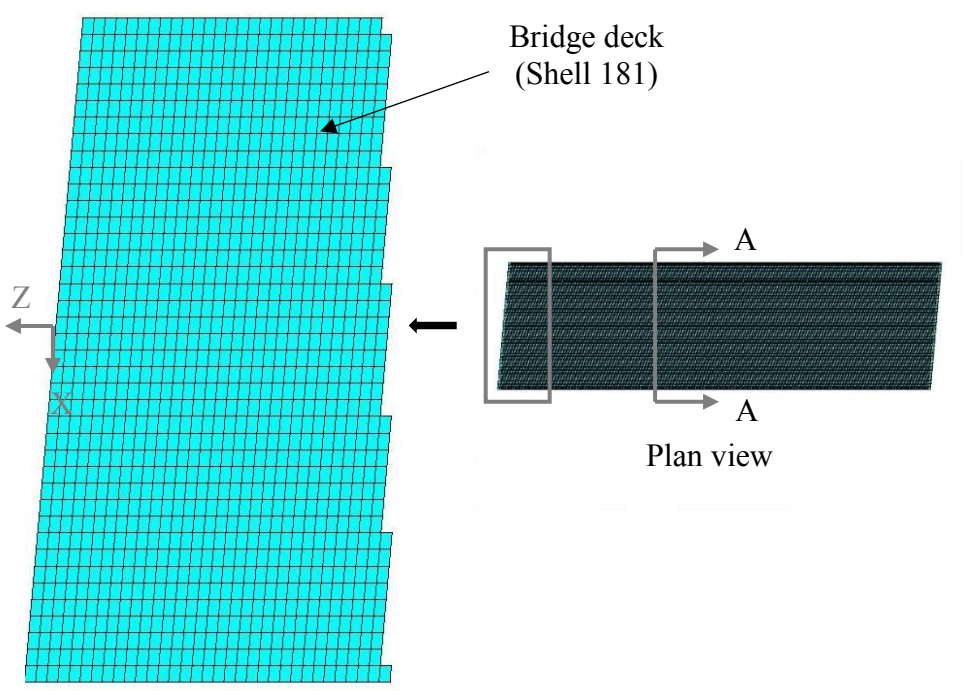

Figure 16. Bridge A finite element model plan view

Figure 17 shows the finite element model of all the components of the bridge, except the abutments and the b2 reinforcement.

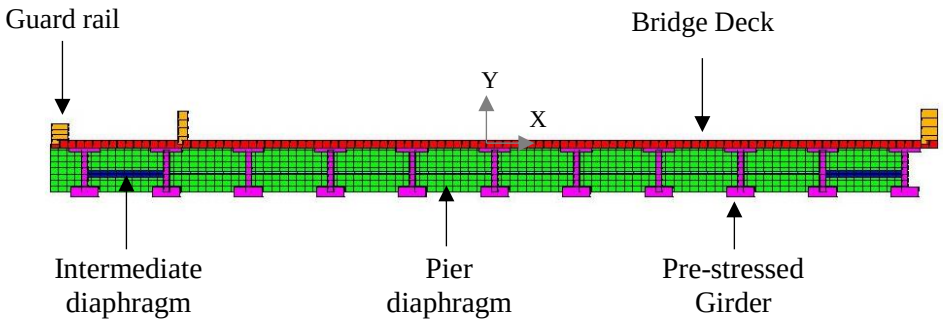

Figure 17. Cross-section A-A

A schematic deck/girder cross-section with reinforcement is shown in Figure 18. The idealized bridge deck and girder model and b2 reinforcement are shown in Figure 19.

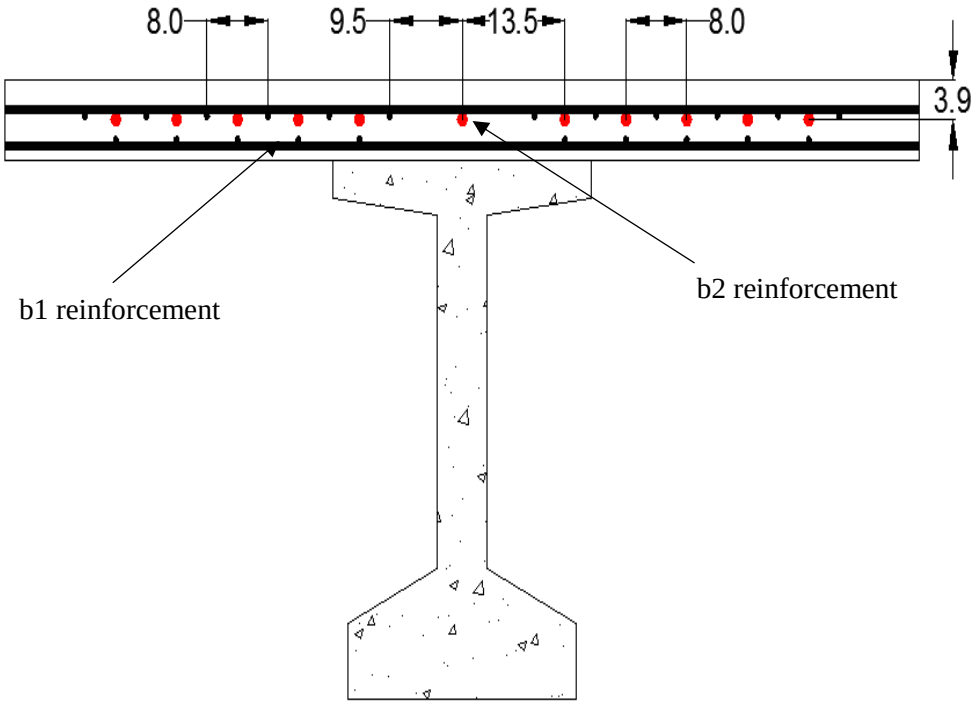

Figure 18. Actual deck, girder, and b2 reinforcement

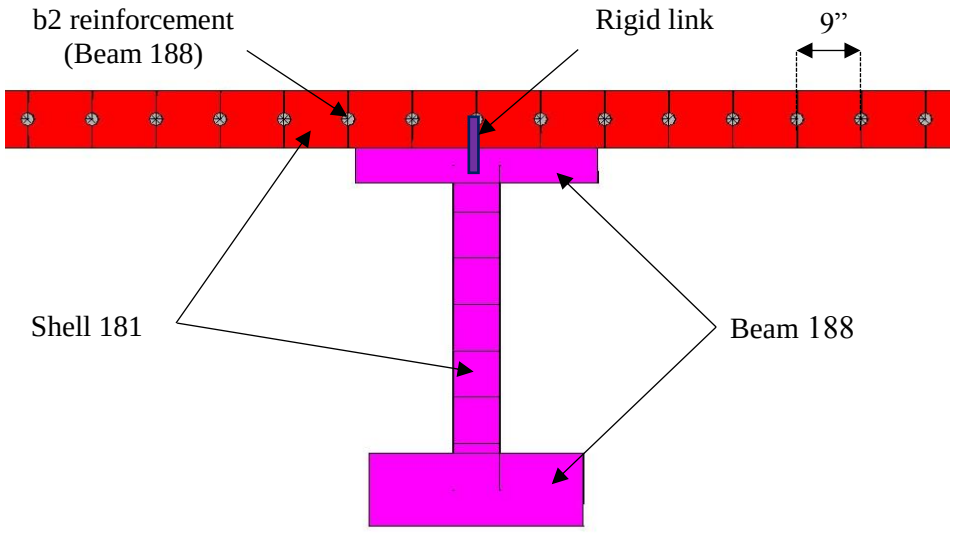

Figure 19. Idealized deck, girder, and b2 reinforcement

Instead of the actual b2 reinforcement spacing, uniform 9 in. spacing was used in the finite element model, with the total amount of reinforcement area remaining the same. The connection between the bridge deck and girders was made using rigid elements, which transfer the degrees of freedom of the master nodes (nodes of the deck elements) to the slave nodes (nodes of the top

flange elements). Rigid links do not contain any material properties. Hence, rigid links cannot be used in an analysis where temperature effects are involved. During the calibration of temperature, the rigid links were replaced with Beam 188 elements with very large stiffness values.

Figure 20 illustrates the idealization of the pier diaphragm.

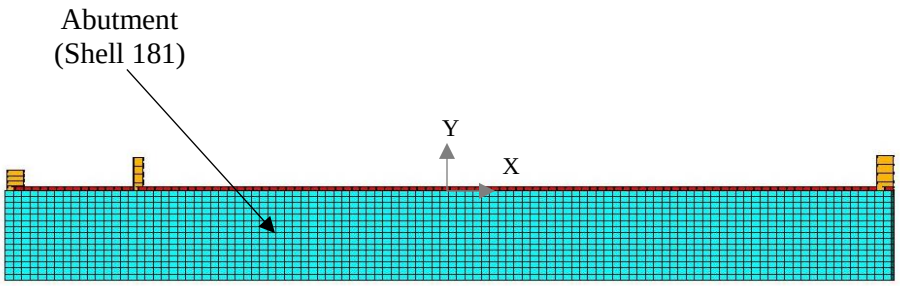

Figure 20. Finite element model of the abutment

Elements in the pier diaphragm were meshed with 6.5-in. (Y direction) by 9-in. (X direction) elements. The girder webs were also meshed with shell elements with 6.5-in. (Y direction) by 9-in. (Z direction) dimensions. Figure 20 shows the finite element model of the abutment. To align the nodes of the deck and girder web, the abutment was meshed with shell elements having 6.5-in. (Y direction) by 9-in. (X direction) dimensions.

4.2.5 Finite Element Model Support Conditions

4.2.5.1 Support Condition at the Pier Diaphragm

The girders of Bridge A are connected to the pier cap through a pintle. The pier cap is supported on five pier columns, which are connected to the pile foundation. The support conditions for the girders at the pier were approximated by a roller support, which restrained the Y direction translation (Figure 21) from movement.

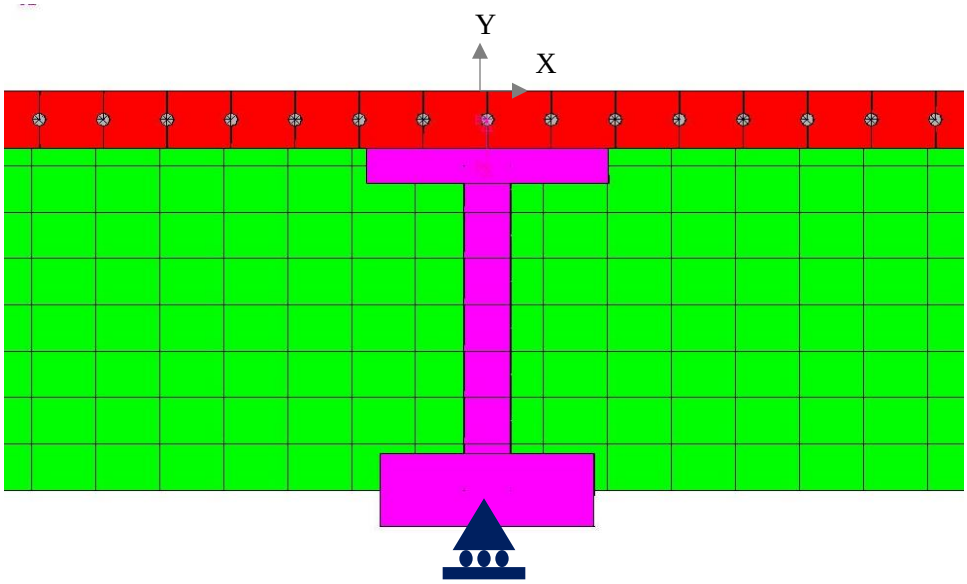

Figure 21. Support condition at the pier diaphragm

4.2.5.2 Support Conditions at the Abutment

Bridge A is an integral abutment bridge. The bottom of the abutment is supported on 21 piles, which are approximately 3.9 ft apart. Also, the ends of the abutments are connected to the wing walls. As an analytical approximation, the soil forces were neglected and the nodes of the abutments at the pile head locations were restrained in the Y direction as shown in Figure 22.

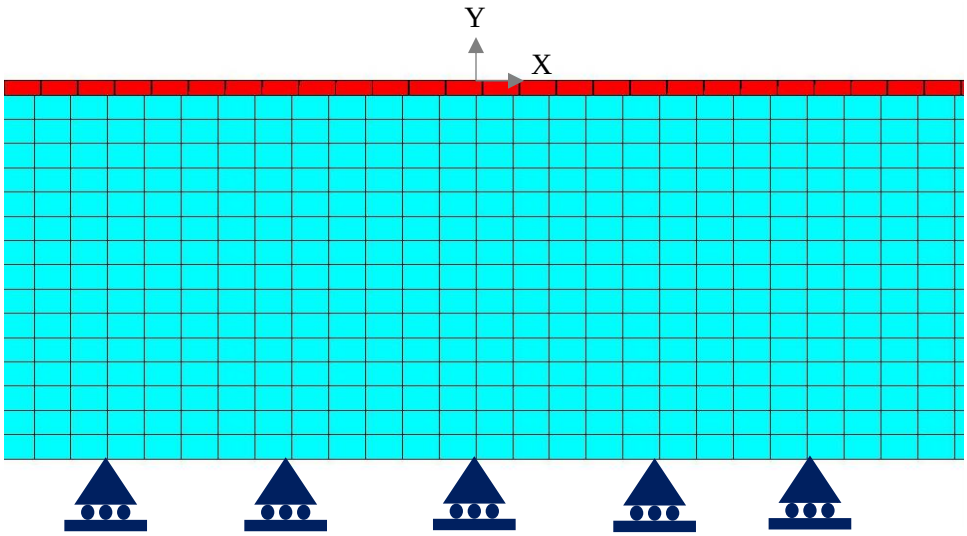

Figure 22. Support conditions at the abutment

4.2.6 Loading Conditions

Four main loading types were applied to the finite element model. The moving truck load was modeled with load steps and with point loads at the truck wheel locations (Figure 8). A uniform surface load was also used for some analyses. Temperature load was applied as a body force. Shrinkage load was applied as an equivalent temperature load.

4.2.7 Model Calibration from Field Test Results

Calibration of the finite element model from the field test results (Chapter 3) involved using data from three sets of gauges: deck gauges, girder gauges, and rosettes. During the calibration process, strain values from the finite element model at the gauge locations were compared with the strain gauge values for all load cases. As described in Chapter 3, gauges near to the truck wheel paths showed larger strain magnitudes than gauges away from the truck wheel paths. In addition to making qualitative assessments regarding the accuracy of the model, peak strain values were used to calculate the percentage strain difference between the finite element model and the field test results as follows:

$$\text{Strain difference percentage} = \frac{|\epsilon_{\text{FEM}} - \epsilon_{\text{Field Test}}|}{\epsilon_{\text{Field Test}}}(100) \quad \textbf{(4)}$$

4.2.7.1 Calibration for the Deck Gauges

The calibration results of the deck gauges of Bridge A are presented in this section (see Figure 23).

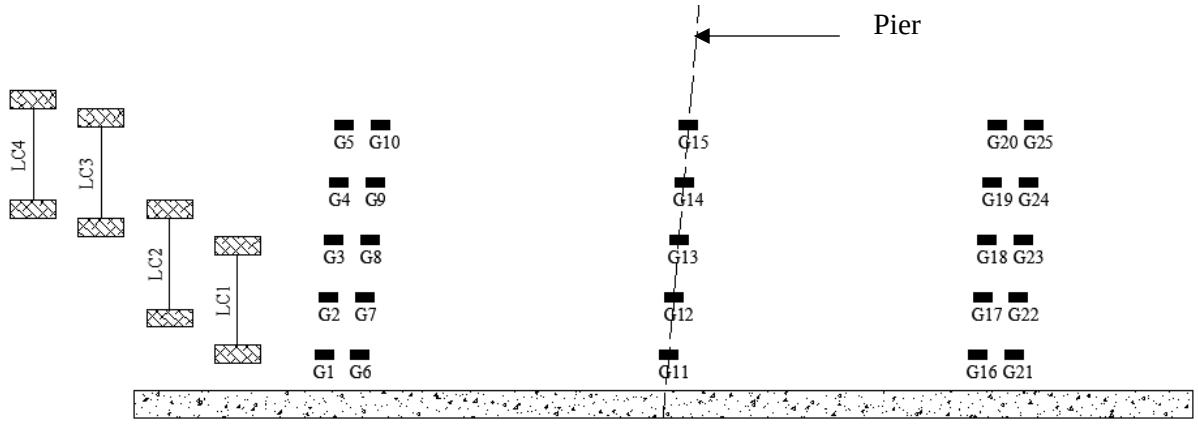

Figure 23. Bridge A instrumentation plan of deck gauges

Comparisons of typical finite element results and field test results from the deck gauges, which are in the vicinity of the truck wheel path, are shown in Figure 24 and Figure 25.

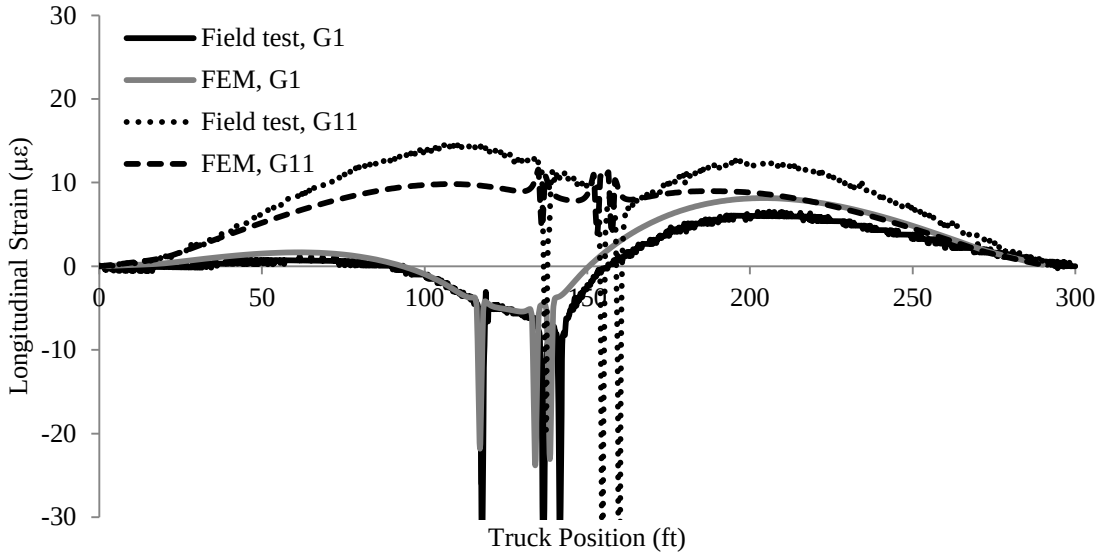

Figure 24. Strain variation of deck gauges (G1 and G11) close to the wheel path, (LC1)

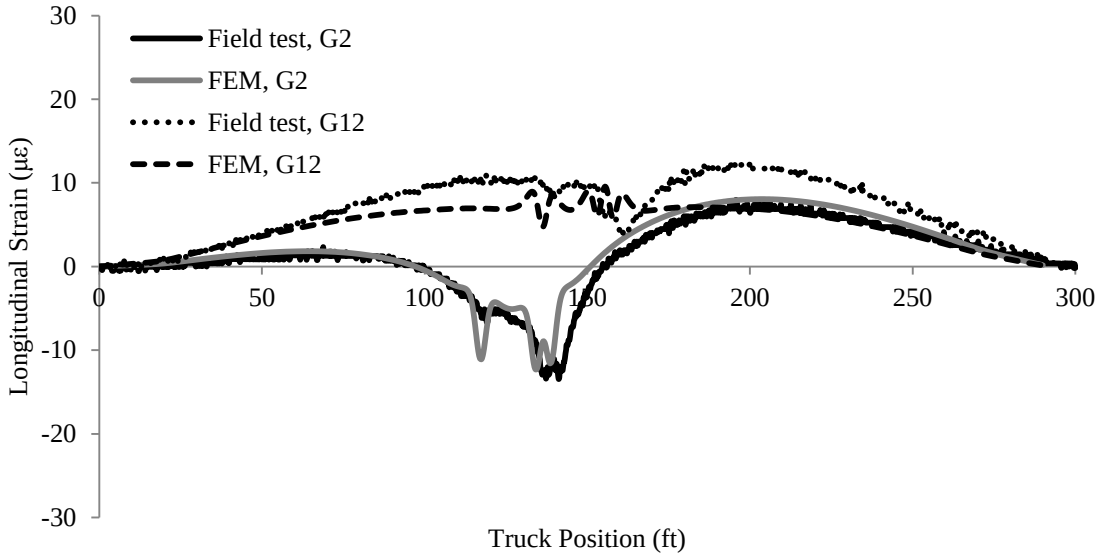

Figure 25. Strain variation of deck gauges (G2 and G12) close to the wheel path, (LC1)

Figure 26 shows the comparisons of typical strain variation of the deck gauges away from the truck wheel path. In general, the finite element results for the deck gauges are in reasonable agreement with the field test results.

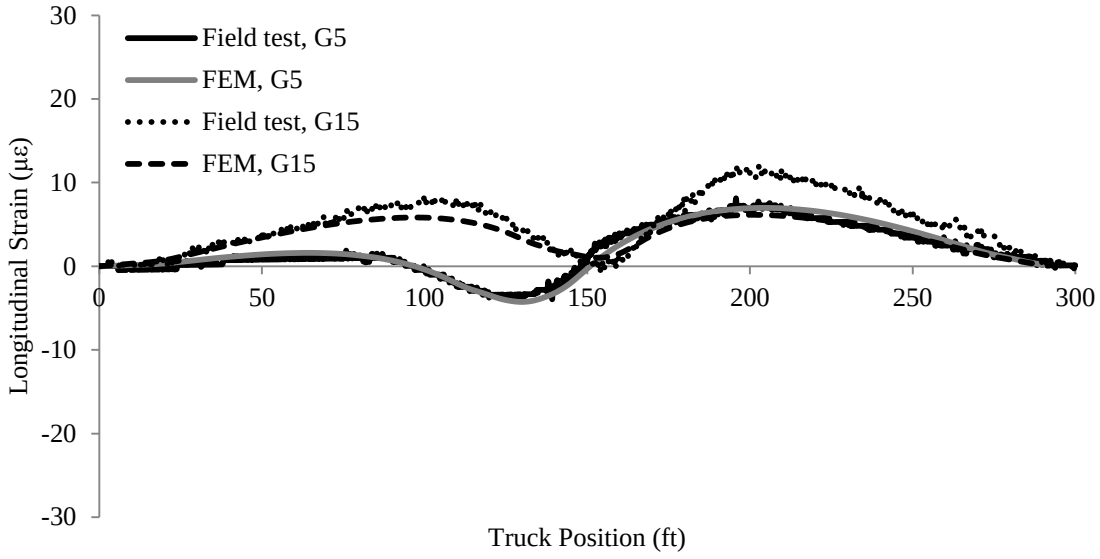

Figure 26. Strain variation of deck gauges (G5 and G15) away from the wheel path, (LC1)

4.2.7.2 Calibration for the Girder Gauges

Calibration results for the girder gauges of Bridge A are presented in this section (see Figure 27).

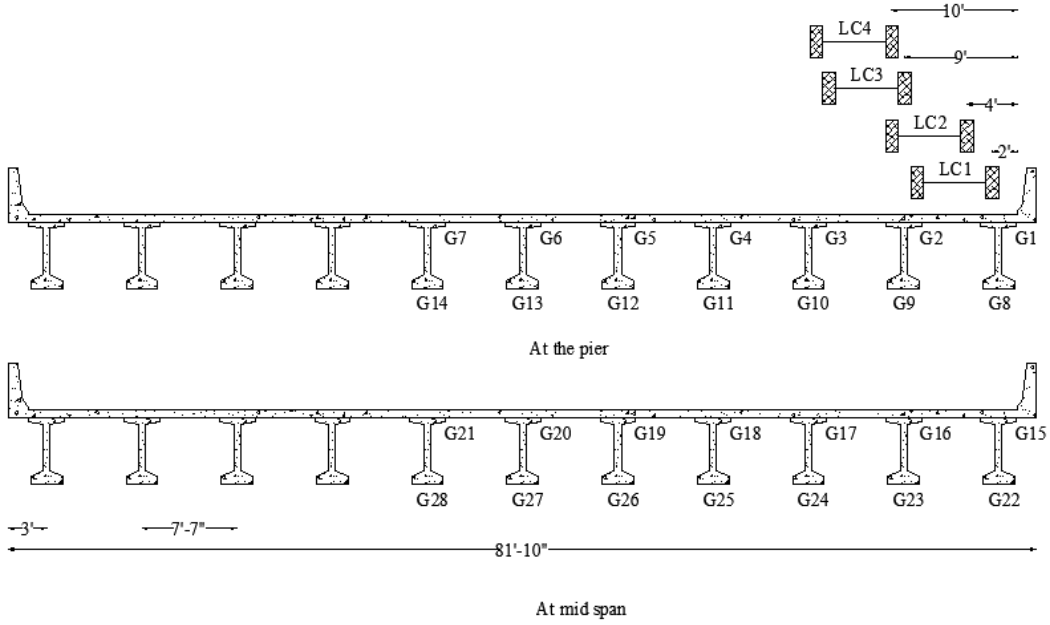

Figure 27. Bridge A instrumentation plan of girder gauges

According to Figure 28, field test results for the gauges at the top flange at the pier and mid-span locations agree with the FEM results. However, strain magnitudes of those gauges are very small.

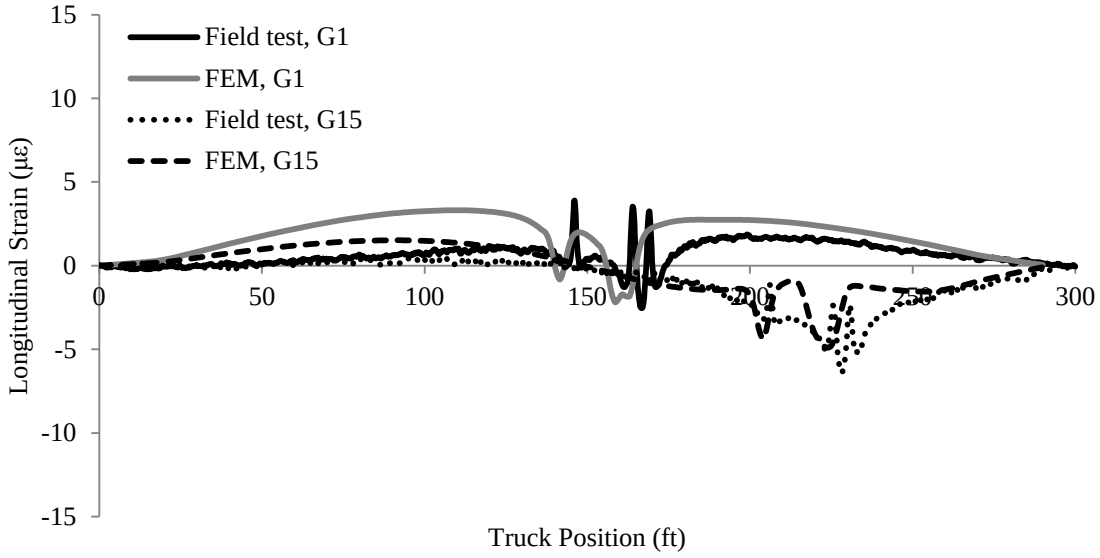

Figure 28. Strain variation of girder gauges (G1 and G15) close to the wheel path, (LC1)

Figure 29 and Figure 30 show the finite element and field test results of girder gauges closer to the truck axles. The pattern of both the finite element and field test results are similar. However, there is a maximum of 30% average strain difference between FEM results and field test results.

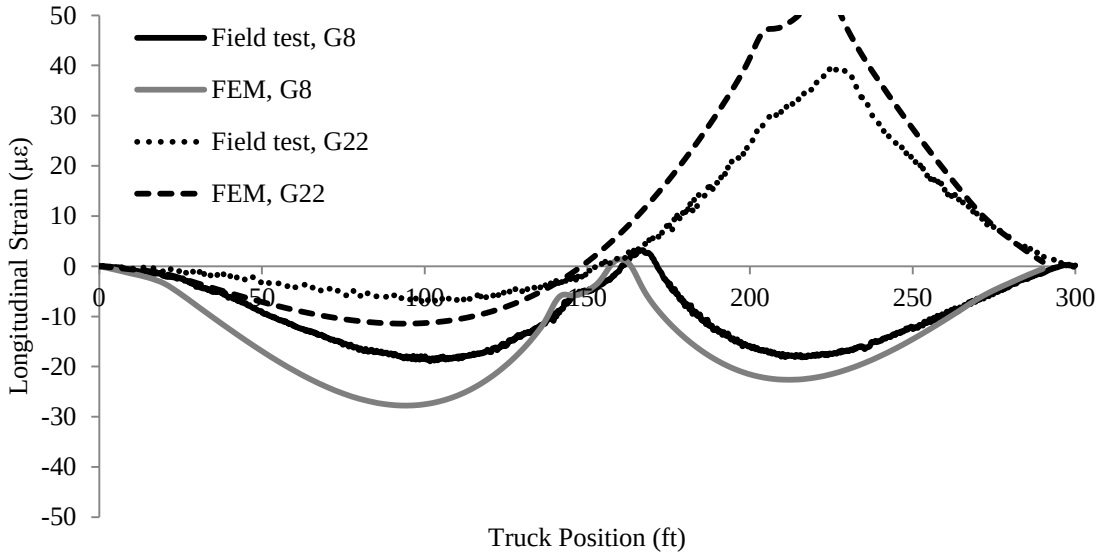

Figure 29. Strain variation of girder gauges (G8 and G22) close to the wheel path, (LC1)

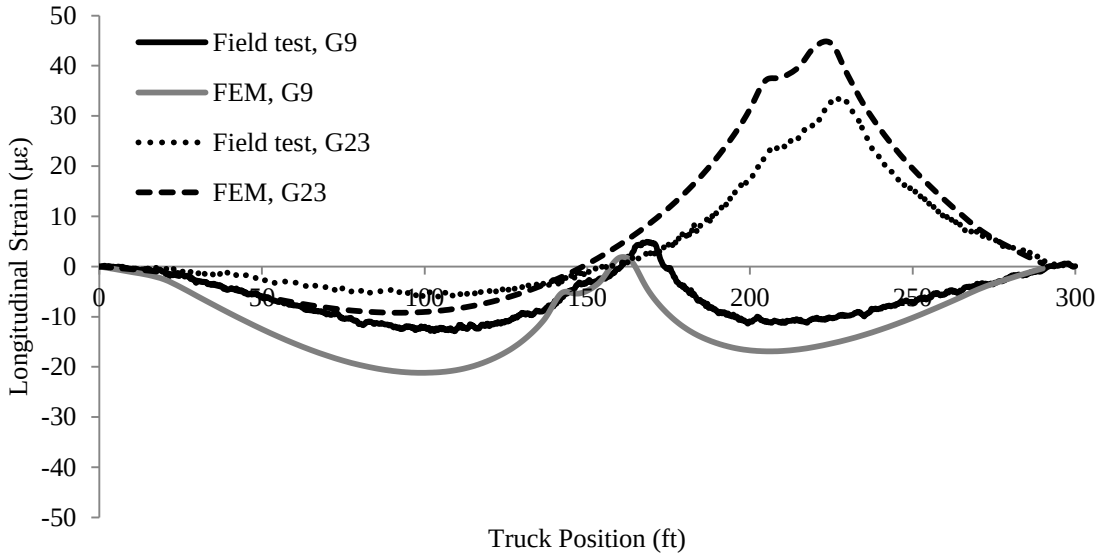

Figure 30. Strain variation of girder gauges (G9 and G23) close to the wheel path, (LC1)

The modulus of elasticity (E) ($57000\sqrt{f'_c}$) of the girders was changed to minimize the percentage strain difference. Figure 31 and Figure 32 show the strain variation of the girder gauge near the pier (G8) and the girder gauge at the mid span (G22), respectively, with various girder f'_c values. These results shows that, with the increase of f'_c and, hence, E of the girders, the strain values approach the field test results.

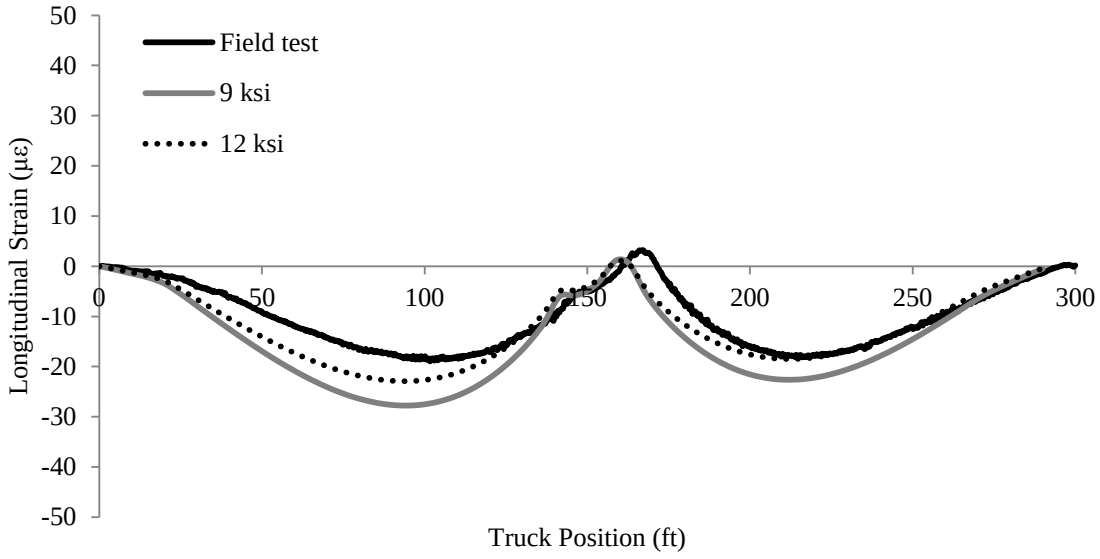

Figure 31. Strain variation of girder gauge G8 with different girder f'_c

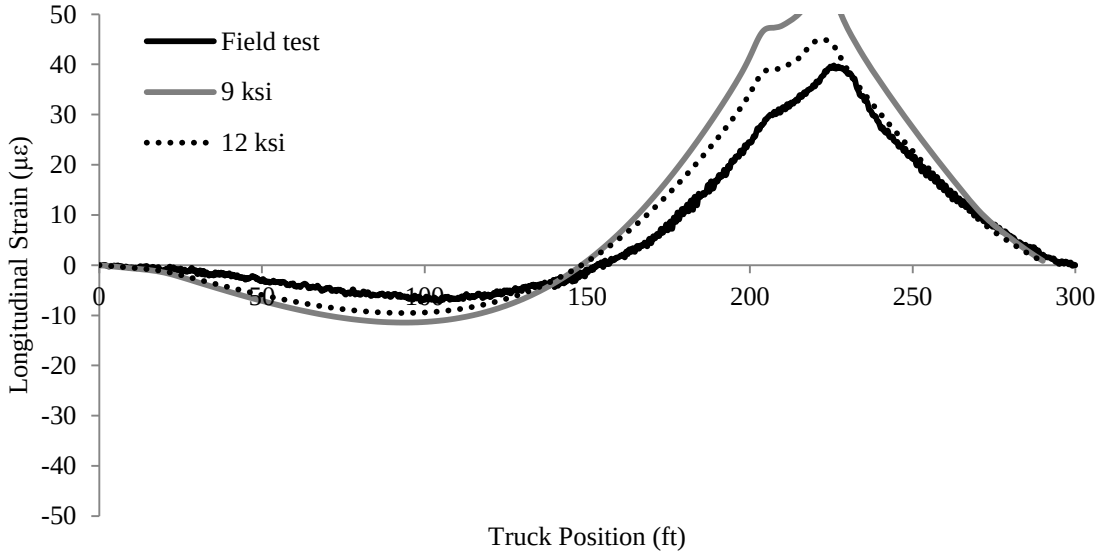

Figure 32. Strain variation of girder gauge G22 with different girder f'_c

Figure 33 and Figure 34 show that the change of the strength and modulus of elasticity of the girder does not significantly affect the strain in the deck.

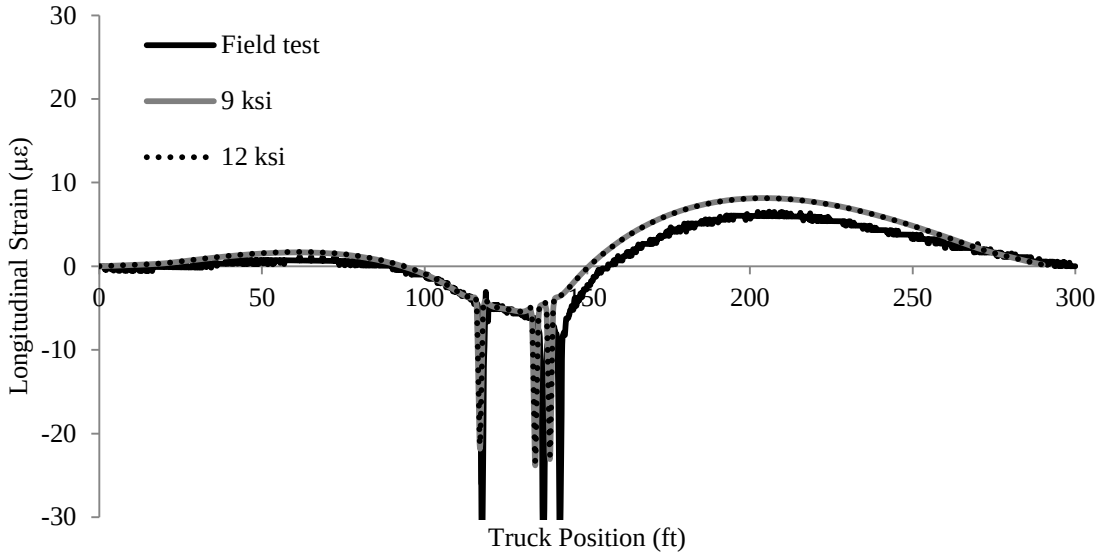

Figure 33. Strain variation of deck gauge G1 with different girder f'_c

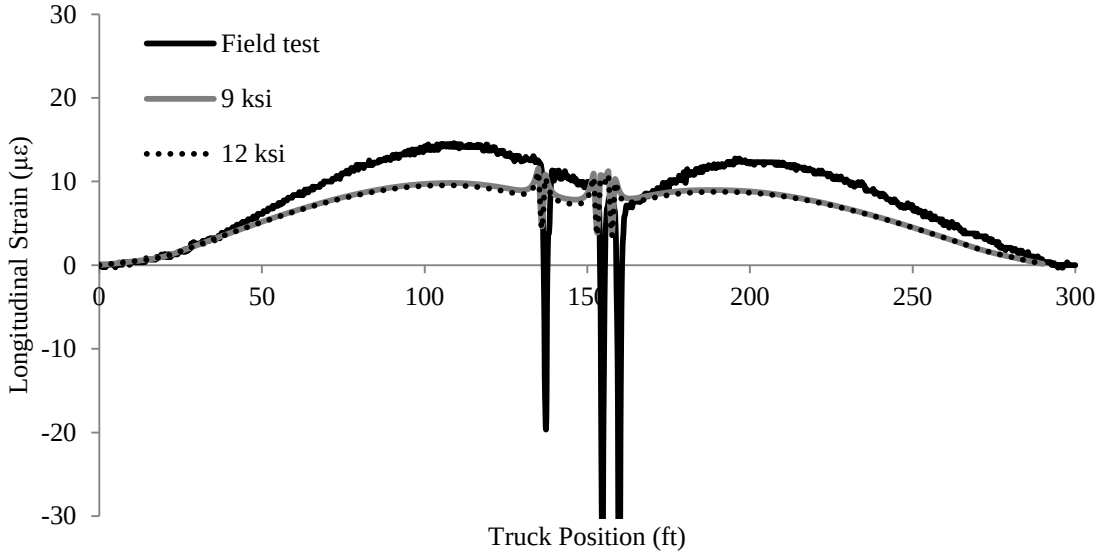

Figure 34. Strain variation of deck gauge G11 with different girder f'_c

Figure 35 shows the variation of the average percentage difference of peak strain with the girder strength. A girder strength of 12 ksi was used for further analysis, which gives about a 23% average difference in the strain peak.

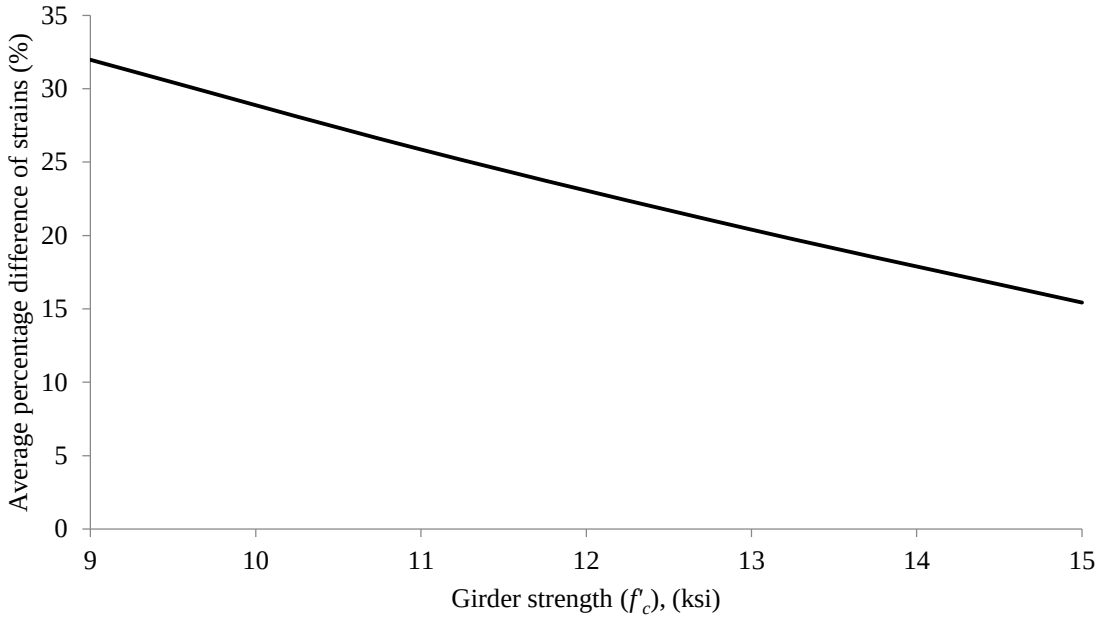

Figure 35. Variation of average % difference with the girder strength

The support conditions at the abutments were changed from rollers (Figure 22) to pinned and fixed conditions in an attempt to further reduce the average percentage difference. Figure 36 and Figure 37 show the strain variation of the girder gauges at the pier and mid-span sections for these different abutment support conditions.

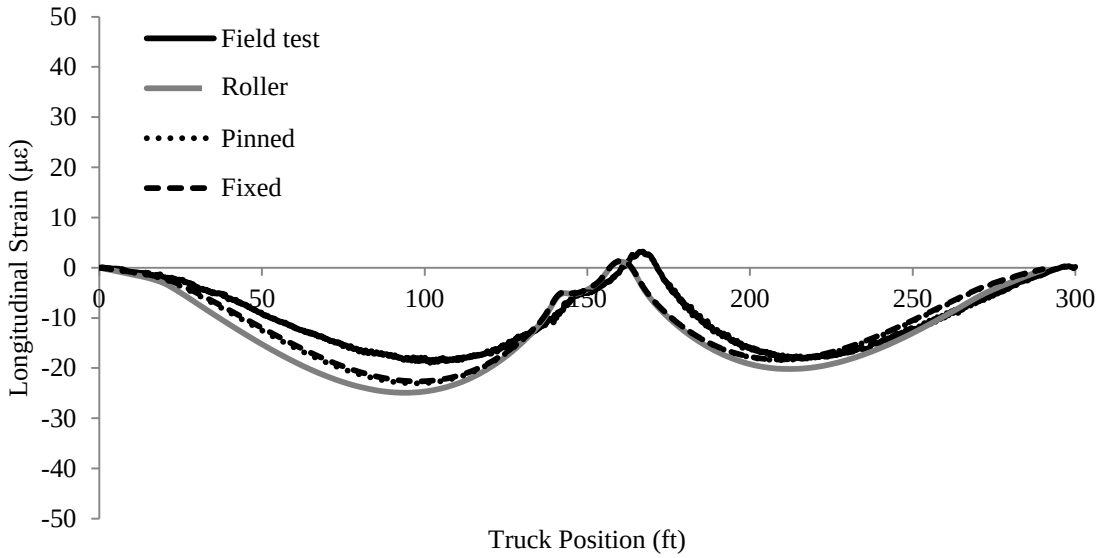

Figure 36. Strain variation of girder gauge G8 with abutment boundary conditions girder $f'_c = 12ksi$

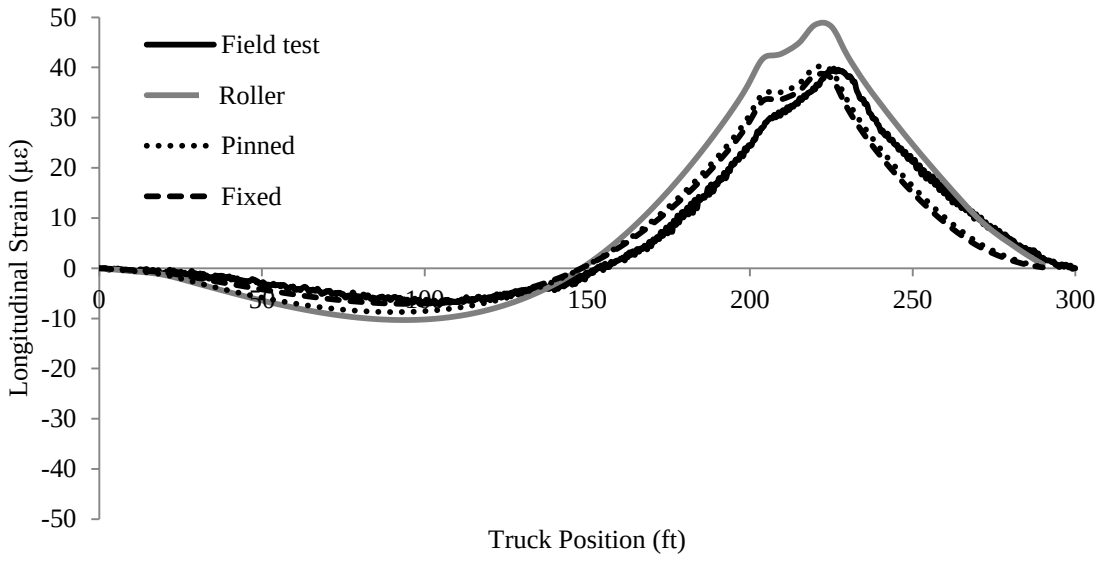

Figure 37. Strain variation of girder gauge G22 with abutment boundary conditions girder $f'_c = 12ksi$

There is no significant difference between the results for the pinned support and the fixed support condition. Both conditions reduce the difference between the FEM results and the field test results.

According to Figure 38, deck strains near the end of the b2 reinforcement do not change significantly with the type of the support conditions at the abutments.

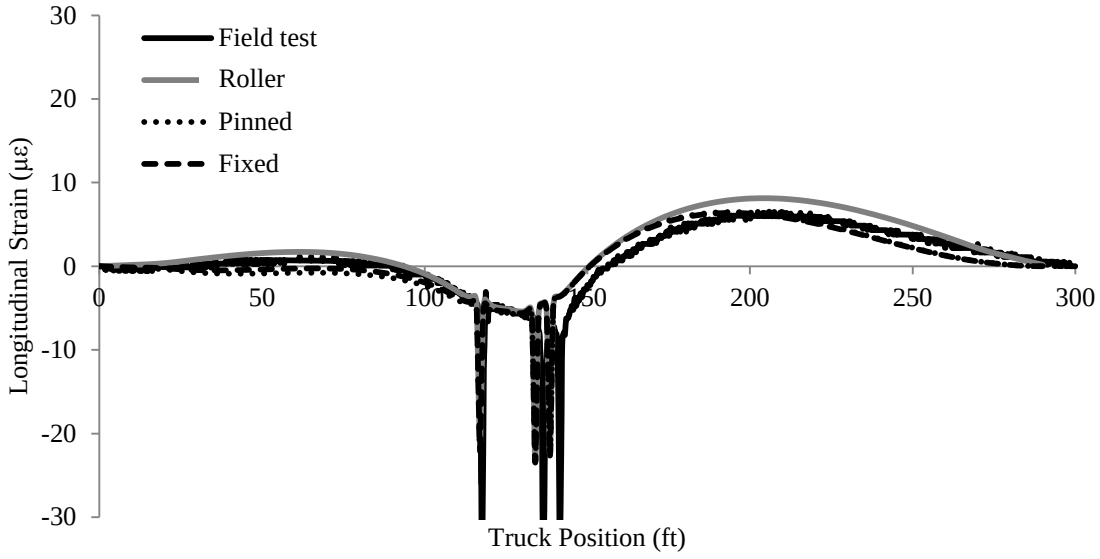

Figure 38. Strain variation of deck gauge G1 with abutment boundary conditions girder $f_c' = 12ksi$

Figure 39 shows that a change of support condition at the abutment affects the deck strains around the pier.

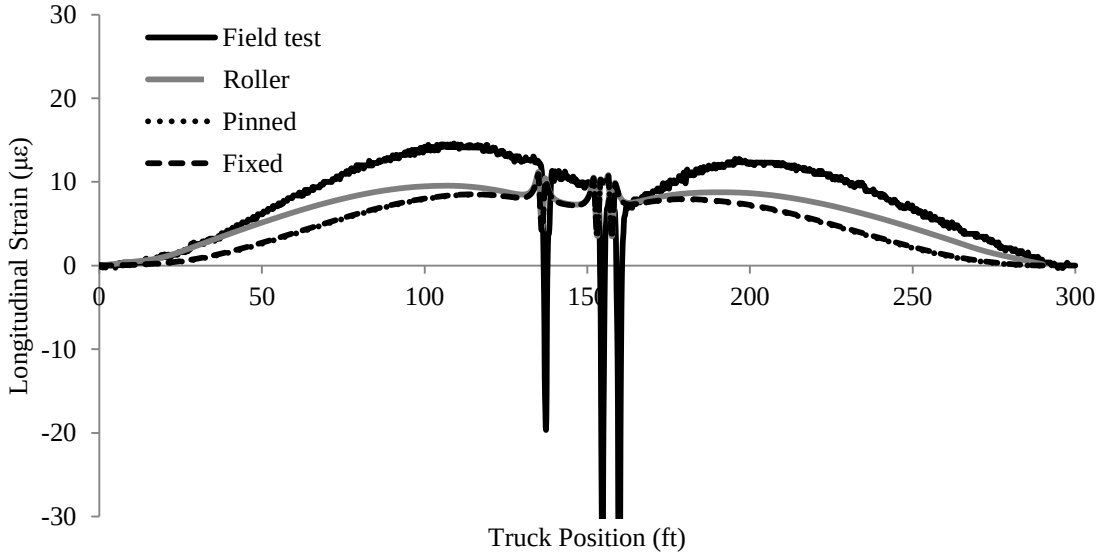

Figure 39. Strain variation of deck gauge G11 with abutment boundary conditions girder $f_c' = 12ksi$

A summary of the calibration results is shown in Table 5.

Table 5. Summary of calibration results

	f'_c of the girders (ksi)	Average error percentage (based on girder gauges) (%)	Average error percentage (based on deck gauges) (%)	Boundary conditions	
				Restraint at the abutment (on piles)	Restraint at the pier (under the girders)
1	9	30	-	Roller	Roller
2	11	25	-	Roller	Roller
3	13	20	-	Roller	Roller
4	15	15	-	Roller	Roller
5	12	25	10	Roller	Roller
6	12	10	10	Pinned	Roller
7	12	10	15	Fixed	Roller

According to these results, Case 6 shows an average of 10% strain difference between the FEM and field test results for both deck and girder gauges. Therefore, Case 6 was selected as the general type of model to be used in the next steps of the research.

4.2.7.3 Calibration for the Rosettes

Comparisons were made between the FEM and field test results of the major principal strains (ε_1) calculated from the rosettes (Figure 40).

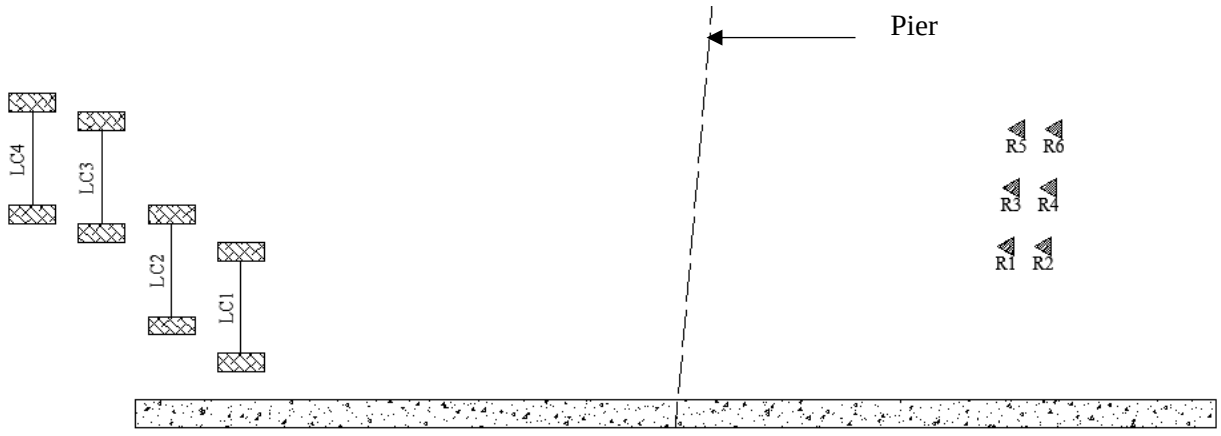

Figure 40. Bridge A instrumentation plan of rosettes

According to Figure 41 and Figure 42, a significant difference between the FEM and field test results for the principal strains can be observed up to the 150 ft truck position. Elsewhere, the finite element results reasonably predict the field test behavior.

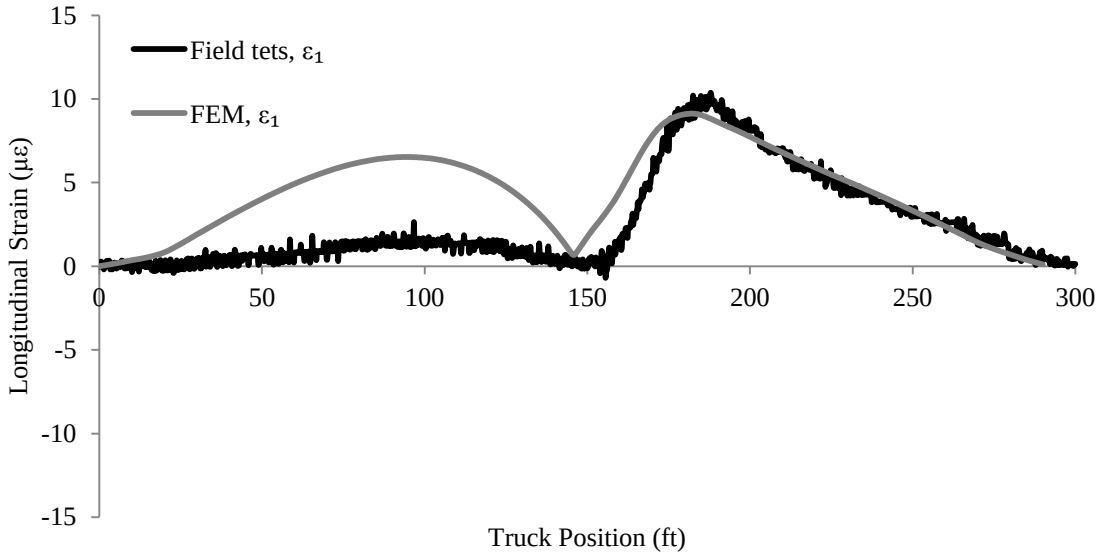

Figure 41. Variation of principal strains of rosette R5 for LC1

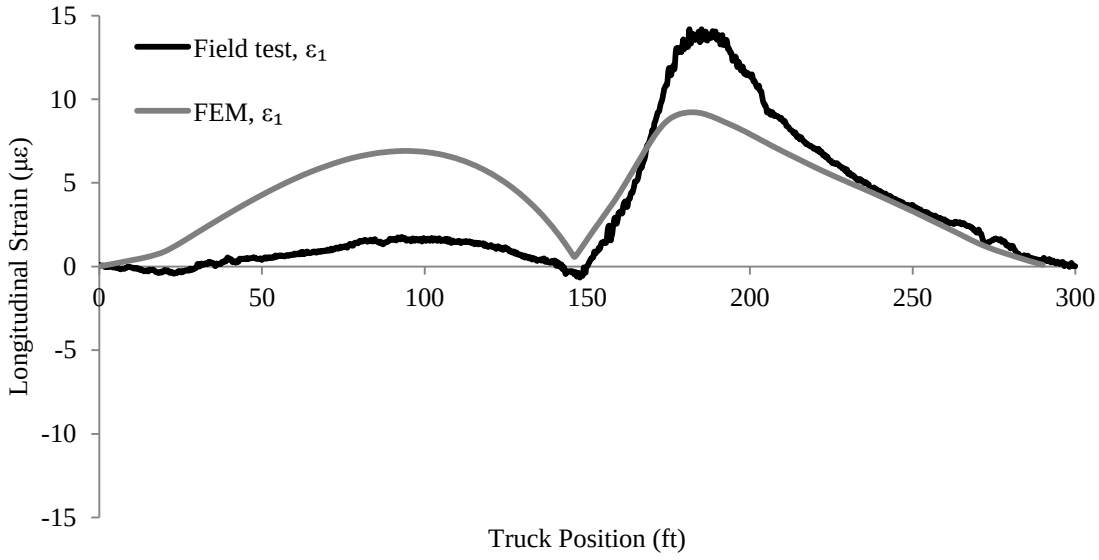

Figure 42. Variation of principal strains of rosette R6 for LC1

4.2.8 Comparison of Cracking Strain with Field Cracks

The finite element analysis results were also compared with cracks observed during the field inspection by the Bridge Engineering Center (BEC) staff and previously completed bridge inspections.

4.2.8.1 Crack Map

Five significant transverse cracks, C1 through C5, were found on the bridge deck through field inspection (Figure 43).

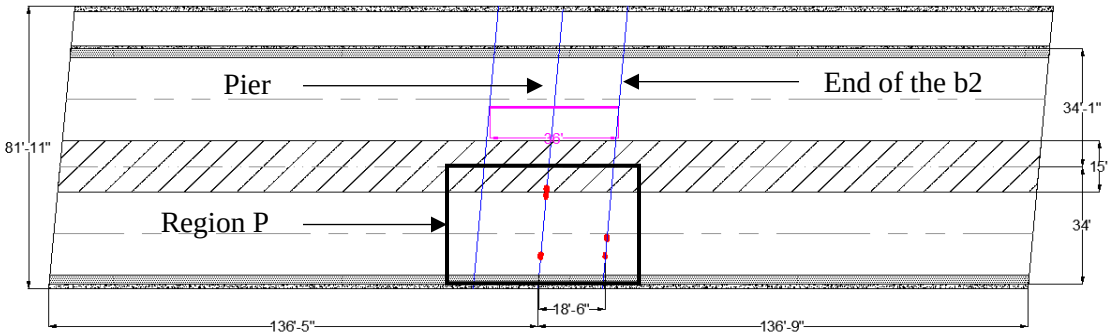

(a) Plan view

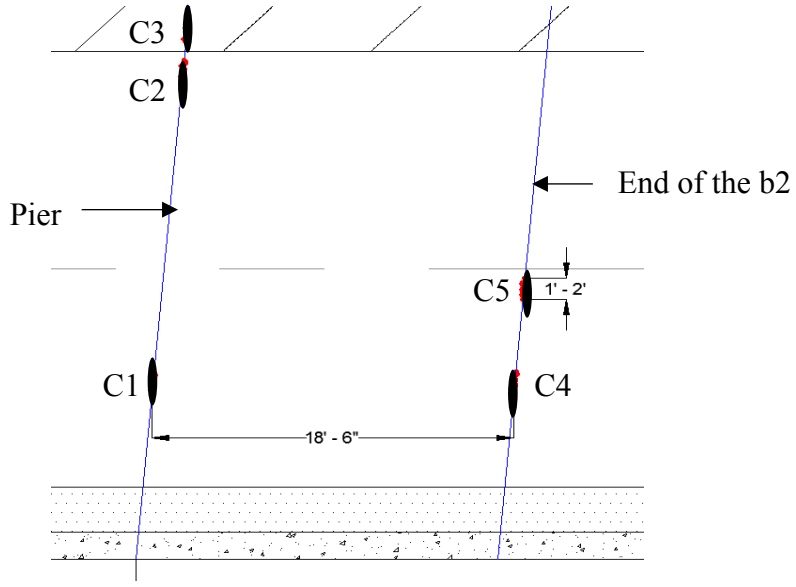

(b) Region P

Figure 43. Crack map

The Bridge Condition Report from 2010 indicated only one transverse crack (C3) on the bridge deck. The Bridge Condition Report from 2012 described the same crack with no other cracks having been reported.

4.2.8.2 Comparison with Live Load Strains

The following relationship can be used to calculate the approximate cracking strain of concrete.

$$\text{Cracking strain of the concrete} = \frac{7.5\sqrt{f'_c}}{57000\sqrt{f'_c}} \approx 130\mu\epsilon \quad \textbf{(5)}$$

The truck used during the field test (Figure 8) was not large enough to generate strains in the bridge deck that would causing cracking of the deck. Therefore, a large truck load, HS20, was used to continue the basic deck cracking study (Figure 44).

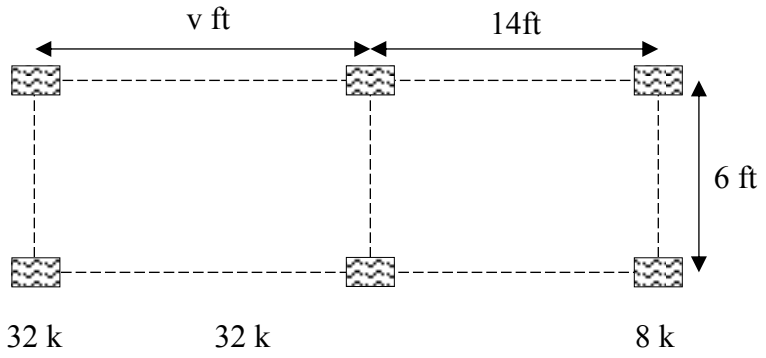

Figure 44. Details of the HS20 truck loading

The HS20 design truck load consists of variable distances (v) between the rear axles, which can vary from 14 ft to 30 ft. An HS20 truck with v equal to 14 ft and 30 ft was run along Lane#1 and Lane#2 to investigate the resulting strain magnitudes. Figure 45 and Figure 46 show typical major principal strain for locations at the end of the b2 reinforcement and over the pier.

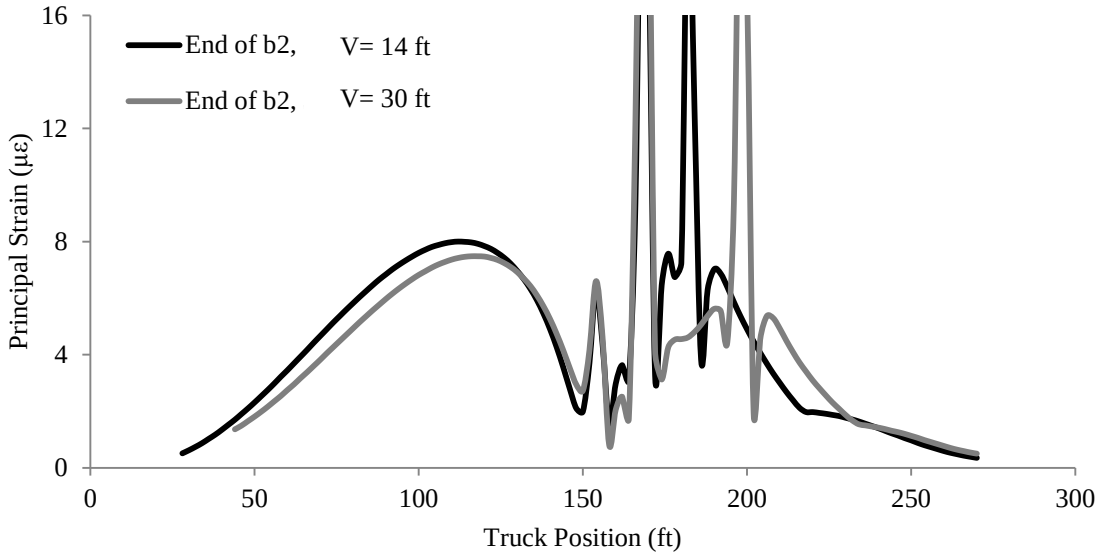

Figure 45. Typical variation of ε_1 strain for truck in Lane1, end of the b2 reinforcement

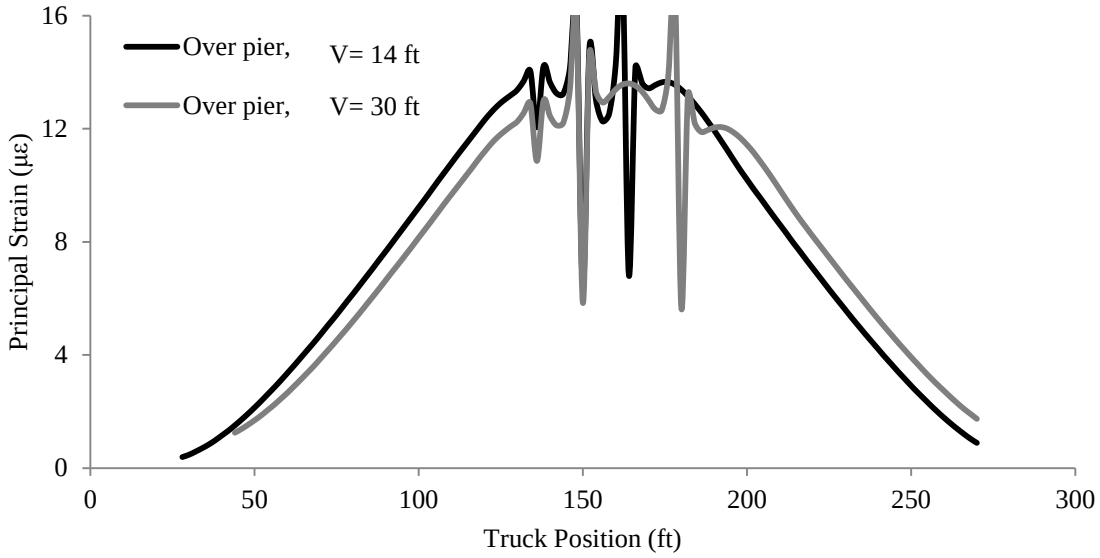

Figure 46. Typical variation of ε_1 strain for truck in Lane1, at the pier

The HS20 truck with 14 ft axle spacing induces larger strains than the HS20 truck with 30 ft axle spacing, but well less than the cracking strain.

Eight trucks were placed at 112 ft and 196 ft front axle positions on Lane #1 to Lane #4 in an attempt to induce large strains.

Strain in the bridge deck was large at the locations of concentrated forces of the truck axles, causing local stress concentrations that were not the focus of this project. These fictitious large strains would sometimes mask the strains of importance to this study. Therefore, a uniform distributed load (UDL) of 0.0004 ksi, somewhat equivalent to eight HS20 trucks, was applied to avoid these stress concentrations. The deck strain in the longitudinal direction (Z direction) (ε_Z), over the pier and at the 1/8 of the span length location, from the eight HS20 truck loadings are compared to the results from the equivalent UDL in Figure 47.

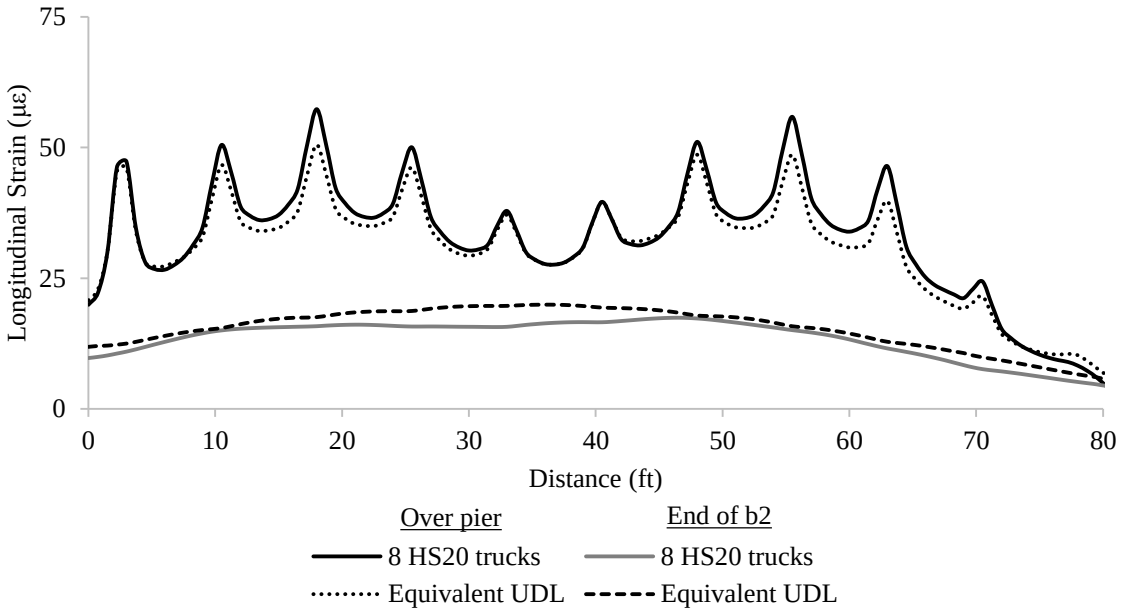

Figure 47. Strain (ε_Z) due to equivalent eight HS20 truck loads

Figure 48 illustrates the major principal strain distribution of Region P (Figure 43), which shows that the finite element analysis predicts no cracking strains at the field crack locations with equivalent UDL.

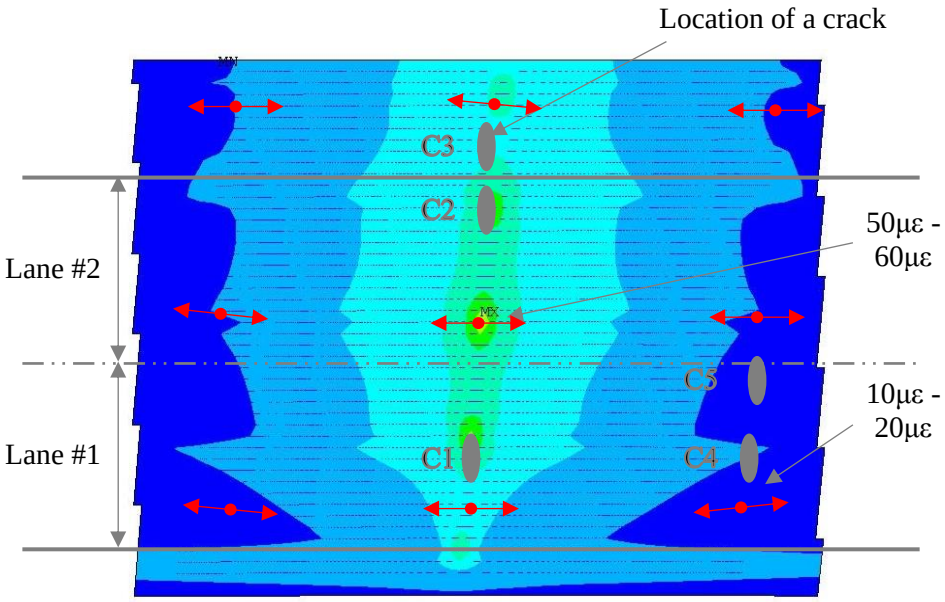

Figure 48. Major principal strain magnitude and direction around Region P, equivalent UDL

4.2.8.3 Comparison with Temperature Load

Cold weather conditions generate tensile stresses over the intermediate supports. A -80°F temperature difference assuming 60°F construction temperature and -20°F cold weather conditions was applied to the model to investigate cracking due to the temperature. The strains induced by the cold temperature were not large enough to simulate the cracking strain on the bridge deck (Figure 49).

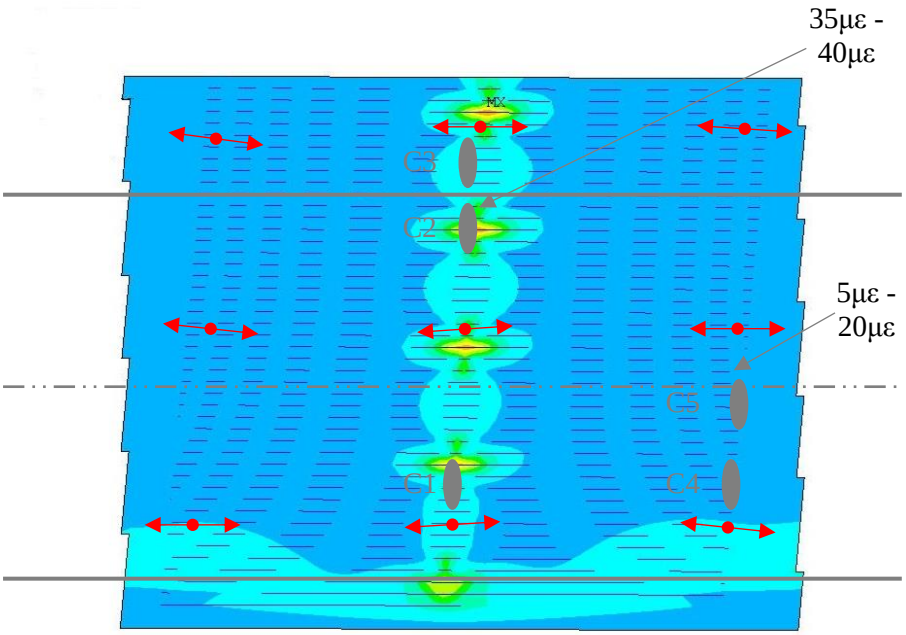

Figure 49. Major principal strain magnitude and direction around Region P due to cold weather

For the temperature and shrinkage loading, the b1 bars were assumed to shrink since they are smeared into the concrete. However, the b2 reinforcement was not allowed to shrink.

4.2.8.4 Comparison with Shrinkage Load

According to literature, about half of the shrinkage of concrete decks takes place during the 56 days following deck placement. Thus, shrinkage strain at 56-days was applied only to the bridge deck. To calculate the shrinkage strain, the following relationship given in the AASHTO LRFD specification was used (AASHTO 5.4.2.3.3-1).

$$(\in_{sh})_t = -k_s k_h \left(\frac{t}{35+t}\right) \times 0.51 \times 10^{-3} = \text{-0.000134} \quad \textbf{(6)}$$

Where:
$(\in_{sh})_t$ = shrinkage strain at time t (56 days)
k_s = Size factor (0.46)
k_h = Humidity factor (0.93)

AASHTO equation C5.4.2.3.3-1 was used to calculate the size factor ks. The volume/surface ratio (V/S) of the deck is used in this equation is the ratio of the total deck volume to the total deck surface area (3.96). AASHTO equation C5.4.2.3.3-2 was used to calculate factor kh by assuming 75% humidity. Finally, the calculated shrinkage strain was applied to the model as an equivalent temperature, which was calculated using Equation 7.

$$T_{equ} = {(\in_{sh})_t}/{\alpha} = \text{-}24.5°\text{F} \quad \textbf{(7)}$$

Where:
T_{equ} = equivalent temperature
α = Coefficient of thermal expansion (0.0000055/°F)

According to Figure 50, the 56-days of shrinkage load does simulate the transverse cracks of the bridge deck, because concrete strains are in the vicinity of the cracking strain.

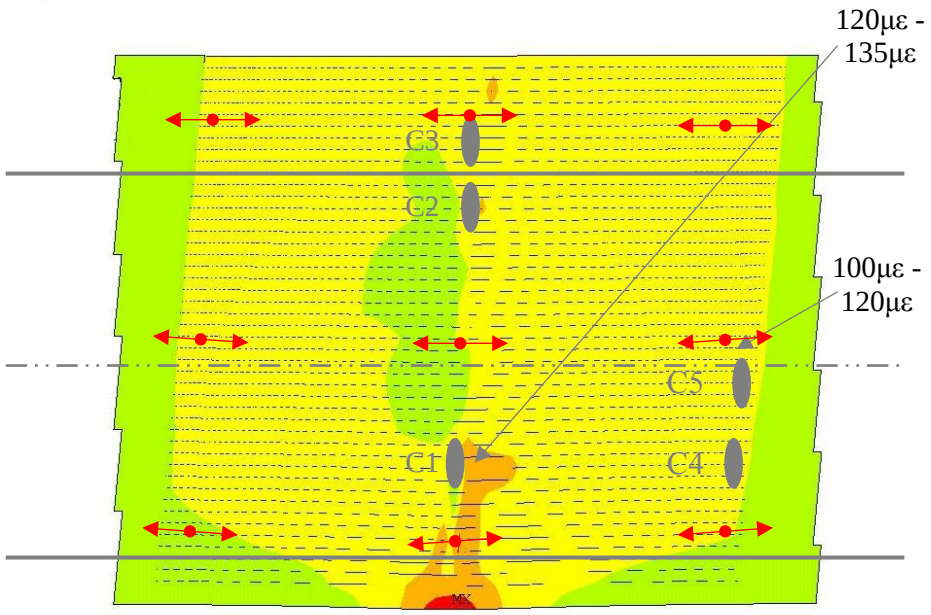

Figure 50. Major principal strain magnitude and direction around Region P due to shrinkage after 56 days

4.3 Finite Element Model of Bridge B

The major difference between Bridge A and Bridge B is that Bridge B has a larger skew angle (42 degrees) than Bridge A (5 degrees). Some other minor differences between these two bridges are listed in Table 6.

Table 6. Comparisons of the properties of Bridge A and Bridge B

Properties	Bridge A	Bridge B
Skew angle (deg)	5	42
Span (ft)	136	156
Girder height (in.)	54	63
Average b2 reinforcement spacing (in.)	9	6
Length of the b2 reinforcement (ft)	36	38
Total b2 reinforcement (in^2/in)	0.140	0.187
Total deck reinforcement (in^2/in)	0.205	0.252

The goal of the Bridge B analysis was to evaluate the influence of skew on the negative moment region behavior in PPCB. The finite element model of Bridge B was developed in a manner similar to that for the finite element model of Bridge A. Figure 51 shows a plan view of the finite element model of Bridge B. The deck of Bridge B was modeled with 6-in. (Z direction) by 6-in. (X direction) shell elements.

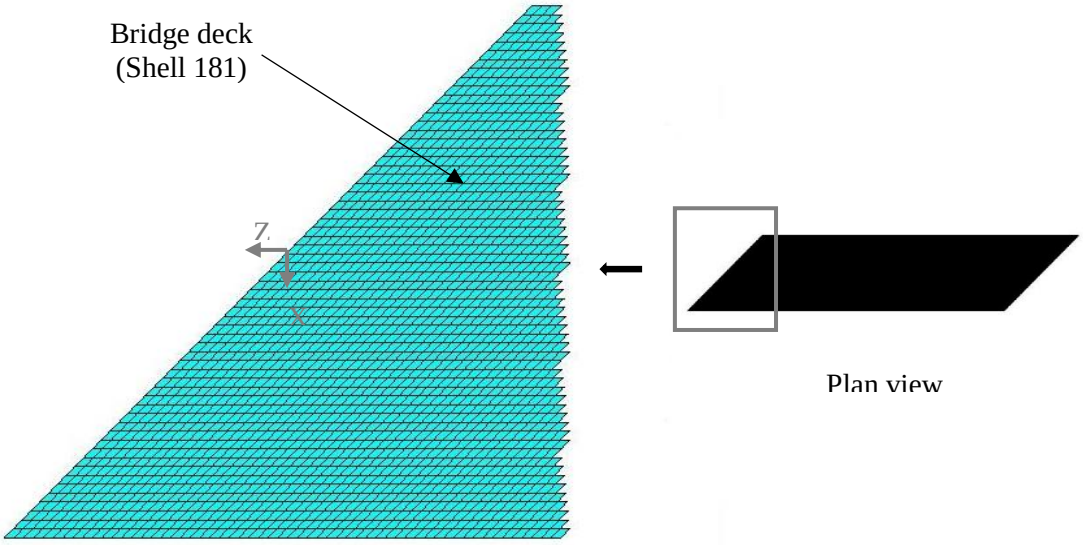

Figure 51. Finite element model of the Bridge B: Plan view

Whereas, Bridge A has one b2 reinforcement layer (Figure 18), Bridge B has two b2 reinforcement layers: one layer above and one below the middle of the deck thickness. However, both b2 reinforcement layers are very close to the mid-depth of the deck. As a result, both b2 reinforcement layers were modeled as one b2 reinforcement layer located at the centroid of the concrete deck.

The live load calibration results of Bridge A were used to establish the initial conditions for Bridge B. As mentioned in Case 6 (Table 5), pinned supports at the abutments and roller supports at the pier were also used as the support conditions of Bridge B. The strength of the girders was as assumed to be 12 ksi, as it was for Bridge A.

4.3.1 Calibration of Bridge B

4.3.1.1 Calibration for the Deck Gauges

Typical calibration results of the deck gauges of Bridge B are presented in this section for deck gauges G1, G 15, G5, and G19 for LC1 (Figure 52).

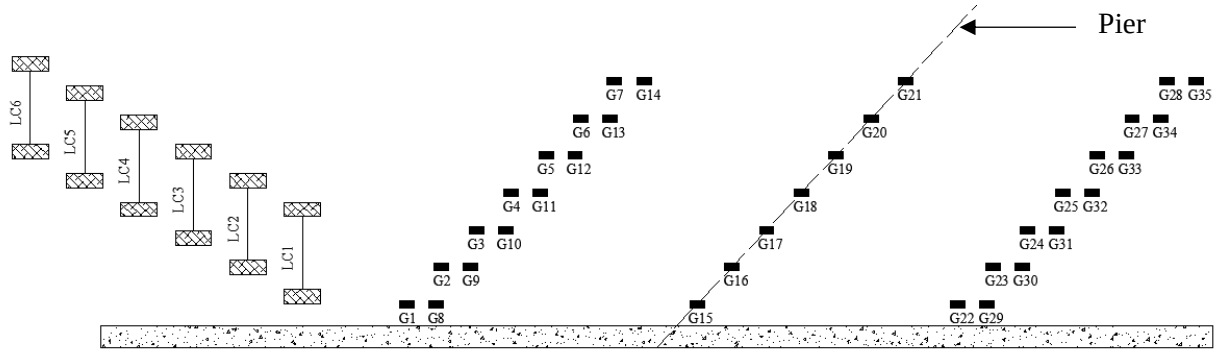

Figure 52. Bridge B instrument plan of deck gauges

Figure 53 shows typical strain comparisons for strain sensors located near the truck load (i.e., G1 and G15).

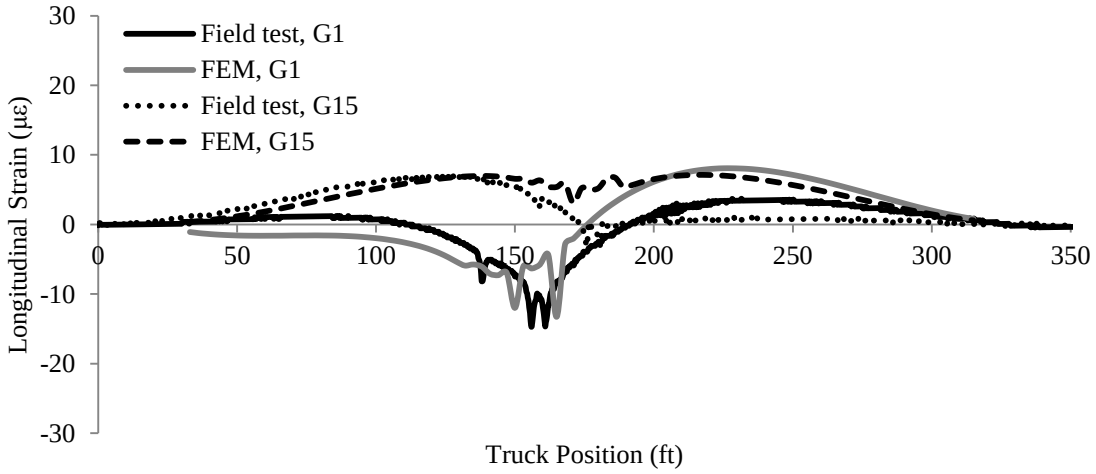

Figure 53. Strain variation of deck gauges (G1 and G15) closer to axles, (LC1)

Figure 54 shows similar comparisons for strain sensors located away from the truck load. In general there were very small differences between the fields collected data and the analytical predictions.

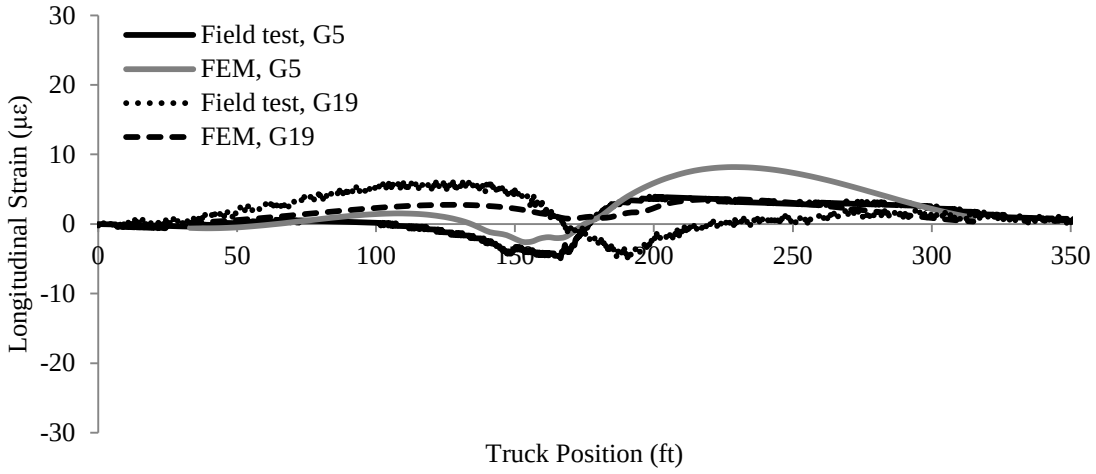

Figure 54. Strain variation of deck gauges (G5 and G19) away from axles, (LC1)

4.3.1.2 Calibration for the Girder Gauges

Analytical and field test results for several of the Bridge B girder gauges (Figure 55) are presented in Figure 56 and Figure 57.

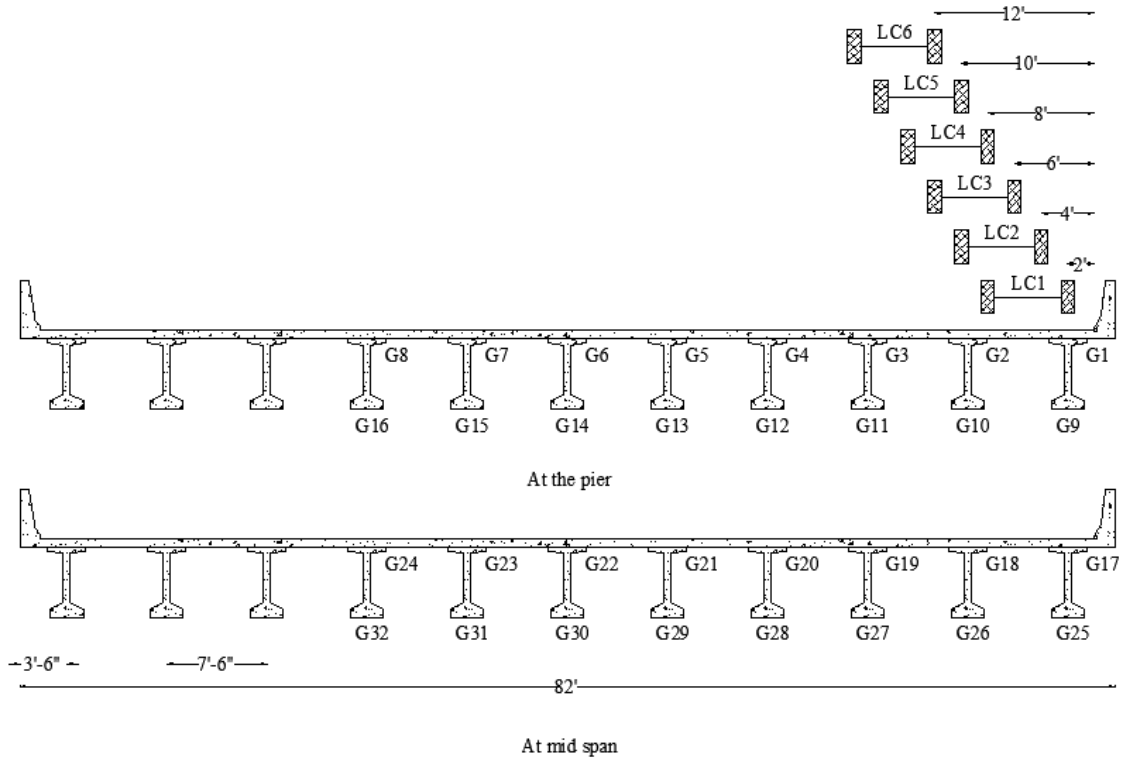

Figure 55. Bridge B instrument plan of girder gauges

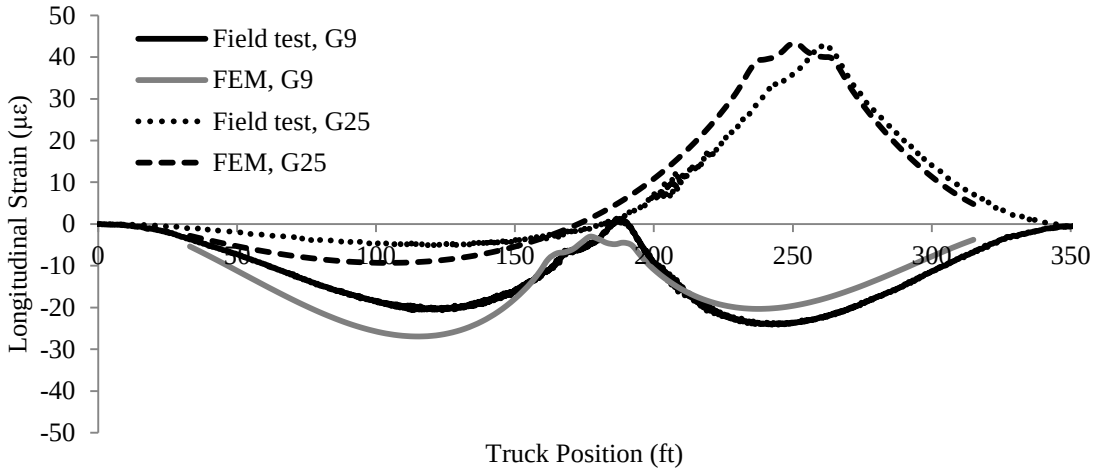

Figure 56. Strain variation of girder gauges (G9 and G25) closer to axles, (LC1)

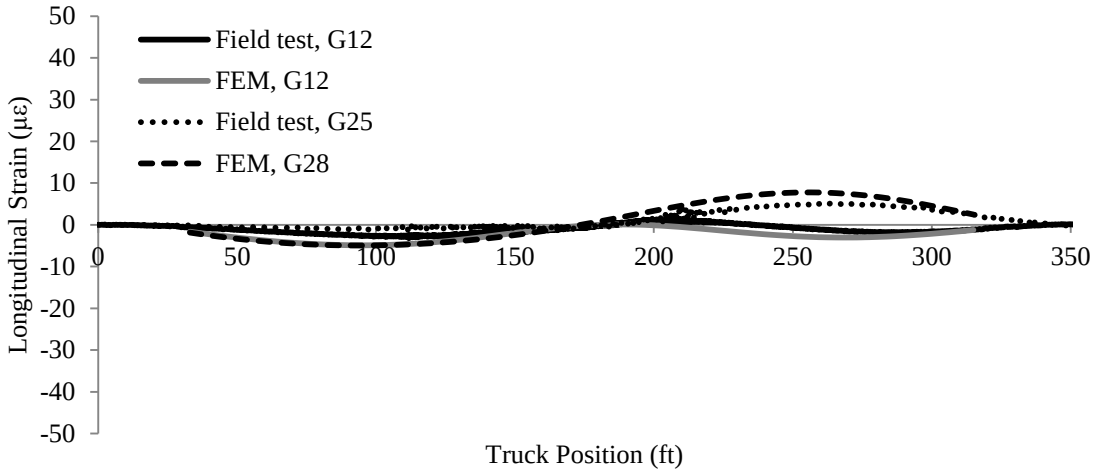

Figure 57. Strain variation of girder gauges (G12 and G28) away from axles, (LC1)

These results show the strain comparisons of girder gauges close to the truck axles and away from the truck axles, respectively. As can be seen, the finite element results are generally in good agreement with the field test results.

4.3.1.3 Calibration for the Rosettes

Comparisons were made between the FEM and the major principal strains (ε_1) determined from field test results (Figure 58).

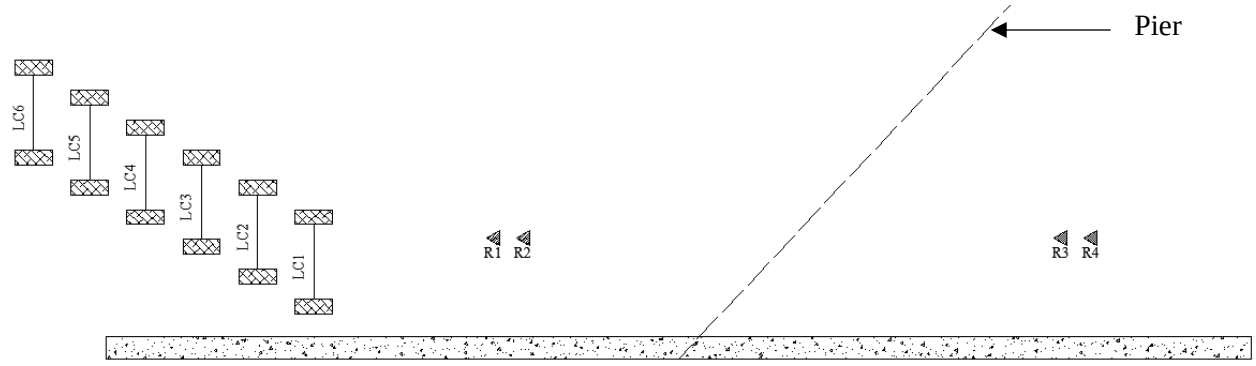

Figure 58. Bridge B instrument plan of rosettes

According to Figure 59, there is a significant difference between the FEM and field test results of the principal strains around the pier may be due to the local effects. Other than that, the finite element model predicts the field test results of the rosettes.

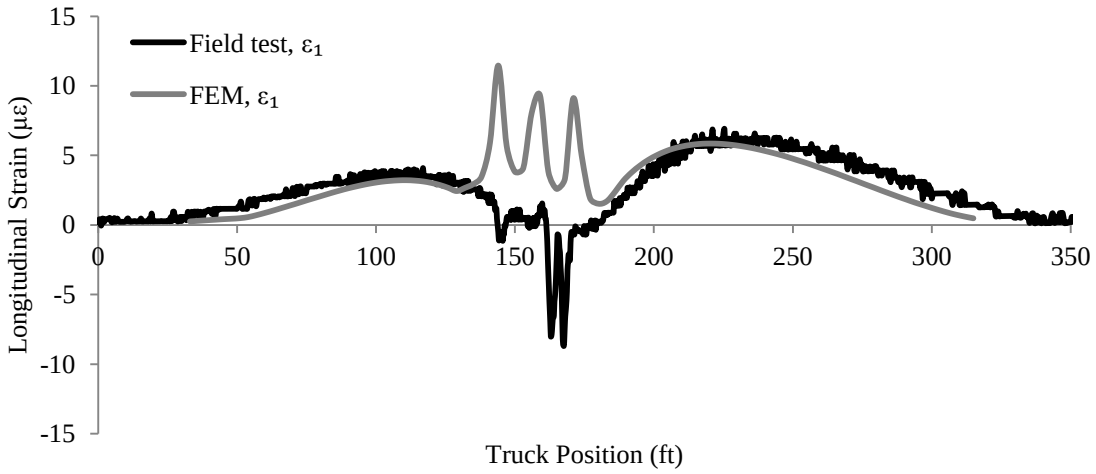

Figure 59. Variation of principal strains of rosette R2 for LC1

Collectively the above-mentioned results for Bridge B show that the deck gauges had small differences and the girder gauges were in agreement with the field test results. However, in an attempt to further minimize the differences three types (Table 7) were studied.

Table 7. Calibration types of Bridge B

Type	f'_c of the deck (ksi)	Boundary conditions	
		Restraint at the abutment (on piles)	Restraint at the pier (under the girders)
1	4	Pinned	Roller
2	5	Pinned	Roller
3	4	Fixed	Roller

Figure 60 shows the comparison of the finite element results of gauge G1 for the different calibration types. No significant strain difference can be observed. Therefore, Type 1 was selected for use in the parametric study of Bridge B.

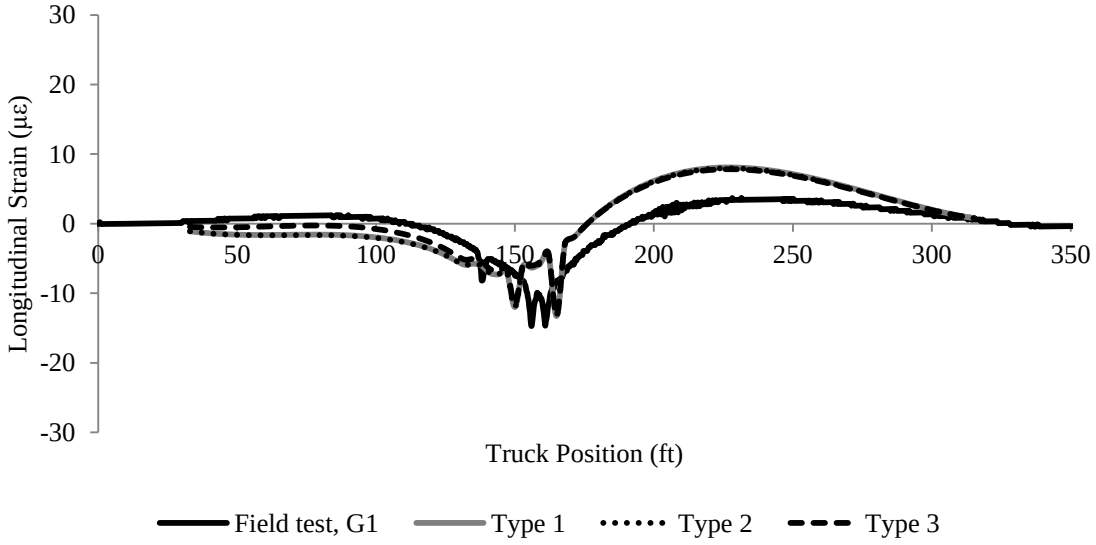

Figure 60. Strain variation of girder gauge G1 with different calibration types

5 PARAMETRIC STUDIES

5.1 Model Configuration

The main objective of this research project was to investigate various aspects of the b2 reinforcement used in the negative moment region of PPCB bridges. To accomplish this, parametric studies were conducted using the basic models described previously.

To understand the behavior of the bridge in multiple states, three different model configurations were utilized: Model 1 - Uncracked Deck, Model 2 - Cracked Deck, and Model 3 - Cracked Deck with Cracked Pier Diaphragm. In many ways, these three models were interpretations of how several states of behavior could be translated into a theoretical design model.

5.1.1 Model 1 - Uncracked Deck

The parametric studies were first conducted on the calibrated bridge models, which consist of fully uncracked section properties. In many ways, the Model 1 configuration is based upon the field-observed behavior (e.g., minimal deck cracking, etc.) and based upon previously observed behavior in other similar bridges. Within the following sections for Model 2 and Model 3, we provide a detailed summary of the results associated with Model 1.

Briefly, based on the parametric study results of Bridge A for both a live load and a 56-day shrinkage load with an uncracked deck model, we can conclude that negative moment b2 reinforcement does not significantly affect the behavior of the bridge deck before cracking. This is because the negative moment b2 reinforcement represents a very small contribution to the overall stiffness of the uncracked concrete deck. As a result, the parametric study was continued by assuming a fully cracked deck (Model 2) in the negative moment region.

5.1.2 Model 2 - Cracked Deck

The goal with Model 2 was to accentuate the contribution of the b2 bars by reducing the stiffness of the surrounding deck concrete to zero (i.e., a fully cracked state). The length, area, and distribution pattern of the b2 reinforcement were the main parameters of the study.

The parametric study with a cracked deck over the pier (Figure 61) was conducted following the steps shown in Figure 62. A parametric study was carried out for both a live load and a 56-day shrinkage load.

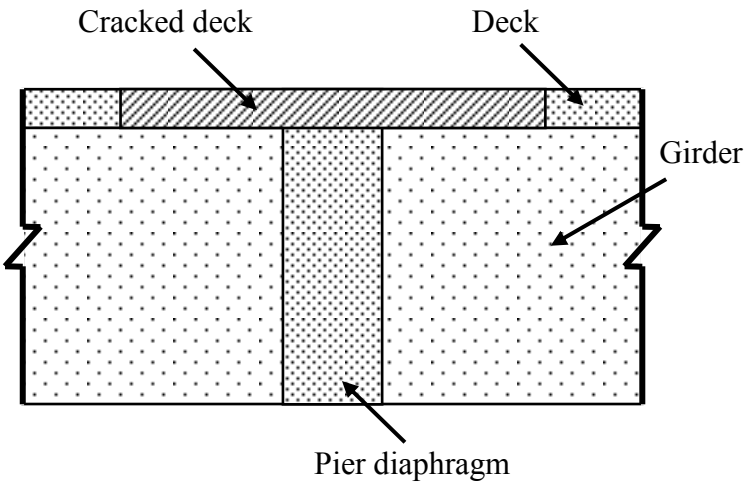

Figure 61. Cracked deck condition

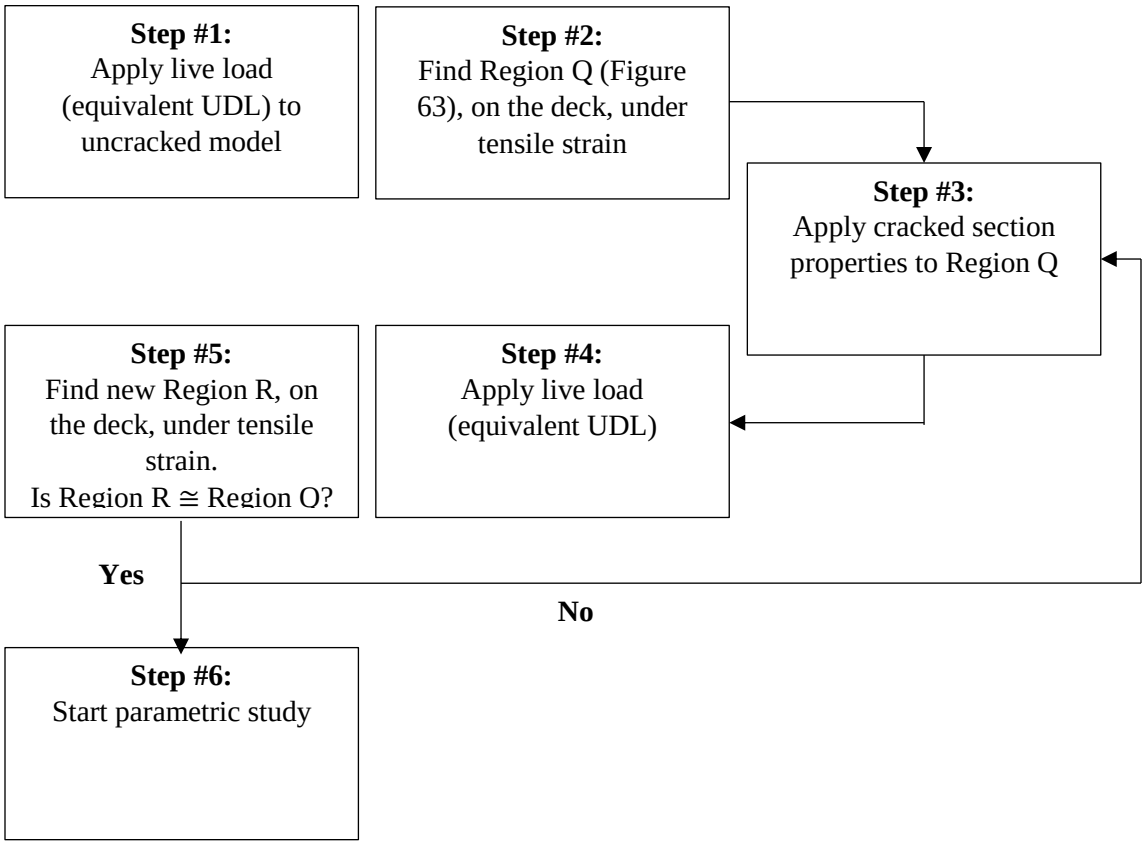

Figure 62. Method to determine cracked section of Model 2

Step 1:

The equivalent UDL of 0.0004 ksi over the four lanes was used to determine the region of the deck that experiences tensile strains.

Step 2:

The longitudinal strain (ε_Z) of the bridge deck along five longitudinal lines is shown in Figure 63, illustrating that (Region Q) the deck, under tensile strain was approximately 30 ft on each side of the pier.

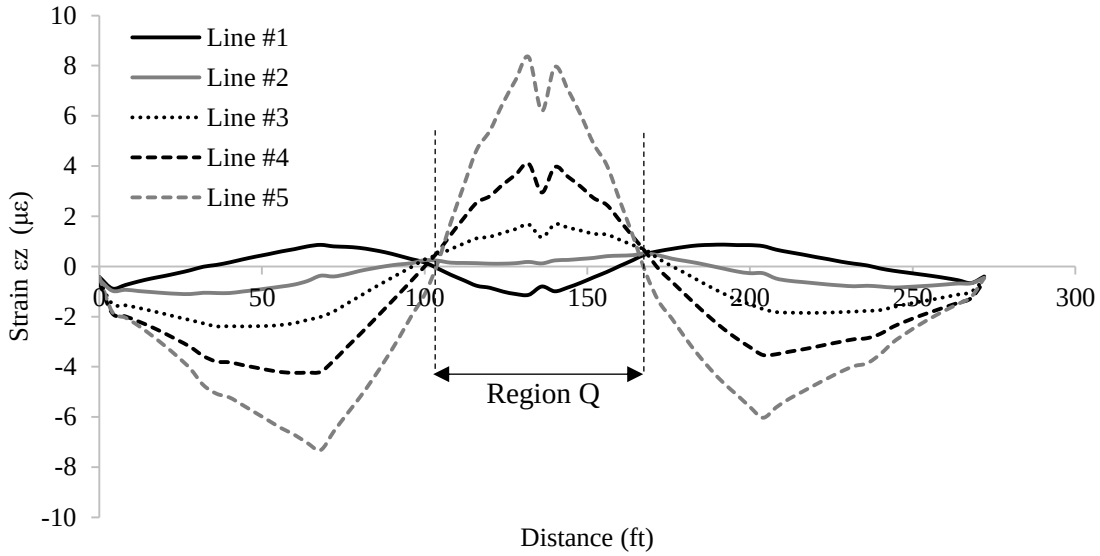

Figure 63. Negative moment region over pier

Step 3:

The effective moment of inertia of the uncracked bridge deck ($I_{Uncracked}$) and cracked deck ($I_{Cracked}$) was then calculated. The modulus of elasticity (E) of the uncracked bridge deck finite elements was proportioned by the $I_{Cracked}/I_{Uncracked}$ ratio (0.006) to calculate the cracked section properties for Region Q.

Step 4:

The equivalent UDL of 0.0004 ksi was again placed on the model with the updated cracked section properties in Region Q.

Step 5:

The negative bending moment region with cracked section properties (Region R) was found to be approximately equal to the negative bending moment region with uncracked section properties (Region Q), about 30 ft to each side of the pier. Thus, it was determined that the Region Q approximation was acceptable.

Step 6:

A parametric study of Bridge A with the cracked deck in Region Q was then conducted.

5.1.3 Model 3 - Cracked Deck with Cracked Pier Diaphragm

Following discussions with the Iowa DOT, it was determined that the Iowa DOT designs the continuity connection at the pier diaphragm by assuming a fully cracked deck and diaphragm (i.e., the girders resist no tension). Therefore, a cracked deck with a cracked pier diaphragm at the pier was studied to simulate the conditions assumed for design (Figure 64). It was assumed that the diaphragm had cracked to more than 1/2 of the total girder depth.

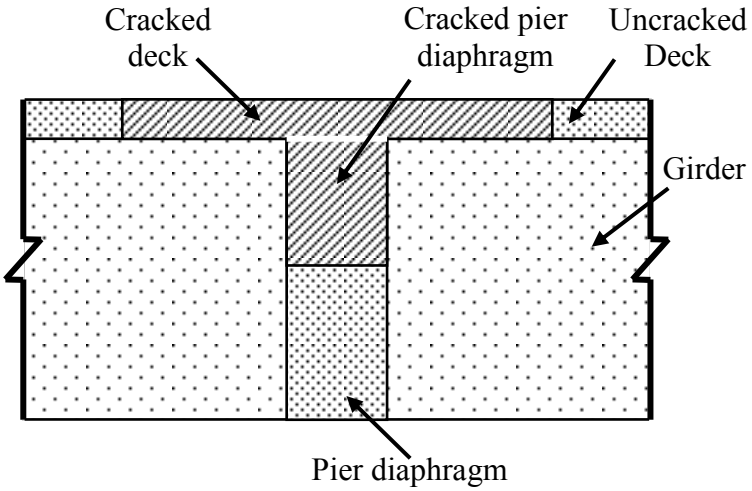

Figure 64. Uncracked deck condition

5.2 Parametric Studies of Bridge A

Parametric studies were conducted with live load (equivalent UDL, Chapter 4) and a 56-day shrinkage load (Chapter 4) to specifically investigate the effects of the length (L), area (A), and distribution pattern of the b2 reinforcement on the negative bending behavior of PPCB bridges. By changing the parameters, strain over the pier, at the 1/8 of the span length location and at the 1/4 of the span length location (Figure 65) were compared to formulate conclusions.

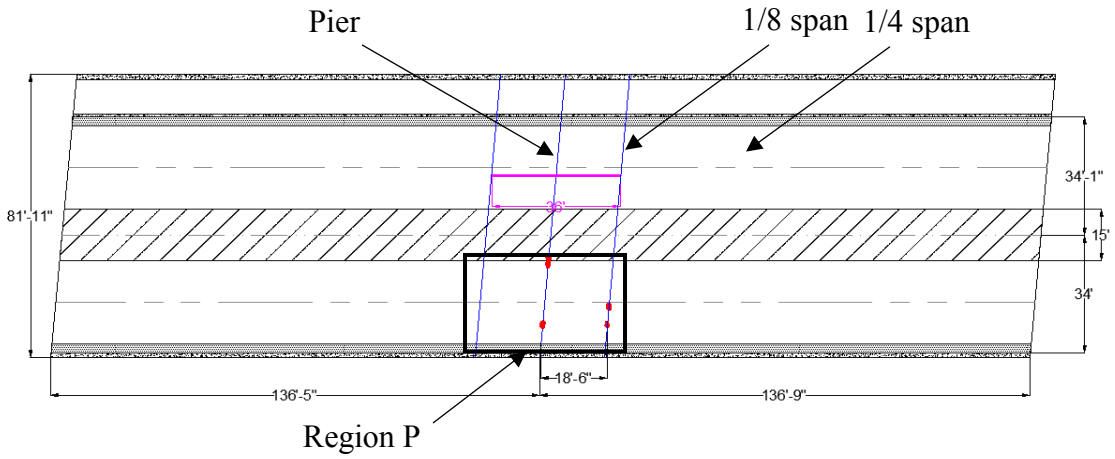

Figure 65. Parametric study region

5.2.1 Live Load

Figure 66(a) shows the major principal strain (ε_1) distribution of Bridge A with an uncracked deck (Model 1) due to the equivalent UDL. Strains are smaller than the cracking strain (Equation 5) over the pier and at the 1/8 of the span length location of the deck.

Figure 66(b) shows the ε_1 strain distribution of Bridge A with twice the length of the b2 reinforcement. The strain distribution pattern and magnitude are similar to the strain distribution for the as-built b2 reinforcement length (Figure 66(a)).

The strain distribution of Bridge A with twice the b2 reinforcement area is shown in Figure 66(c). When compared with the strain distribution of the as-built b2 reinforcement area (Figure 66(a)), no significant difference can be observed.

Finally, Figure 66(d) shows the ε_1 strain distribution of Bridge A with 36-ft and 72-ft staggered b2 reinforcement. When compared with the strain distribution of the as-built b2 reinforcement distribution pattern (Figure 66(a)), no significant difference can be observed.

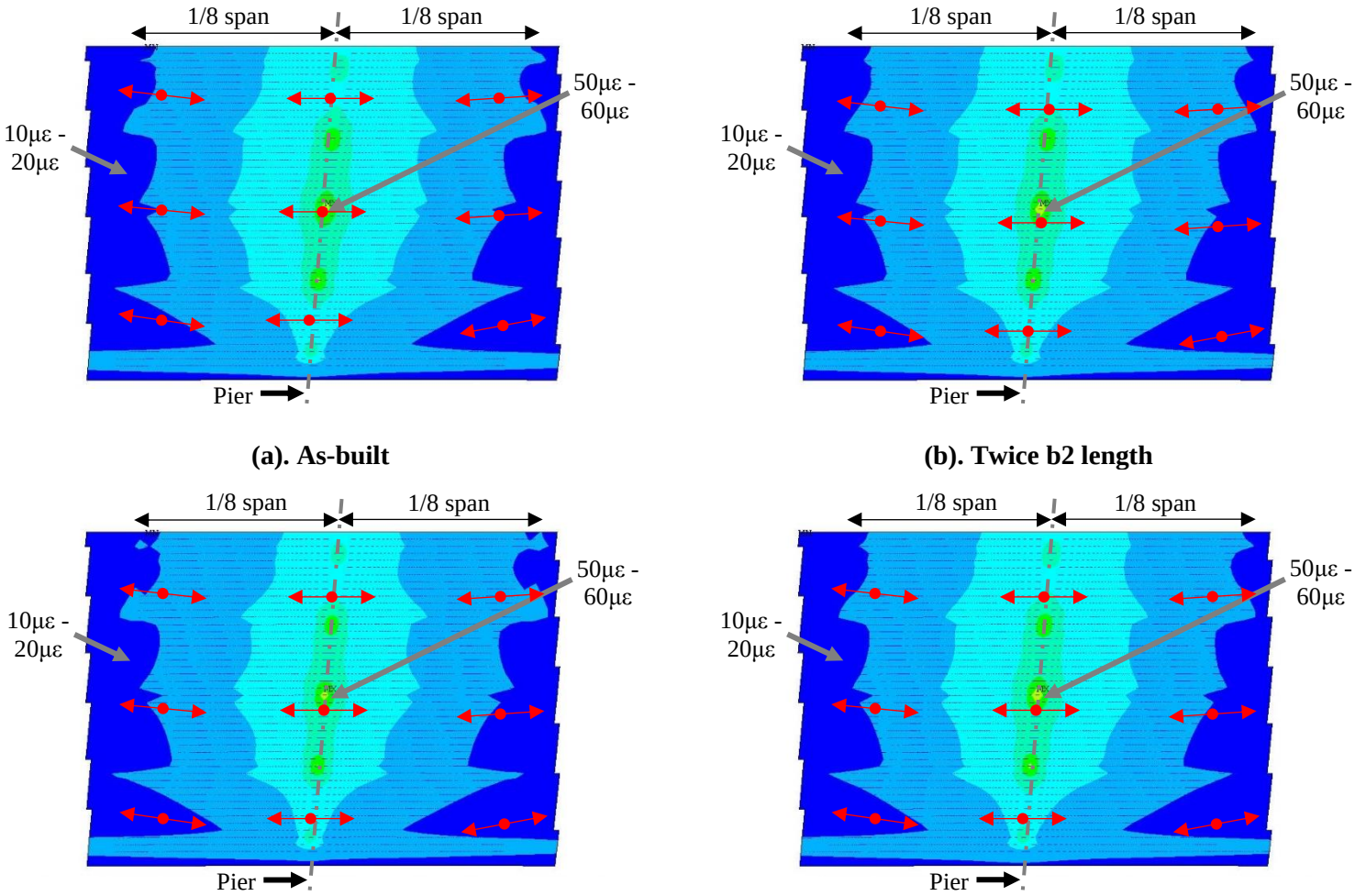

(a). As-built

(b). Twice b2 length

(c). Twice b2 area

(d). Staggered b2 pattern

Figure 66. Major principal strain magnitude and direction of Bridge A of Model 1, Load = Equivalent UDL

Table 8 illustrates the average longitudinal strains (ε_z) at three different locations on Bridge A with the as-built properties, twice the length, twice the area, and a staggered distribution pattern of the b2 reinforcement using the three different, previously described models under live load (equivalent UDL, Chapter 4).

Table 8. Average longitudinal strain (με) of Bridge A due to the live load

	Model 1			Model 2			Model 3		
Parameter	**Pier**	**1/8 span**	**1/4 span**	**Pier**	**1/8 span**	**1/4 span**	**Pier**	**1/8 span**	**1/4 span**
As-built	26	6	-9	197	39	-12	304	94	-12
Twice length	26	6	-9	198	8	-12	259	6	-14
Twice area	25	7	-9	152	49	-12	197	56	-14
Staggered b2 at 1/8 span and 1/4 span	26	6	-9	198	22	-12	258	21	-14

Compared to Model 1, much higher strains were observed on the top surface of the bridge deck of Model 2 and Model 3. As can be seen, sometimes the strains are much larger than the cracking strain (130 με), indicating that it is possible to develop cracks. Furthermore, these analysis results would seem to indicate that once cracking starts (i.e., moving from Model 1 conditions to Model 2 conditions to Model 3 conditions), cracks could be expected to continue to develop and grow. In general, the higher strains over the pier and girders (regardless of the model type) would seem to indicate a higher density of cracks and/or wider cracks occur in these areas.

As expected, the parametric study results under live load indicate higher tensile strains over the pier for all model configurations. Furthermore, at the 1/8 of the span length location, the results indicate approximately 20% to 30% lower tensile strains than those at the pier. Even further, at the 1/4 of the span length location, the deck is in compression under the simulated live load.

The length of the b2 reinforcement was changed to twice the as-built b2 reinforcement length to investigate the effect of the b2 reinforcement length. Therefore, the termination point of the b2 reinforcement with twice the initial length would be at the 1/4 of the span length location. Compared to the results from the as-built condition, Model 1 does not show a significant different difference due to a lengthening of the b2 reinforcement. Model 2 and Model 3 show a significant reduction in average longitudinal strain only at the 1/8 of the span length location.

The effect of the b2 reinforcement area was studied by doubling the as-built b2 reinforcement area. Due to the b2 reinforcement area change, no significant strain difference is observed in Model 1. Compared to the as-built condition, Model 2 and Model 3 show a small reduction of longitudinal strain over the pier.

The b2 reinforcement was terminated at 1/8 of the span length and 1/4 of the span length locations to develop the staggered reinforcement distribution pattern. Compared to the as-built

condition, no noticeable strain differences were found in Model 1. Average longitudinal strains only at the 1/8 of the span length location were decreased in Model 2 and Model 3.

5.2.2 Shrinkage Load

To investigate the effect of the b2 reinforcement, a shrinkage load at 56 days (Chapter 4) was applied to the bridge deck. As shown in Figure 67(a), strains over the pier and at the 1/8 of the span length location of the b2 reinforcement are in the vicinity of the cracking strain of the concrete (Equation 5).

For Model 1, Figure 67(b) presents the strain distribution with twice the length of b2 reinforcement. Compared to Figure 67(a), no significant strain difference is observed over the pier, but a small difference is apparent at the 1/8 of the span length location.

The strain distribution of Bridge A with twice the b2 reinforcement area is shown in Figure 67(c). Compared to Figure 67(a), there is no noticeable difference between the strain distributions.

Finally, the major principal strain distribution of Bridge A with the staggered b2 reinforcement area is shown in Figure 67(d). Compared to Figure 67(a), no significant strain difference can be found over the pier. Small differences can be found at the 1/8 of the span length location.

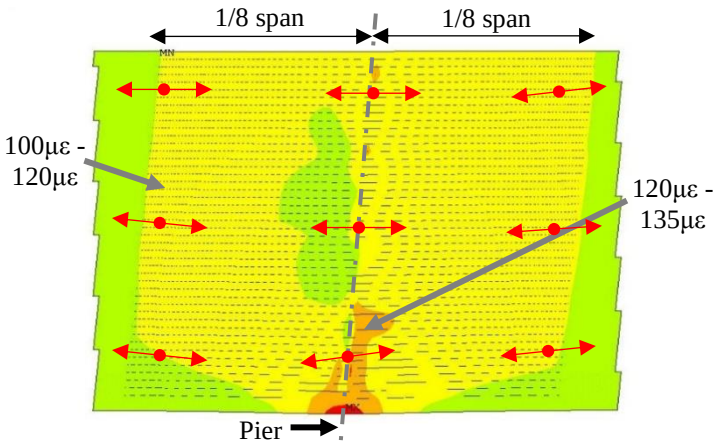

(a). As-built

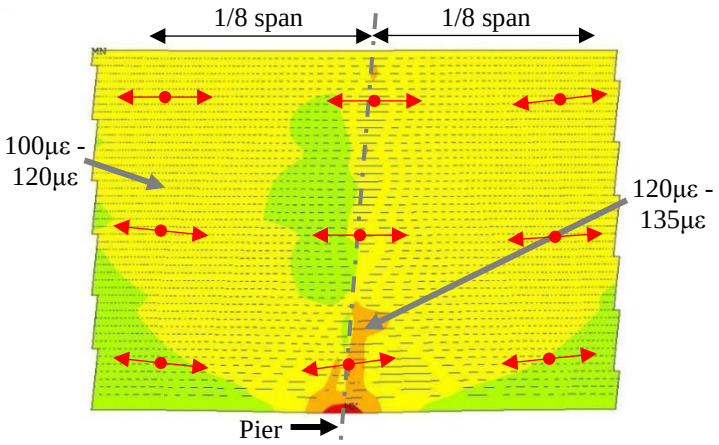

(b). Twice b2 length

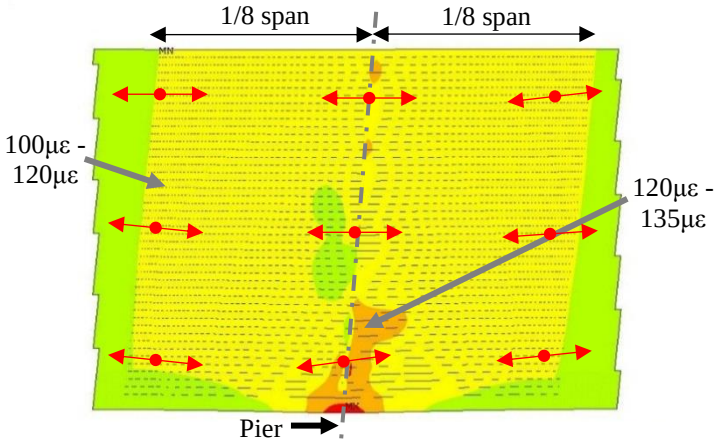

(c). Twice b2 area

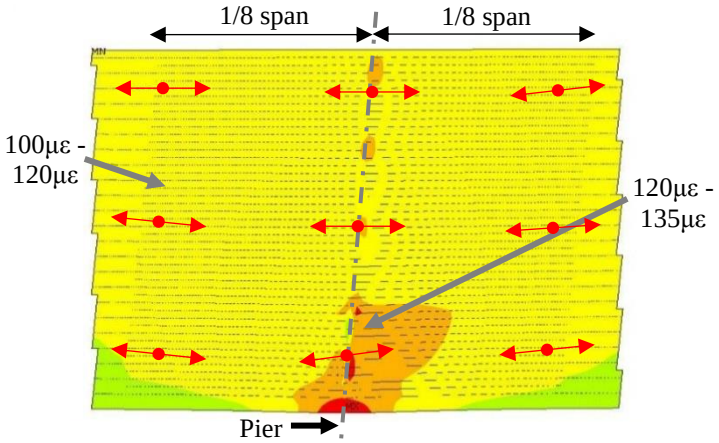

(d). Staggered b2 pattern

Figure 67. Major principal strain magnitude and direction of Bridge A of Model 1, Load = Shrinkage (56 days)

Table 9 presents the average longitudinal strains (ε_z) at three different locations on Bridge A with the as-built properties, twice the length, twice the area, and staggered distribution pattern of the b2 reinforcement using the three different, previously described models for the 56-day shrinkage load (Chapter 4).

Table 9. Average longitudinal strain (με) of Bridge A due to 56-day shrinkage load

	Model 1			Model 2			Model 3		
Parameter	**Pier**	**1/8 span**	**1/4 span**	**Pier**	**1/8 span**	**1/4 span**	**Pier**	**1/8 span**	**1/4 span**
As-built	86	103	96	112	218	52	175	255	52
Twice length	86	107	97	127	187	58	161	186	56
Twice area	87	107	96	108	228	52	130	234	51
Staggered b2 at 1/8 span and 1/4 span	86	106	96	121	225	55	155	225	53

Change of b2 parameters does not significantly affect the strain distribution due to the 56-day shrinkage load. Results show the tensile strains with the highest strain occurring at the 1/8 of the span length location. Compared to the results from the as-built condition, a change in b2 reinforcement length with either Model 2 or Model 3 shows a significant reduction in average longitudinal strain only at the 1/8 of the span length location. No significant difference can be observed due to the b2 reinforcement area or pattern change with Model 2 and Model 3.

5.2.3 Summary

Parametric studies of Bridge A were conducted by changing the length, area, and distribution pattern of the b2 reinforcement. Three different types of conditions, Model 1 - Uncracked Deck, Model 2 - Cracked Deck, and Model 3 - Cracked Deck with Cracked Pier Diaphragm, were used in the study of the strain distribution and magnitude in the negative bending moment region.

The bridge with the uncracked deck showed no significant difference in the strain distribution due to the live load or the 56-day shrinkage load. Both the cracked deck and the cracked deck with cracked pier diaphragm models show similar strain distributions, except that the cracked deck with cracked pier diaphragm condition shows slightly larger strains over the girders. The results show that an increase of b2 reinforcement area reduces the strain magnitudes over the pier, whereas an increase of length of the b2 reinforcement decreases the strain level at the 1/8 of the span length location of the b2 reinforcement. The staggered b2 reinforcement distribution pattern also reduces the strains at the 1/8 of the span length location of the b2 reinforcement.

5.3 Parametric Studies of Bridge B

The parametric studies of Bridge B were conducted similar to the parametric studies of Bridge A by changing the length (L), area (A), and distribution pattern of the b2 reinforcement and considering the differences in behavior under a live load (equivalent UDL, Chapter 4) and a 56-day shrinkage load (Chapter 4).

5.3.1 Live Load

Figure 68 shows the major principal strain distribution around Region P (Figure 65) of the uncracked Bridge B due to the live load. Comparing Figure 66 to Figure 68, a significant reduction of strain is seen over the pier due to the increased skew. Strains are lower than the cracking strain (Equation 5) over the pier and at the 1/8 of the span length location of the deck.

Figure 68(b), (c), and (d) show the ε_1 strain distribution of Bridge B with twice the length, twice the area, and staggered b2 reinforcement at 1/4 of the span length and 1/8 of the span length locations, respectively. When compared with the strain distribution of the as-built b2 reinforcement condition (Figure 68(a)), no significant difference can be observed.

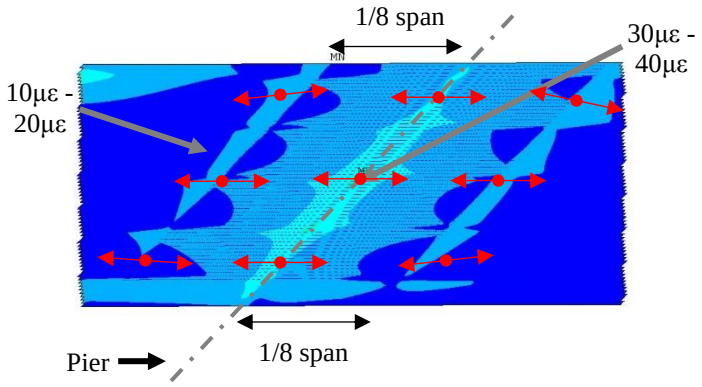

(a). As-built

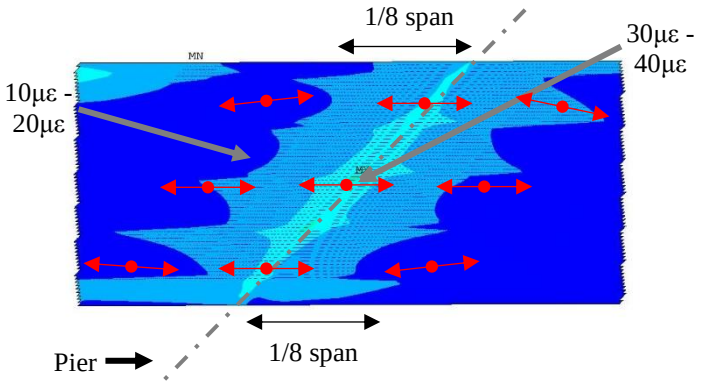

(b). Twice b2 length

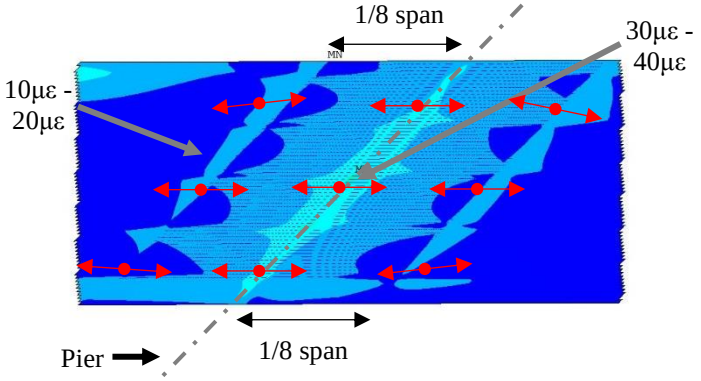

(c). Twice b2 area

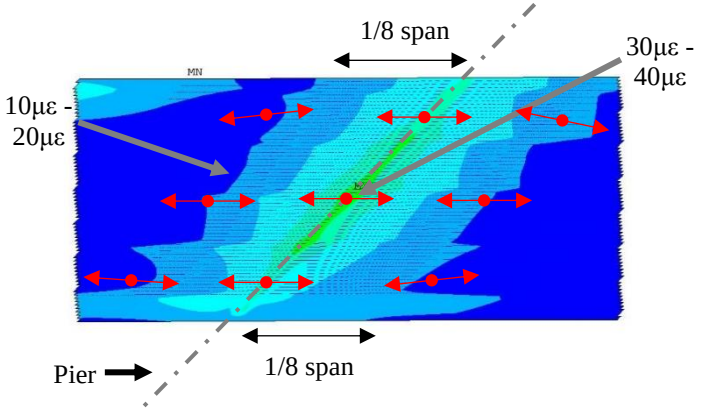

(d). Staggered b2 pattern

Figure 68. Major principal strain magnitude and direction of Bridge B of Model 1, Load = Equivalent UDL

Table 10 present the average longitudinal strains (ε_z) at three different locations on Bridge B with the as-built properties, twice the length, twice the area, and a staggered distribution pattern of the b2 reinforcement for the previously described three different models under live load (equivalent UDL, Chapter 4).

Table 10. Average longitudinal strain (με) of Bridge B due to the live load

	Model 1			Model 2			Model 3		
Parameter	**Pier**	**1/8 span**	**1/4 span**	**Pier**	**1/8 span**	**1/4 span**	**Pier**	**1/8 span**	**1/4 span**
As-built	15	10	-5	32	76	-33	38	82	-35
Twice length	15	7	-3	33	2	4	39	2	7
Twice area	15	10	-5	32	76	-33	38	82	-35
Staggered b2 at 1/8 span and 1/4 span	24	10	-6	161	31	-35	219	39	-49

Similar to the Bridge A results, compared to Model 1, much higher strains were observed on the top surface of the bridge deck of Model 2 and Model 3, indicating possible crack development.

The parametric study results under live load indicate higher tensile strains over the pier for all model configurations. At the 1/8 of the span length location, the results indicate lower tensile strains than those at the pier. At the 1/4 of the span length location, the deck appears to be in compression under the simulated live load.

Similar to Bridge A parametric study results, changing the b2 reinforcement parameters does not show a significant difference when Model 1 is used. Twice the b2 reinforcement length shows a significant reduction in average longitudinal strain only at the 1/8 of the span length location for Model 2 and Model 3.

Compared to the as-built condition, Model 2 and Model 3 show a small reduction of longitudinal strain over the pier due to doubling the as-built b2 reinforcement area. Compared to the as-built condition, the staggered b2 reinforcement pattern shows lower longitudinal strains only at 1/8 of the span length locations in Model 2 and Model 3.

5.3.2 Shrinkage Load

A simulated shrinkage load at 56 days was also applied to Bridge B as part of the parametric studies. Figure 69 presents the strain distribution around the negative moment region (Region P). Compared to Figure 67, a small increase in strain magnitude over the pier can be observed.

The parametric studies were carried out by changing the length (L) (Figure 69(b)), area (A) (Figure 69(c)), and distribution pattern of the b2 reinforcement (Figure 69(d)). No significant differences were observed.

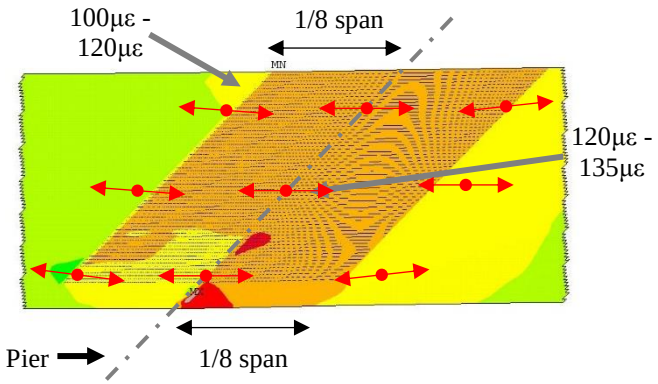

(a). As-built

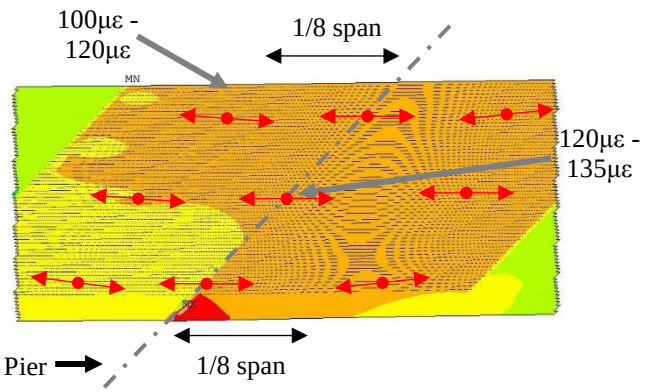

(b). Twice b2 length

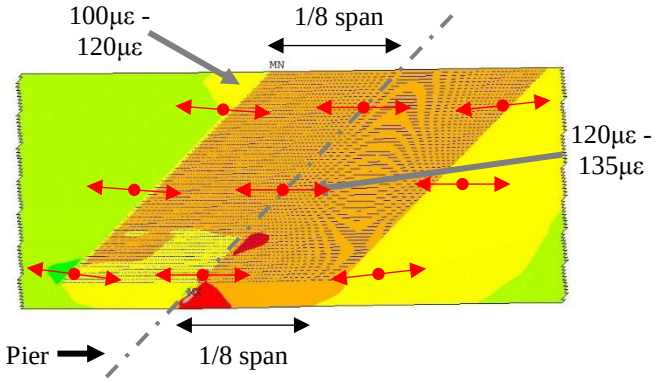

(c). Twice b2 area

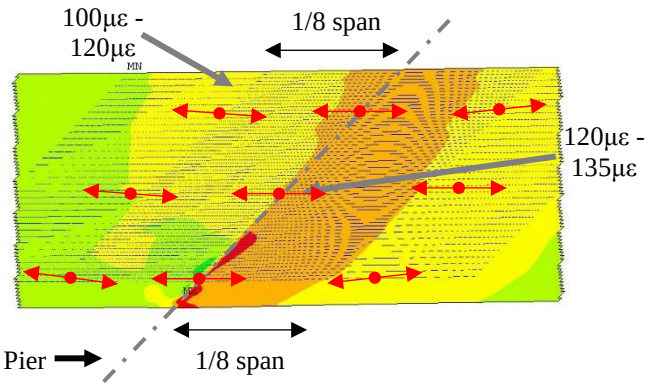

(d). Staggered b2 pattern

Figure 69. Major principal strain magnitude and direction of Bridge B of Model 1, Load = Shrinkage (56 days)

Table 11 shows the average longitudinal strains (ε_z) at three different locations on Bridge B for the previously described models due to the 56-day shrinkage load (Chapter 4).

Table 11. Average longitudinal strain (με) of Bridge B due to 56-day shrinkage load

	Model 1			Model 2			Model 3		
Parameter	**Pier**	**1/8 span**	**1/4 span**	**Pier**	**1/8 span**	**1/4 span**	**Pier**	**1/8 span**	**1/4 span**
As-built	79	118	100	95	239	236	97	242	235
Twice length	77	124	108	98	147	479	100	147	481
Twice area	79	118	100	95	239	236	97	242	235
Staggered b2 at 1/8 span and 1/4 span	74	115	103	112	196	351	138	198	344

The parametric study results of Model 1 due to the 56-day shrinkage load does not significantly affect the behavior of the bridge. Due to the shrinkage load, higher tensile strains were observed at the 1/8 of the span length location. Compared with the as-built condition, twice the b2 reinforcement length of either Model 2 or Model 3 shows a significant reduction in average longitudinal strain only at 1/8 of the span length locations. Whereas, no significant difference can be observed due to the change in b2 reinforcement area or pattern with Model 2 and Model 3.

5.3.3 Summary

Bridge B was used to study the effect of skew angle on the negative moment of the PPCB bridge decks. The parametric studies of Bridge B were conducted similar to those of Bridge A. The results are similar, except that Bridge B shows smaller strains over the pier due to the live load. However, compared to Bridge A, a slight increase in strains over the pier due to the 56-day shrinkage load of Bridge B can be observed.

6 EVALUATION OF SECONDARY MOMENTS OF BRIDGE A

6.1 Introduction

The construction sequence of a continuous multi-span PPCB bridge helps to understand the development of secondary moments at intermediate supports. The typical construction sequence and development of the secondary moments can be explained in five steps.

First, the PPCB bridge girders are placed on supports and behave like a simply supported structure under its self-weight (Figure 70(a)).

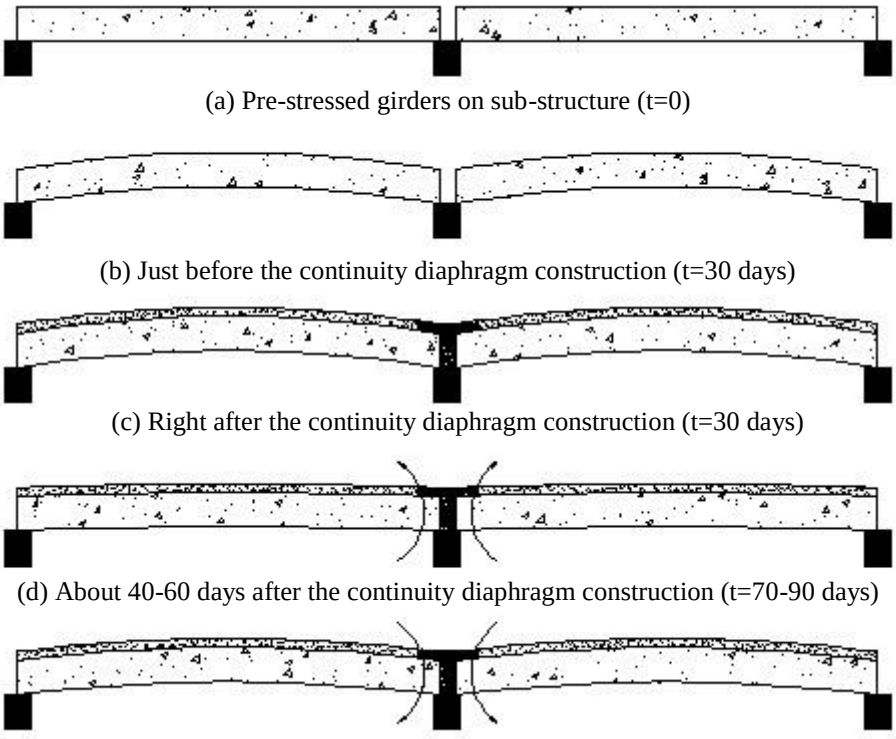

(a) Pre-stressed girders on sub-structure (t=0)

(b) Just before the continuity diaphragm construction (t=30 days)

(c) Right after the continuity diaphragm construction (t=30 days)

(d) About 40-60 days after the continuity diaphragm construction (t=70-90 days)

(e) About 1-3 years after the continuity diaphragm construction (t=1-3 years)

Figure 70. Construction sequence and development of secondary moments in a two-span continuous bridge

Until the cast-in-place deck placement and construction of the continuity diaphragm (30 days, for example), these girders experience an upward deformation due to the creep of the pre-stressing force, which is partially counteracted by the dead load of the girders (Figure 70(b)).

After the cast-in-place deck and the continuity diaphragm concrete have been placed and fully cured, the structure behaves as a continuous beam (Figure 70(c)).

During the next 40 to 60 days or so, the structure develops negative secondary moments (Figure 70(d)) (Newhouse 2005) due to the differential shrinkage between the fresh concrete deck and the precast concrete girders.

During these 40 to 60 days and for the next 1 to 3 years, positive secondary moments continue to increase due to the creep in the girders (Figure 70(e)).

In addition to the positive secondary moment increase due to creep, temperature gradients also induce the positive secondary moment at the intermediate supports (Ghimire 2009).

Often, the positive secondary moment at the intermediate supports is greater than the negative secondary moment. However, the positive secondary moment might develop cracks in the bottom of the continuity diaphragm at the intermediate supports, which reduce the degree of continuity at the intermediate support (McDonagh and Hinkley 2003). The secondary moments that can be developed in a continuous PPCB are investigated in the following sections.

6.2 Calculation of Secondary Moments

Evaluation of the secondary moments involve several uncertainties due to the time-dependent nature of their development. Several methods have been proposed during the past couple of decades to calculate these secondary moments. The PCA method was the first method. The CTL method, P-method, WSDOT RMCalc software, RESTRAINT program, and the modified RESTRAINT program are also available to estimate the secondary moments.

6.2.1 Portland Cement Association (PCA) Method

Based on Mattock's research findings (1960), Freyermuth proposed a detailed procedure to calculate the secondary moments of PPCB bridges due to creep and shrinkage (Freyermuth 1969). An elastic structural analysis considering monolithic behavior of the deck and girders was used to calculate the positive secondary moments due to creep. The negative secondary moment due to the differential shrinkage between the cast-in-place deck and the concrete girders can be calculated by the formulas given in the PCA report (Freyermuth 1969).

6.2.2 Construction Technology Laboratory (CTL) Method

The performance of bridges designed according to the PCA method has been acceptable. However, after 20 years with additional research in the prediction of concrete creep and shrinkage properties , an investigation and improvement of the accuracy of the PCA method was proposed.

As a result of a National Cooperative Highway Research Program (NCHRP) project, Oesterle et al. (1989) developed a method called the CTL method to calculate these secondary moments, which is also known as the BridgeRM program. The CTL method was based on the PCA method, but it can be used to calculate the complete time-history of the secondary moments rather than just the secondary moment at a particular age of the structure.

6.2.3 P-Method

In 1998, Peterman and Ramirez stated that both the PCA and CTL methods overestimate the secondary moments due to the absence of the effect of the cracks in the concrete deck (see Figure 71).

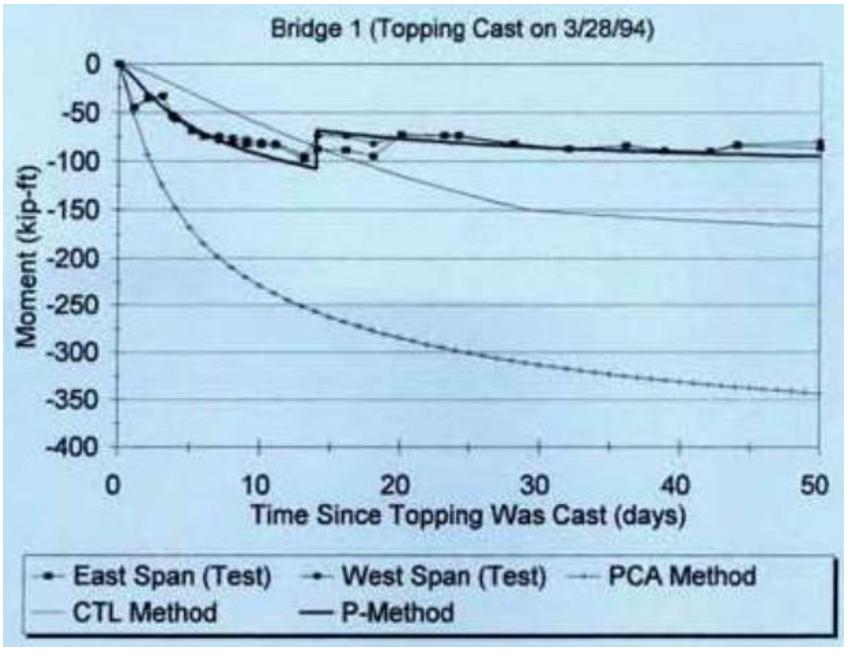

Peterman and Ramirez 1998

Figure 71. Restraint moments from laboratory tests, PCA, CTL and P-Methods

Using both the PCA and CTL method and incorporating the effects of the cracks in the concrete, Peterman and Ramirez developed a method (called the P-method) to calculate the secondary moments of pre-stressed concrete bridges with cast-in-place concrete toppings.

6.2.4 RMCalc Program

In 2003, McDonagh and Hinkley developed a program (RMCalc) to calculate the secondary moments. The RMCalc program is actually a repackaging of BridgeRM and uses the same algorithms.

6.2.5 RESTRAINT Program

Miller et al. (2004) developed a spreadsheet-based program called RESTRAINT to calculate the secondary moments of PPCB bridges. The RESTRAINT program is also based on the PCA and CTL methods with some modifications.

6.2.6 mRESTRAINT Program by Chebole

The original RESTRAINT program was intended to calculate the secondary moments of bridges with equal spans. It can handle limited section properties such as the girder type and

strand properties. Furthermore, the original RESTRAINT program does not use the properties of the continuity diaphragm to calculate the secondary moments.

In 2006, Chebole identified these drawbacks of the original RESTRAINT program and proposed several modifications (Chebole 2011). The modified RESTRAINT program by Chebole is known as the mRESTRAINT program.

Chebole also showed that the secondary moments calculated with the PCA method are not similar to the RMCalc and RESTRAINT programs. This may be due to the absence of incremental time-step analysis in the PCA method. The RMCalc results are similar to the results obtained from the RESTRAINT program (see Figure 72).

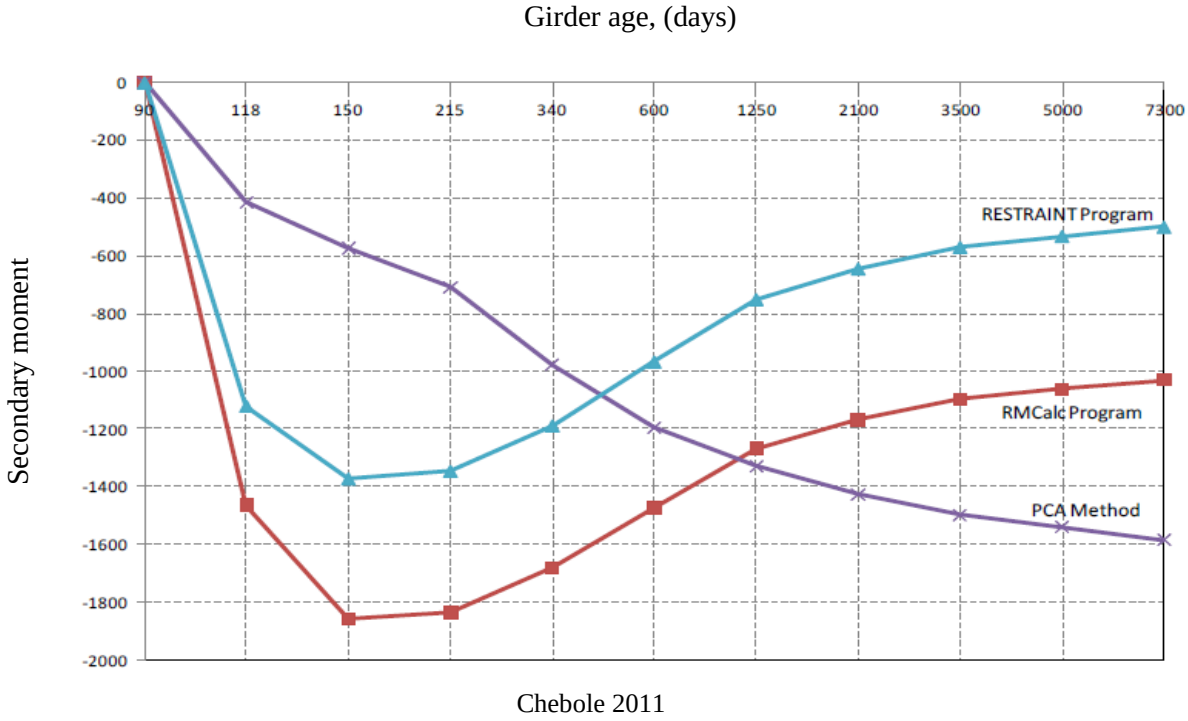

Figure 72. Secondary moment values versus age of girder

6.2.7 mRESTRAINT Program by Ghinire

Until 2009, apparently no one considered the effects of the thermal gradient in the girders of the secondary moment calculations. In 2009, Ghinire re-modified the mRESTRAINT program developed by Chebole to accommodate the thermal gradient of the girders on the secondary moments.

6.3 Comparison of Secondary Moment of Bridge A

The main focus of this portion of the project was to calculate the secondary moments in Bridge A (on Meredith Drive over I-35/I-80) and compare it with the live load negative moment over the intermediate support to evaluate the significance of the secondary moments, given the hypothesis that the secondary moments may be contributing to the historically

"good" performance of PPCB bridges in Iowa. The RMCalc (Version 2.2.2, 2005) was used and results are summarized in Figure 73.

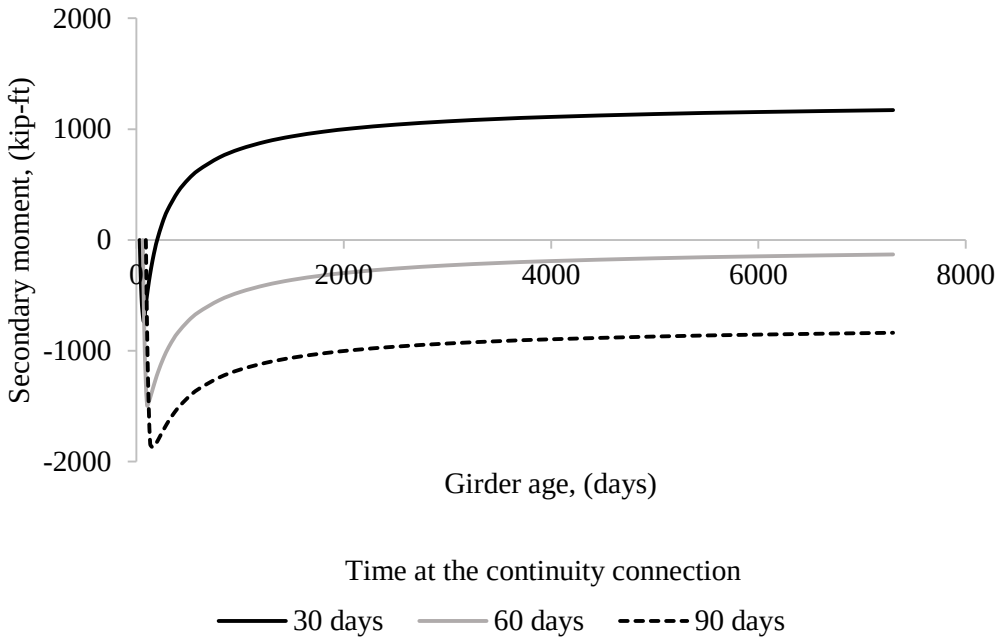

Figure 73. Variation of secondary moments with girder age at the continuity connection construction

For the calculations, it was assumed that the pre-stressing force was released two days after girder concrete placement and that both the cast-in-place deck and the continuity diaphragm were constructed together. The secondary moments are sensitive to the age of the girders when the continuity connection construction is made for 30, 60, and 90 days, as shown in Figure 73. For the first 40 to 60 days after the continuity diaphragm construction, negative secondary moment developed due to the self-weight and differential shrinkage (Figure 70(d)). After this, the negative moment is counteracted by positive secondary moment due to creep (Figure 70(e)). If the continuity connection construction is made at 30 days, the positive secondary moment after 20 years is 1,170 kip-ft.

6.4 Live Load Moment

The negative moment at the intermediate support of Bridge A due to the live load was calculated using the BEC ANALYSIS program (Bridge Engineering Center n.d.). In this case, Bridge A was treated as a two-span continuous beam (Figure 74) having a composite deck girder cross-section. As shown in Figure 74, a HS 20 moving truck load was used for the analysis. The maximum live load negative moment over the intermediate support of Bridge A was calculated as 923 kip-ft.

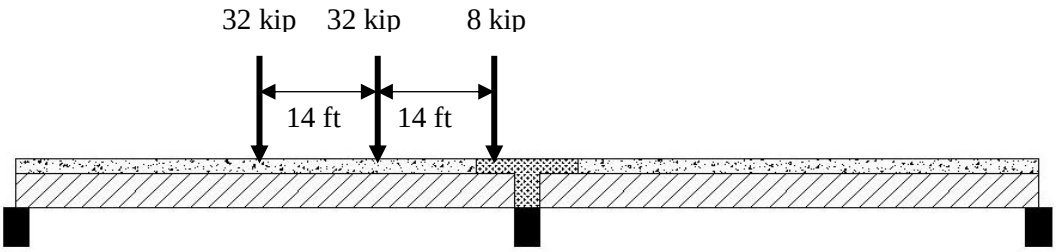

Figure 74. Simplified model of Bridge A used to calculate live load negative moment

6.4.1 Summary

According to the RMCalc program, positive secondary moments could become large enough to counteract the live load negative moment at the intermediate pier. This suggests that the secondary moments may play an important role in the long-term structural performance of PPCB bridges. Usually, the negative moment deck reinforcement design is based only on the live load negative moments at the intermediate support. If secondary moments are present and reliable, lesser amounts (or none) of negative moment b2 reinforcement could be appropriate. However these secondary moments are highly time-dependent and many uncertainties are associated with them. Therefore, further field/laboratory tests may be required to confidently consider the secondary moments in the negative moment reinforcement design process.

7 CONCLUSIONS AND RECOMMENDATIONS

Multi-span PPCB bridges made continuous, for live loads, usually experience a negative live load moment region over the intermediate supports. Sufficient reinforcement (longitudinal continuous deck reinforcement (b1) plus additional longitudinal reinforcement over the intermediate supports (b2)) must be provided to satisfy the strength and serviceability requirements within this negative moment region.

The AASHTO LRFD Bridge Design Specifications (2004) recommend that the negative moment reinforcement be extended beyond the inflection point (into a zone of deck compression). Based upon satisfactory previous performance and judgment, the Iowa DOT terminates the b2 reinforcement at 1/8 of the span length. Although the Iowa DOT OBS policy results in approximately 50% shorter b2 reinforcement than the AASHTO LRFD specifications indicate, the Iowa DOT has not experienced any significant deck cracking over the intermediate supports. The objectives of this project were as follows.

- Investigate the Iowa DOT OBS policy regarding the required amount of b2 reinforcement to provide negative moment continuity
- Investigate the OBS policy regarding the termination length of b2 reinforcement
- Investigate the impact of the b2 reinforcement termination pattern
- Investigate the effect of secondary moments on the performance of PPCB bridges

7.1 Summary

7.1.1 Literature Review

In PPCB bridges, the predominant mode of deck cracking is transverse cracking, which usually occurs over the transverse reinforcement. The effects of numerous contributing factors and mitigation procedures are not yet fully understood. Most research work has focused on the construction materials, mix designs, construction practices, and environmental conditions during construction to determine why transverse cracks occur on bridge decks. Very little research has been carried out on the effects of structural design factors such as girder type, shear stud configuration, deck thickness, reinforcement size and type, and the effect of vibrations on deck cracking.

Secondary moments due to creep of the girders as well as differential shrinkage between the deck and the girders are known to play an important role in the design of the reinforcement at the bottom of the continuity connection. Several research projects developed and improved methods to calculate the secondary moments and some of them developed more efficient positive moment connections to mitigate the cracks at the bottom of the continuity connection due to these secondary moments. Researchers have also concluded that the positive reinforcing steel at the support has no significant effect on the resulting negative moment.

7.1.2 Field Testing

Five bridges with different characteristics (numbers of spans, span lengths, widths, skew angles, number of girders, and girder types) were used during a field test program to

investigate the effects of various bridge characteristics on the negative bending behavior near the piers.

To investigate the effects of the b2 reinforcement, a suite of strain gauges, including rosettes, were placed on the deck top surface 1 ft within and 1 ft beyond the end of the b2 reinforcement. Another set of strain gauges were located on the top surface of the deck over the pier. Girder strain gauges were attached to both top and bottom flanges at a mid-span location and at one depth of the girder away from the pier. A standard snooper truck provided by the Iowa DOT crossed the bridge along multiple transverse paths at a crawl speed to generate pseudo-static strain responses in the test bridges.

Even though the field tests involved five bridges with different properties, the strain profiles from the deck and girder gauges look similar in terms of pattern and magnitudes. For example, the strain gauges 1 ft beyond the b2 reinforcement showed slightly higher strains than the strain gauges within the b2 reinforcement. When the truck axles were in the vicinity of the rosettes, an expected compression and tension behavior of the bridge was observed in the two-span bridges. Major and minor principal strains of approximately the same magnitudes with opposite signs were observed when the truck axles were away from the rosettes. In the three-span bridges, principal strains of the same magnitudes with opposite signs were always observed.

7.1.3 Calibration

A significant focus of the research was to investigate the effects of b2 reinforcement on both skewed and non-skewed bridges with bulb-tee girders. From the five field-tested bridges, Bridge A (on Meredith Drive over I-35/I-80) with a smaller skew angle and Bridge B (on I-80 over US 65) with a larger skew angle were selected for further study with calibrated finite element models.

7.1.3.1 Bridge A

A finite element model of Bridge A was calibrated with the field test results in the vicinity of the negative moment region. The field test results from the deck gauges agreed with the finite element results. The modulus of elasticity of the girders was increased and the support conditions were modified to minimize the difference between the finite element model and the field test.

The finite element model was then compared with the cracking strain of the concrete to simulate the transverse field cracks. It was found that a UDL approximately equivalent to eight HS20 trucks was not sufficient to produce cracking strains. Furthermore, an 80-degree temperature drop was also found to not be sufficient to develop cracks. A deck shrinkage load of 56 days was applied to the model and it was found that this amount of deck shrinkage could induce strain that exceeded cracking levels.

7.1.3.2 Bridge B

The live load calibration results of Bridge A were used as the initial conditions for calibrating Bridge B, followed by a refined calibration with Bridge B field test results. The finite element results of Bridge B generally agreed with the field test results.

7.1.4 Parametric Studies

7.1.4.1 Bridge A

Three different types of models for Bridge A were used in the parametric studies: Model 1 - Uncracked Deck, Model 2 - Cracked Deck, and Model 3 - Cracked Deck with Cracked Pier Diaphragm. The length, area, and distribution pattern of the b2 reinforcement were the primary parameters of the study. Linear static analysis was used to conduct the parametric study with live load (equivalent UDL) and 56-day shrinkage load.

The parametric study results showed that Model 1 had no significant difference in the strain distribution for different b2 parameters under either the live load or the 56-day shrinkage load. Both Model 2 and Model 3 show similar strain distributions. An increase of b2 reinforcement area slightly reduces the strain magnitudes over the pier. Increased length of b2 reinforcement slightly reduces the strains of the deck at the 1/8 of the span length location. A staggered b2 reinforcement pattern also slightly reduces the strains of the deck at the 1/8 of the span length location.

7.1.4.2 Bridge B

The parametric studies of Bridge B were conducted similar to that for Bridge A to demonstrate the effect of skew angle coupled with changes in the b2 reinforcing details. Results of the parametric study of Bridge B are similar to Bridge A, except Bridge B shows smaller strains over the pier due to the live load and slightly larger strains over the pier due to the shrinkage load.

7.1.5 Secondary Moment

Compared to the AASHTO guidelines, the Iowa DOT uses b2 reinforcement that is approximately one half that specified. However, no significant effect of the b2 reinforcement was observed in the parametric studies nor had any anecdotal evidence been identified to suggest that the b2 reinforcement was not performing adequately.

Secondary moments may be positively impacting the negative moment performance. The RMCalc program was used to compare the magnitude of the secondary moments with live load negative moment. It was found that the secondary moments may actually be large enough to counteract any negative moments resulting from live loads. Due to uncertainties associated with these secondary moments, further research may be required to gain more confidence in the consideration of secondary moments.

7.2 Conclusions

- The parametric study results show an increased area of the b2 reinforcement slightly reduces the strain over the pier. Whereas, increased length and a staggered reinforcement pattern slightly reduce the strains of the deck at 1/8 of the span length.
- Finite element results suggested that the transverse field cracks over the pier and at 1/8 of the span length, are mainly due to deck shrinkage.
- Bridges with larger skew angles have lower strains over the intermediate supports.
- Secondary moments affect the behavior in the negative moment region. The impact may be significant enough such that no tensile stresses in the deck may be experienced.

7.3 Recommendations

- Based on the finite element results, termination of b2 reinforcement at 1/8 of the span length is acceptable.

- Secondary moments may reduce the amount and length of the b2 reinforcement required. Further field tests and laboratory tests are recommended.

Further field tests and laboratory tests related to secondary moments are recommended. This additional research should include a broad experimental program coupled with a detailed analytical evaluation and should result in the development and recommendation of design tools for considering secondary moments in PPCB design and detailing.

REFERENCES

AASHTO. *AASHTO LRFD Bridge Design Specifications.* Washington, DC: American Association of State Highway and Transportation Officials, 2004.

ANSYS, Inc. *ANSYS APDL V14 Documentation Manual.* Canonsburg, PA: ANSYS, Inc., 2011.

Babaei, K., and R. Purvis. *Prevention of Cracks in Concrete Bridge Decks.* Harrisburg, PA: Pennsylvania Department of Transportation, 1994.

Bridge Engineering Center. *BEC ANALYSIS: A Live Load Structural Analysis Program for Bridge Structures and Components.* Ames, IA: Bridge Engineering Center, Iowa State University, n.d.

Chebole, Veeravenkata S. Murthy. *Long-Term Continuity Moment Assessment in Pre-stressed Concrete Girder Bridges, Master of Science Thesis.* Baton Rouge, LA: Department of Civil and Environmental Engineering, Louisiana State University, 2011.

Cheng, T. T., and D. W. Johnson. *Incidence Assessment of Transverse Cracking in Bridge Decks: Construction and Material Consideration.* Washington, DC: Federal Highway Administration, 1985.

French, Catherine, Laurice Eppers, Quoc Le, and Jerome F. Hajjar. "Transverse Cracking in Concrete Bridge Decks." *Transportation Research Record: Journal of the Transportation Research Board.* No. 1688 (2007): 21-29.

Freyermuth, C. L. "Design of Continuous Highway Bridges with Precast, Prestressed Concrete Girders." *Journal of the Prestressed Concrete Institute.* Vol. 14, no. 2 (1969).

Frosch, R. J., R. D. Radabaugh, and D. T. Blackman. "Investigation of Transverse Deck Cracking." *Structures Congress Proceedings.* Reston, VA: ASCE, 2002.

Ghimire, Sushovan. *Restraint Moments Due to Thermal Gradients in Continuous Prestressed Concrete Girder Bridges.* Baton Rouge, LA: Department of Civil and Environmental Engineering, Louisiana State University, 2009.

Hadidi, R., and M. Saadeghvaziri. "Transverse Cracking of Concrete Bridge Decks: State-of-the-Art." *Journal of Bridge Engineering.* Vol. 10, no. 5 (2005): 503–510.

Hastak, Makarand, Amir Mirmiran, Richard Miller, Ronak Shah, and Reid Castrodale. "State of Practice for Positive Moment Connections in Prestressed Concrete Girders Made Continuous." *Journal of Bridge Engineering.* Vol. 8, no. 5 (2003): 267–272.

Issa, M. "Investigation of Cracking in Concrete Bridge Decks at Early Ages." *Journal of Bridge Engineering.* Vol. 4, no. 2 (1999): 116-124.

Kochanski, T., J. Parry, D. Pruess, L. Schuchardt, and J. Ziehr. *Premature Cracking of Concrete Bridge Decks Study.* Madison, WI: Wisconsin Department of Transportation, 1990.

Krauss, P. D., and E. A. Rogalla. *Transverse Cracking in Newly Constructed Bridge Decks.* Washington, DC: Transportation Research Board, National Research Council, 1996.

Kwak, Hyo-Gyoung, and Young-Jae Seo. "Numerical Analysis of Time-Dependent Behavior of Pre-Cast Pre-Stressed Concrete Girder Bridges." *Construction and Building Materials.* Vol. 16, no. 1 (2002): 49–63.

Mattock, A. H. "Precast-Prestressed Concrete Bridges 5. Creep and Shrinkage Studies." *Development Department Bulletin D46,* 1960.

McDonagh, Michael D., and Kevin B. Hinkley. "Resolving Restraint Moments: Designing for Continuity in Precast Prestressed Concrete Girder Bridges." *PCI Journal.* Vol. 48, no. 4 (2003): 104-119.

McKeel, W. T. *Evaluation of Deck Durability on Continuous Beam Highway Bridges.* Charlottesville, VA: Virginia Highway and Transportation Research Council, 1985.

Miller, R. A., R. Castrodale, A. Mirmiran, and M. Hastak. *NCHRP Report 519: Connection of Simple-Span Precast Concrete Girders for Continuity.* Washington, DC: National Cooperative Highway Research Program, 2004.

Newhouse, Charles D. *Design and Behavior of Precast, Prestressed Girders Made Continuous - An Analytical and Experimental Study, Doctor of Philosophy Dissertation.* Blacksburg, VA: Department of Civil and Environmental Engineering, Virginia Polytechnic Institute and State University, 2005.

Oesterle, R. G., J. D. Glikin, and S. C. Larson. *NCHRP Report 322: Design of Precast Prestressed Girders Made Continuous.* Washington, DC: National Cooperative Highway Research Program, 1989.

Oesterle, Ralph G., Armin B. Mehrabi, Habib Tabatabai, Andrew Scanlon, and Chris A. Ligozio. "Continuity Considerations in Prestressed Concrete Jointless Bridges." *Structures 2004: Building on the Past, Securing the Future.* Nashville, TN: American Society of Civil Engineers, 2004. 1-8.

Peterman, R. J., and J. A. Ramirez. "Restraint Moments in Bridges with Full-Span Prestressed Concrete Form Panels." *PCI Journal*, 1998.

Ramey, G, A Wolff, and R Wright. "Structural Design Actions to Mitigate Bridge Deck Cracking." *Practice Periodical on Structural Design and Construction.* Vol. 2, no. 3 (1997): 118–124.

Schmitt, T. R., and D. Darwin. *Cracking in Concrete Bridge Decks.* Topeka, KS: Kansas Department of Transportation, 1995.

Vishay Precision Group. *Strain Gauge Rosettes: Selection, Application and Data Reduction.* Wendell, NC: Vishay Precision Group, Micro-Measurements, 2010.

Wassef, Wagdy G., Christopher Smith, Chad M. Clancy, and Martin J. Smith. *Comperhensive Design Example for Prestressed Concrete (PSC) Girder Superstructure Bridge with Commentary.* Harrisburg, PA: Modjeski and Masters, Inc., 2003.

APPENDIX: FIELD TEST RESULTS FOR EACH BRIDGE

A summary of the field test results with figures showing typical results is presented in Chapter 3. This appendix provides a summary of the field test results for each of the five bridges. A plan view of the bridge, locations of the deck gauges, locations of the girder gauges, locations of the rosettes, and load case details are included. Results of deck gauges and girder gauges are given only for Load Case 1 (LC1). Results for LC4 are approximately symmetric with LC1 results.

A.1 Bridge 1: On County Road C50 over US 218

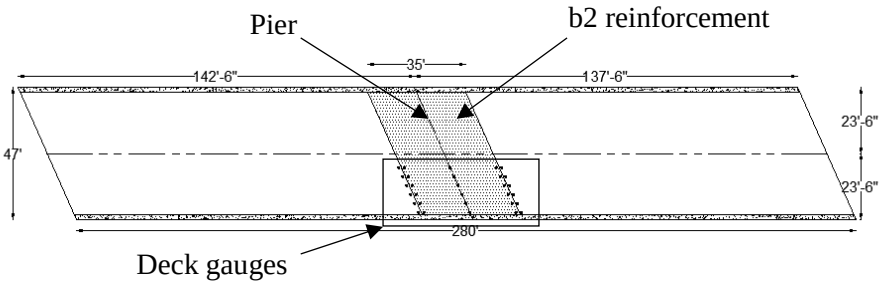

Figure A.1.1. Bridge 1 plan view

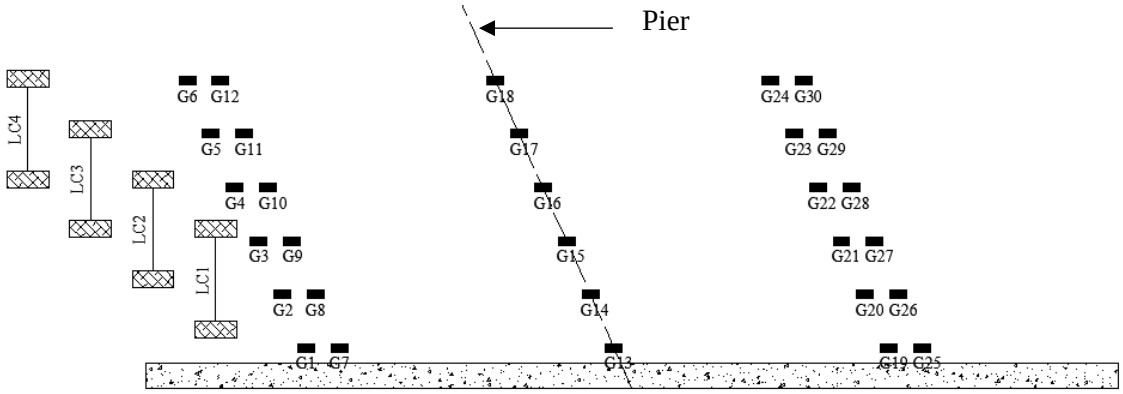

Figure A.1.2. Bridge 1 deck gauge instrumentation plan

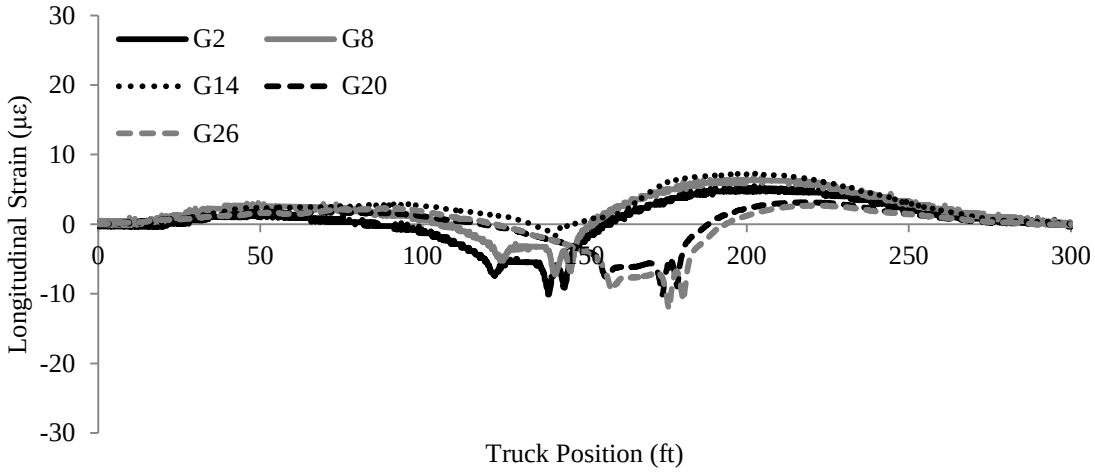

Figure A.1.3. Bridge 1 typical deck gauge longitudinal strain variations close to the wheel path (LC1)

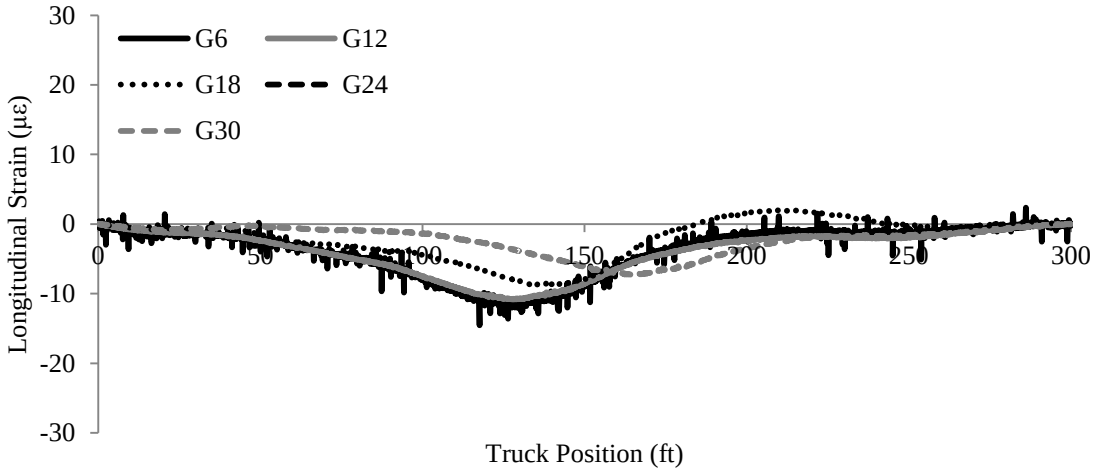

Figure A.1.4. Bridge 1 typical deck gauge longitudinal strain variations away from the wheel path (LC1)

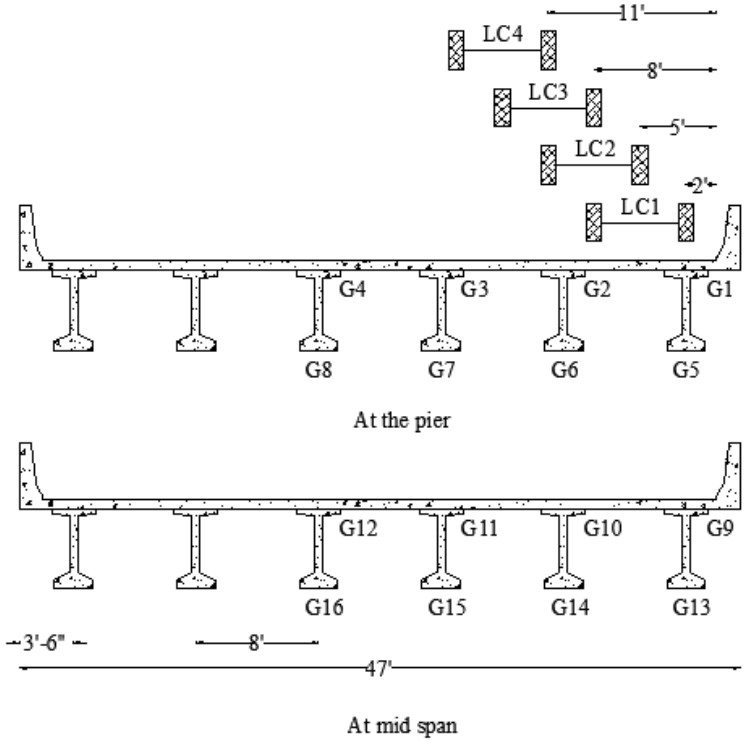

Figure A.1.5. Bridge 1 girder gauge instrumentation plan

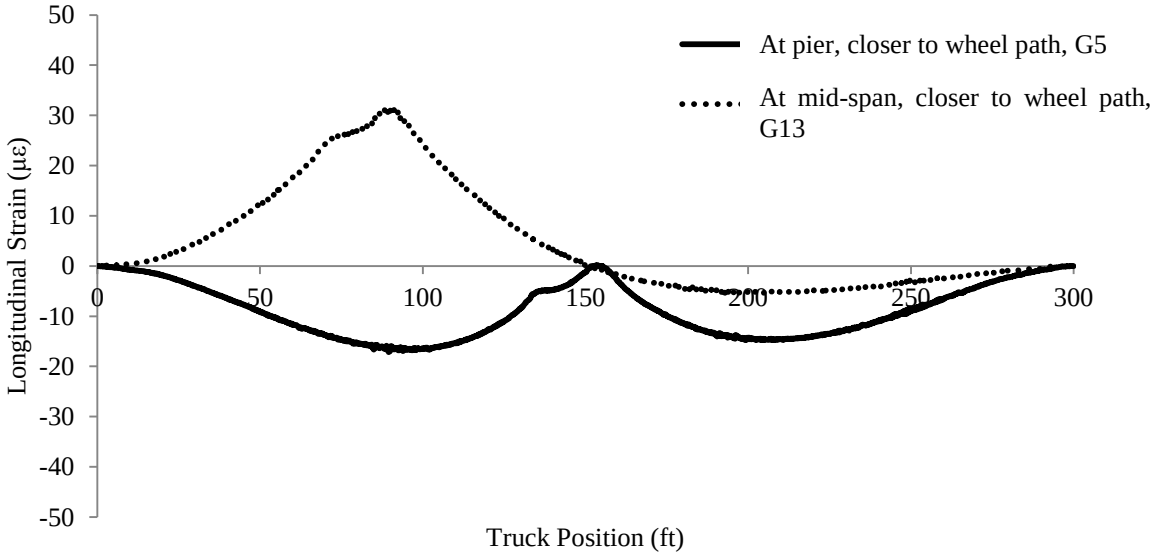

Figure A.1.6. Bridge 1 typical girder gauge strain variations (LC1)

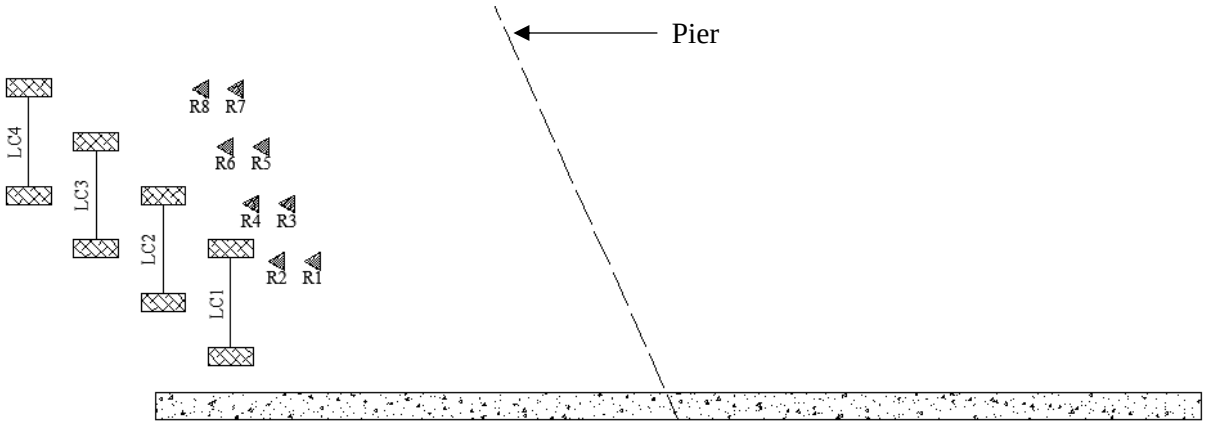

Figure A.1.7. Bridge 1 rosette instrumentation plan

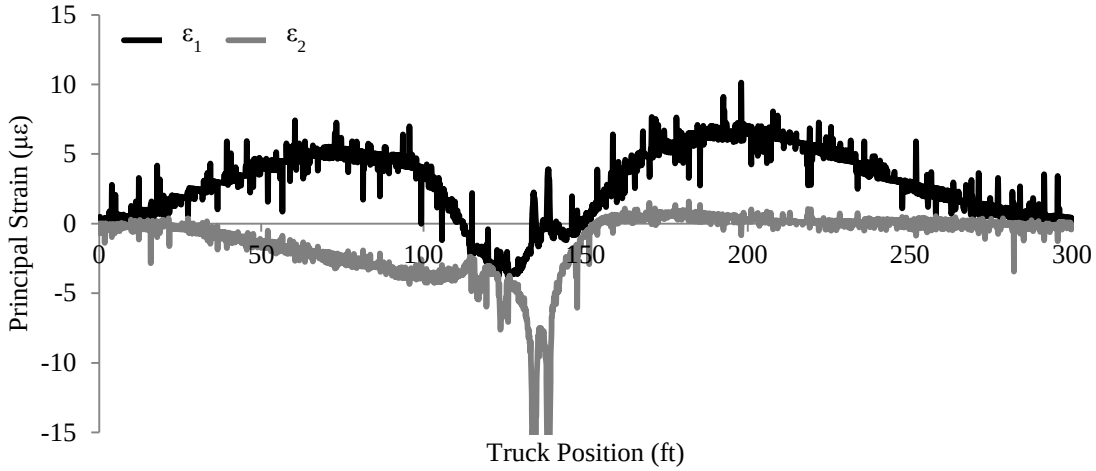

Figure A.1.8. Bridge 1 typical principal strain variations of rosettes (R7) close to wheel path (LC4)

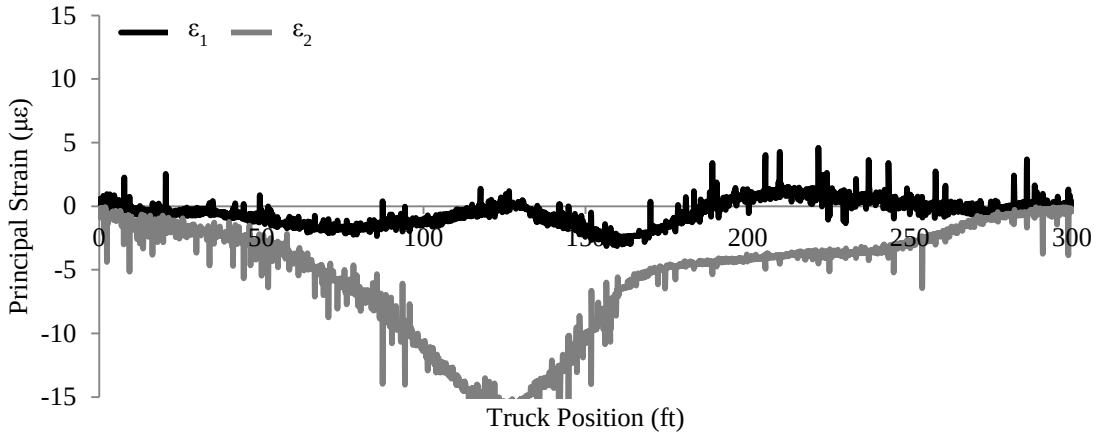

Figure A.1.9. Bridge 1 typical principal strain variations of rosettes (R7) away from wheel path (LC1)

A.2 Bridge 2: On I-80 over US 65

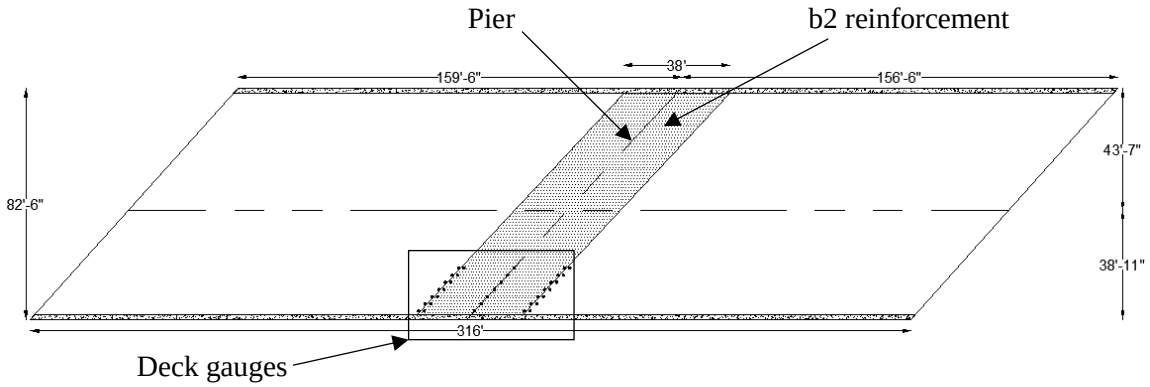

Figure A.2.1. Bridge 2 plan view

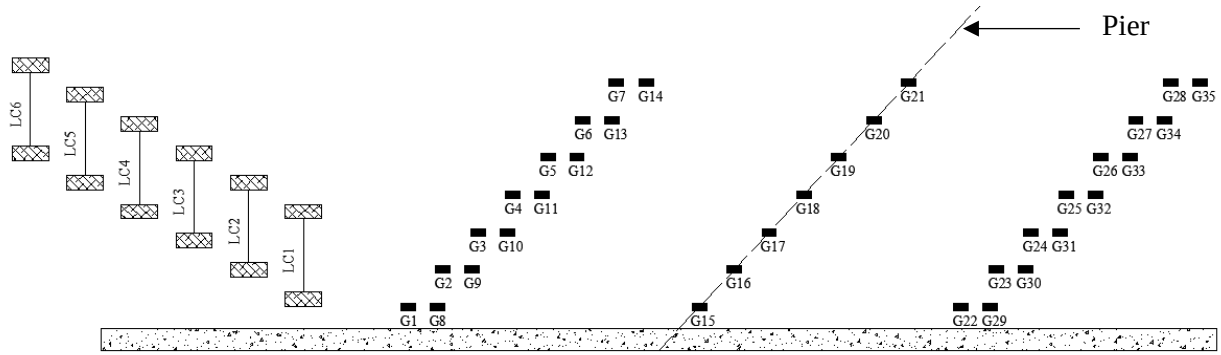

Figure A.2.2. Bridge 2 deck gauge instrumentation plan

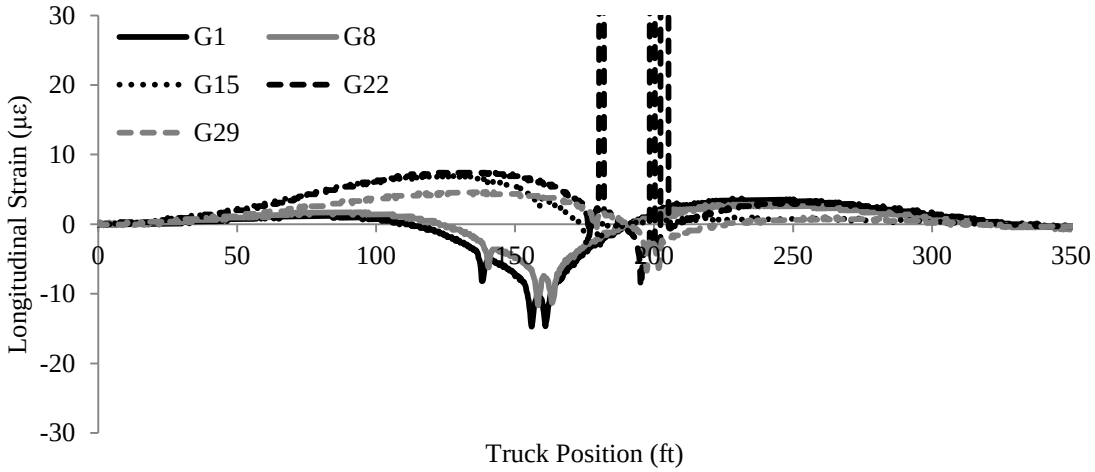

Figure A.2.3. Bridge 2 typical deck gauge longitudinal strain variations close to the wheel path (LC1)

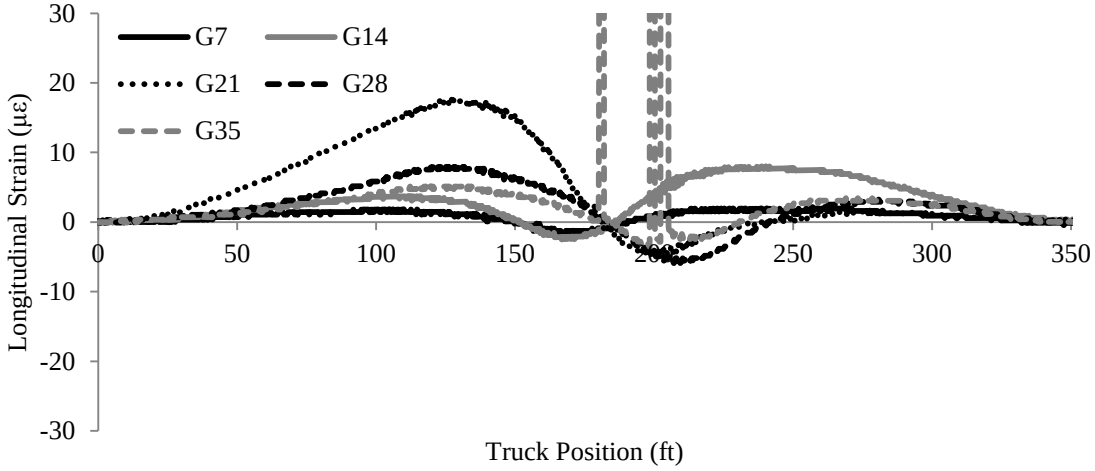

Figure A.2.4. Bridge 2 typical deck gauge longitudinal strain variations away from the wheel path (LC1)

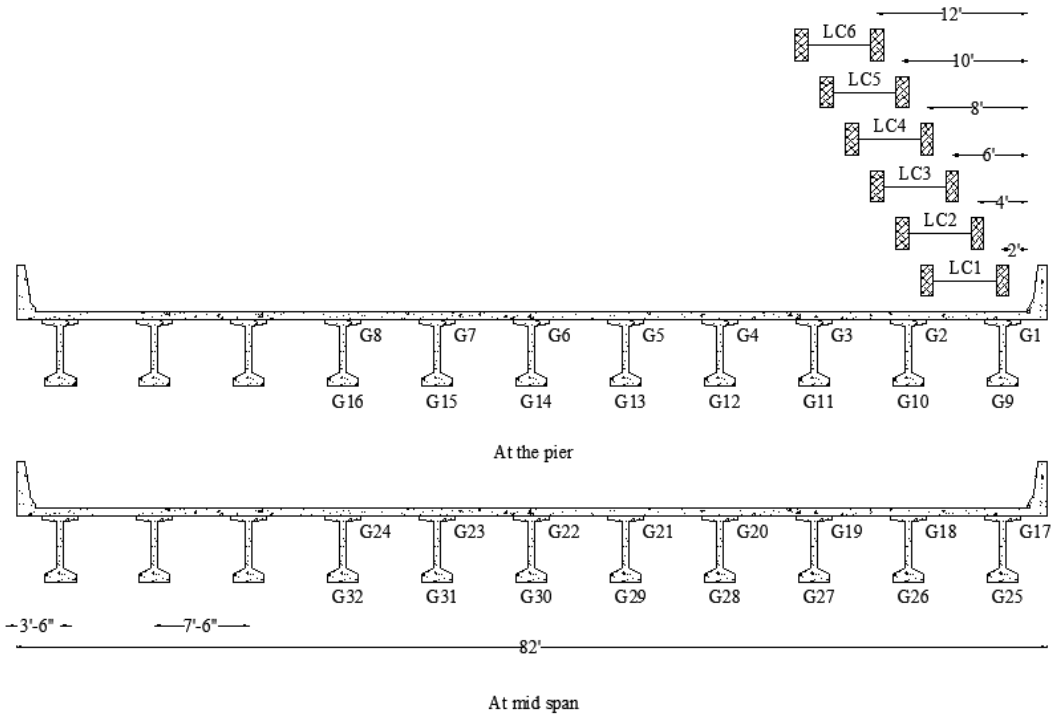

Figure A.2.5. Bridge 2 girder gauge instrumentation plan

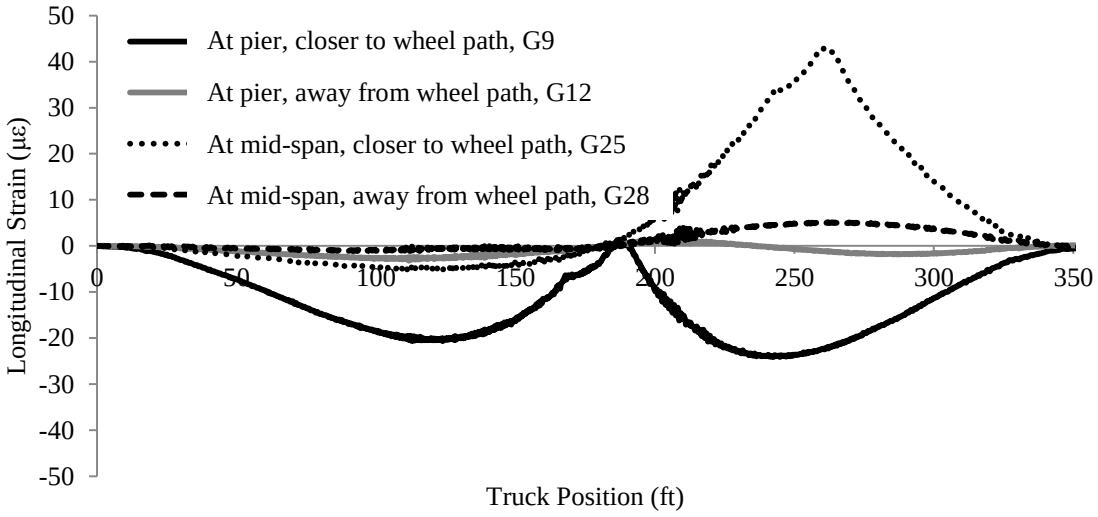

Figure A.2.6. Bridge 2 typical girder gauge strain variations (LC1)

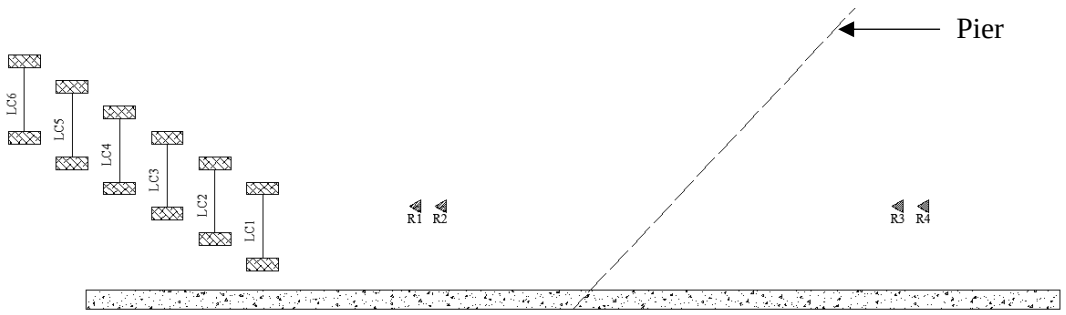

Figure A.2.7. Bridge 2 rosette instrumentation plan

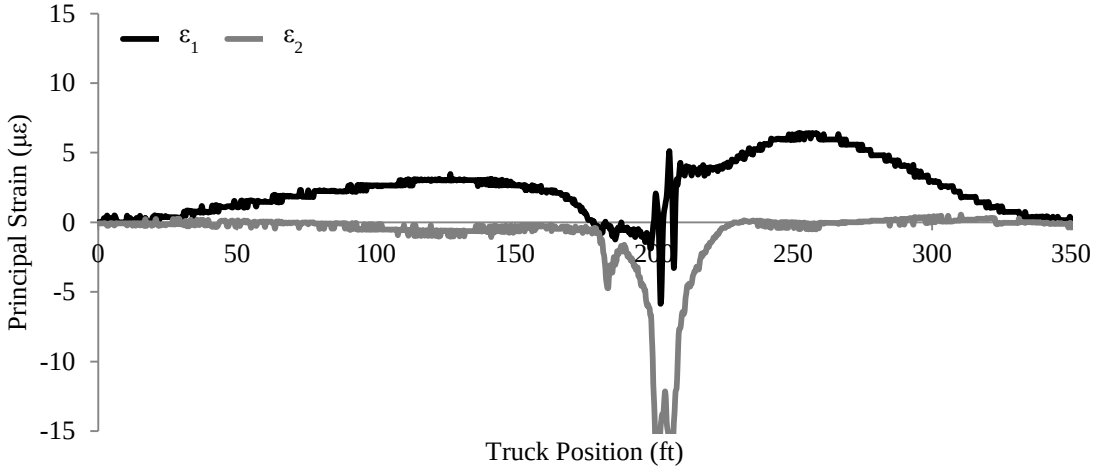

Figure A.2.8. Bridge 2 typical principal strain variations of rosettes (R4) close to wheel path (LC1)

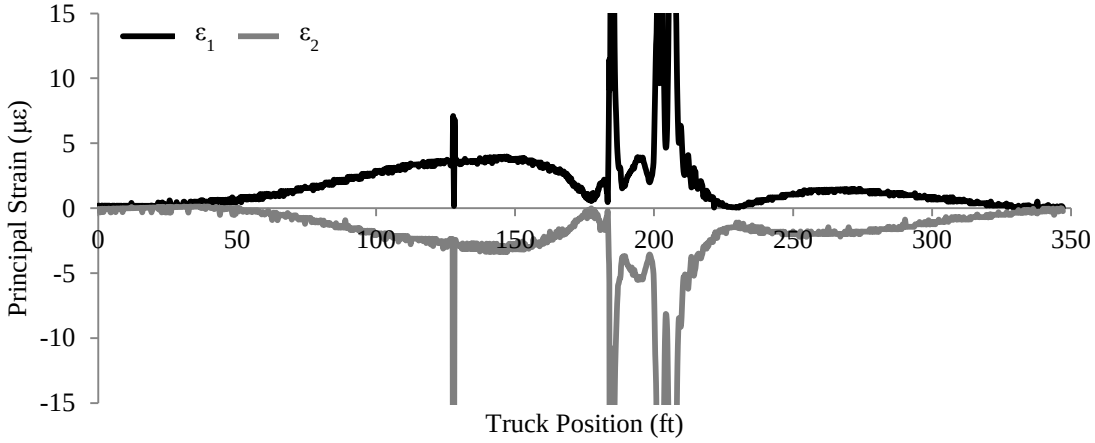

Figure A.2.9. Bridge 2 typical principal strain variations of rosettes (R4) away from wheel path (LC6)

A.3 Bridge 3: On Meredith Drive over I-35/I-80

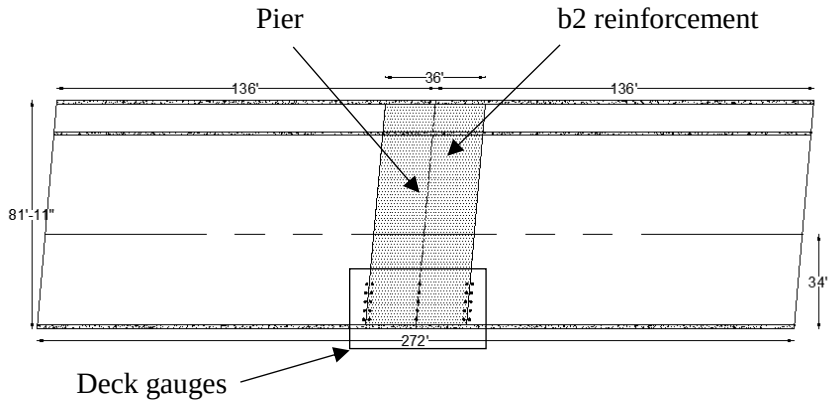

Figure A.3.1. Bridge 3 plan view

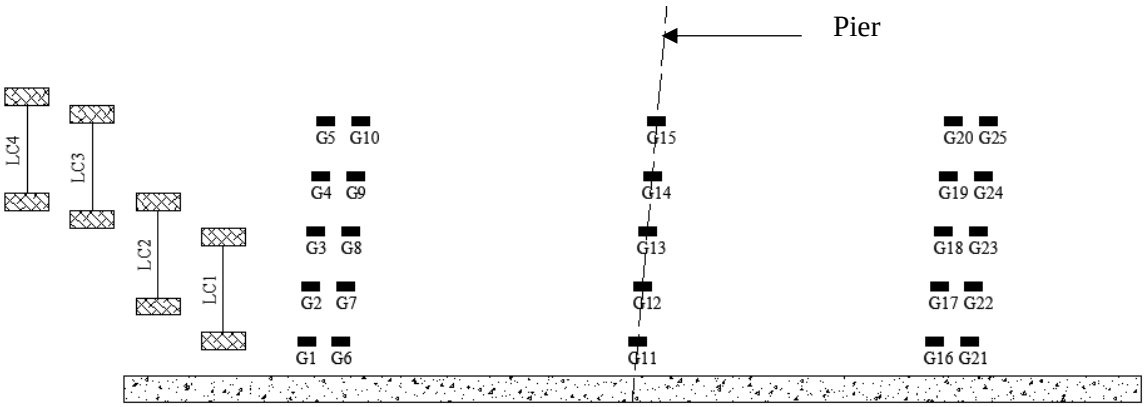

Figure A.3.2. Bridge 3 deck gauge instrumentation plan

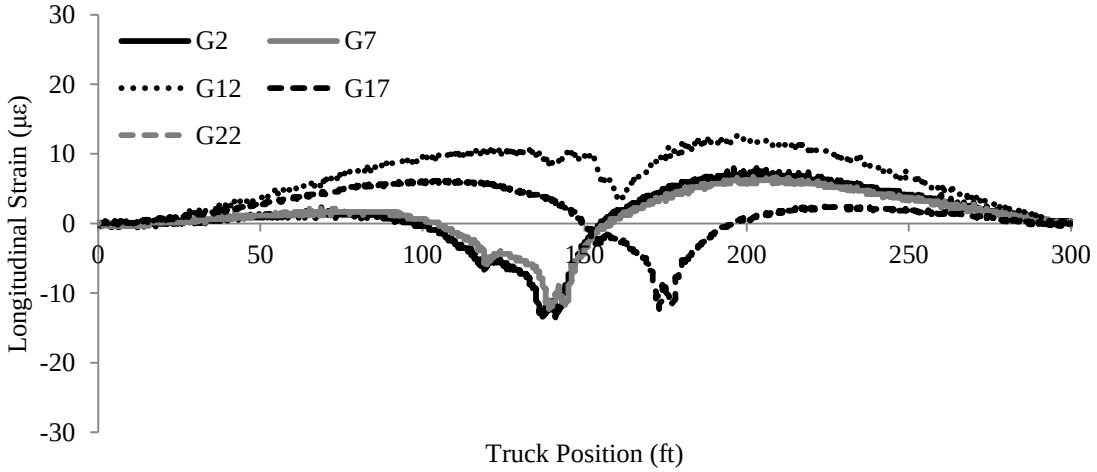

Figure A.3.3. Bridge 3 typical deck gauge longitudinal strain variations close to the wheel path (LC1)

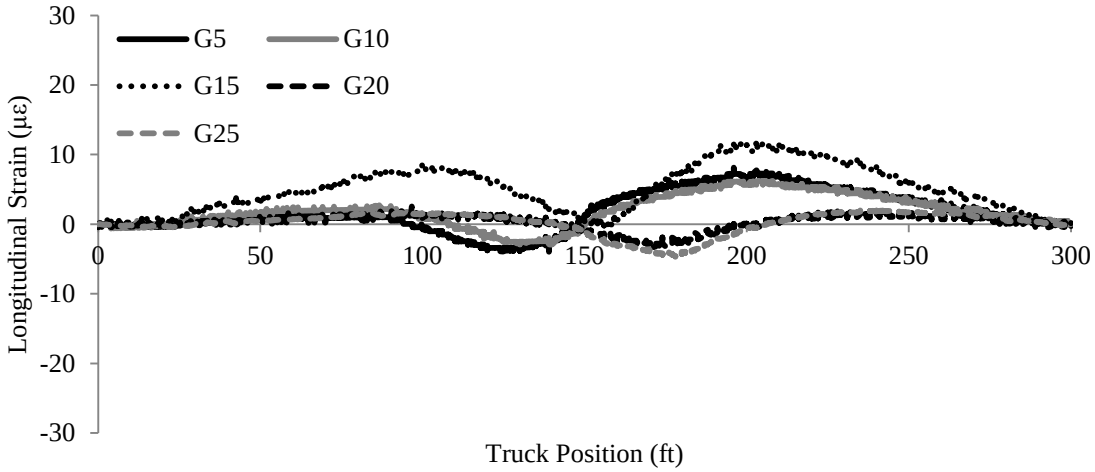

Figure A.3.4. Bridge 3 typical deck gauge longitudinal strain variations away from the wheel path (LC1)

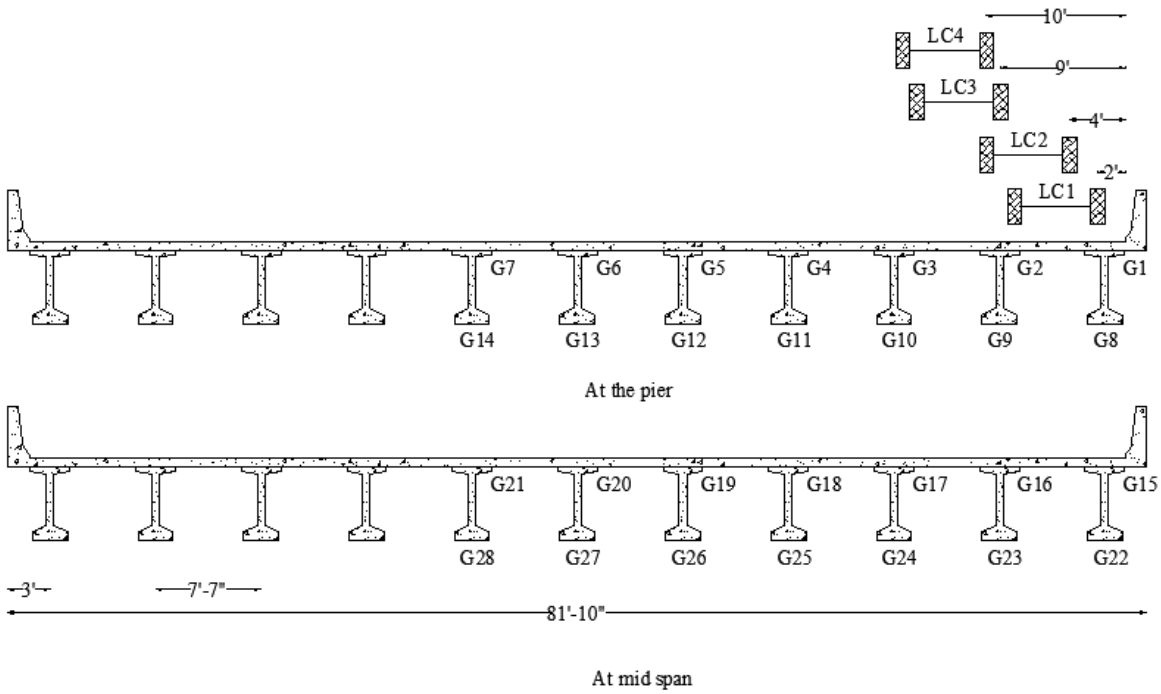

Figure A.3.5. Bridge 3 girder gauge instrumentation plan

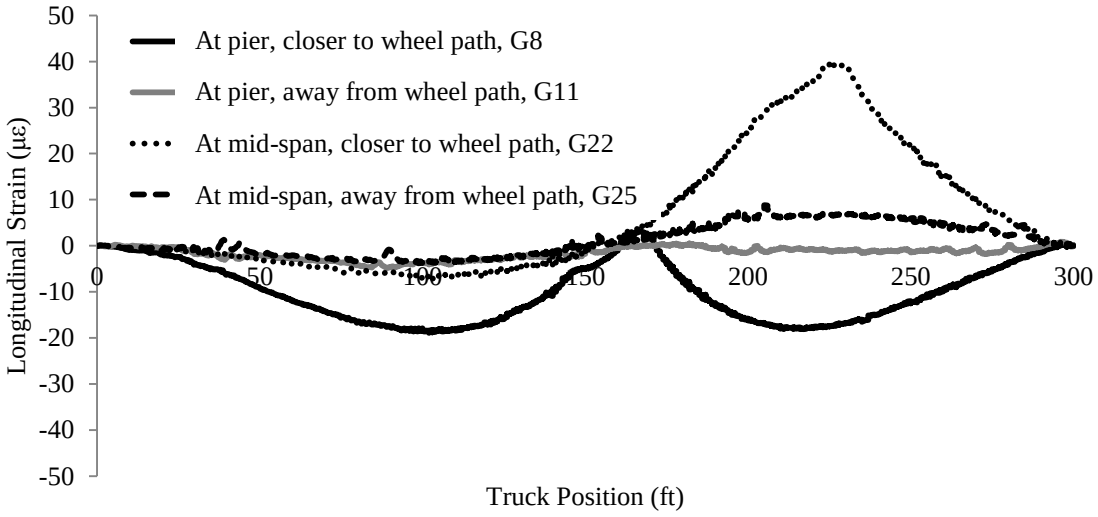

Figure A.3.6. Bridge 3 typical girder gauge strain variations (LC1)

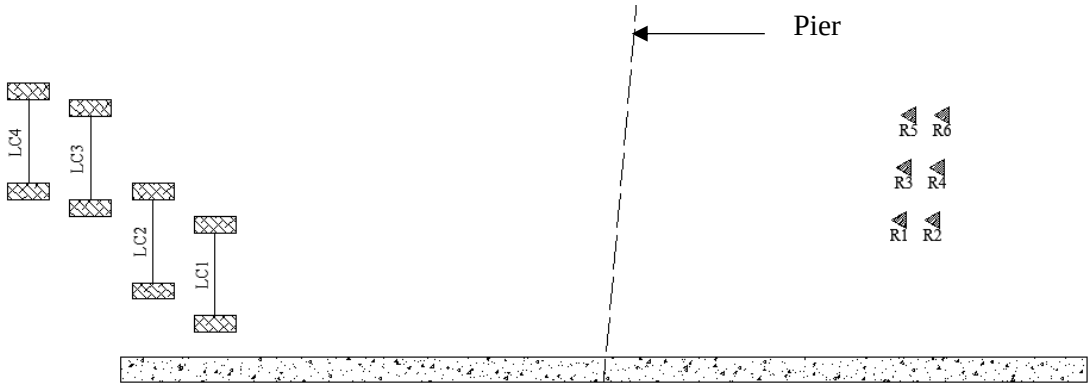

Figure A.3.7. Bridge 3 rosette instrumentation plan

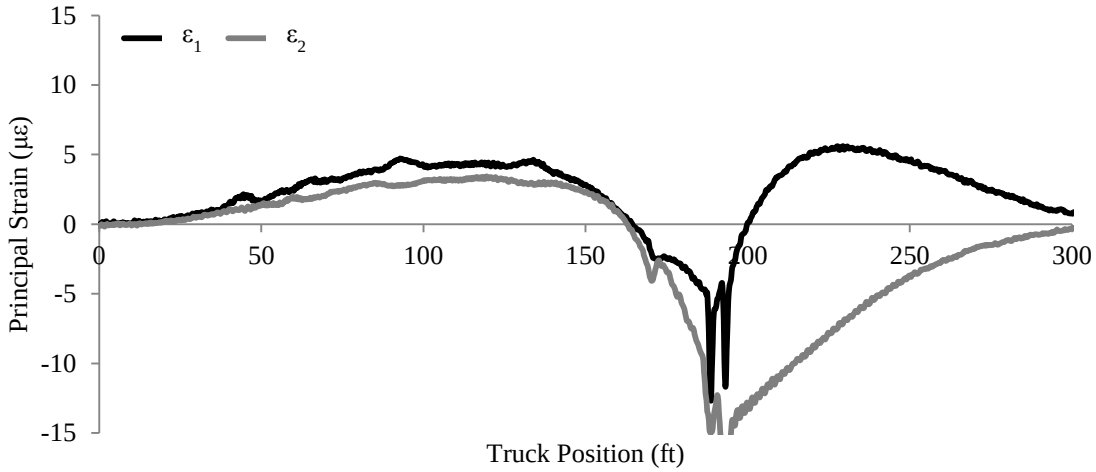

Figure A.3.8. Bridge 3 typical principal strain variations of rosettes (R6) close to wheel path (LC4)

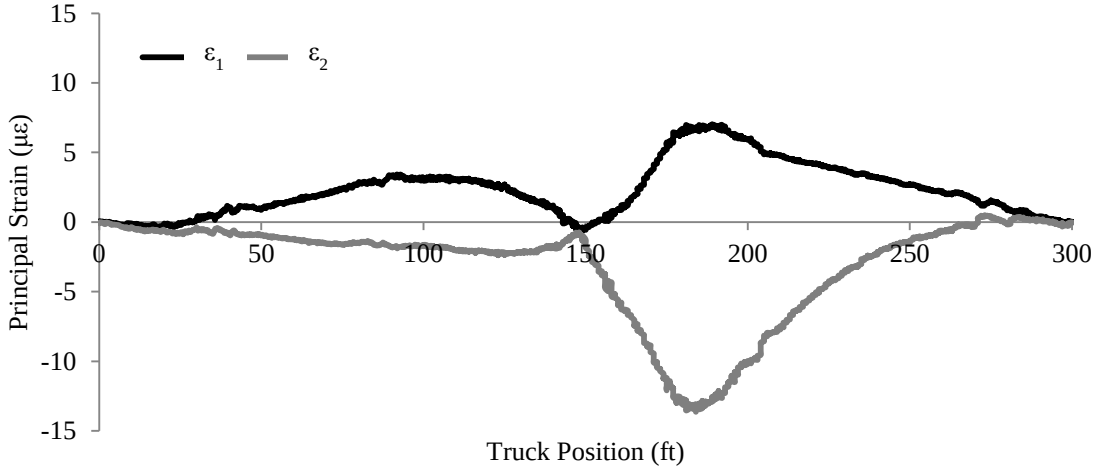

Figure A.3.9. Bridge 3 typical principal strain variations of rosettes (R6) away from wheel path (LC1)

A.4 Bridge 4: On Mt. Pleasant Bypass over Big Creek

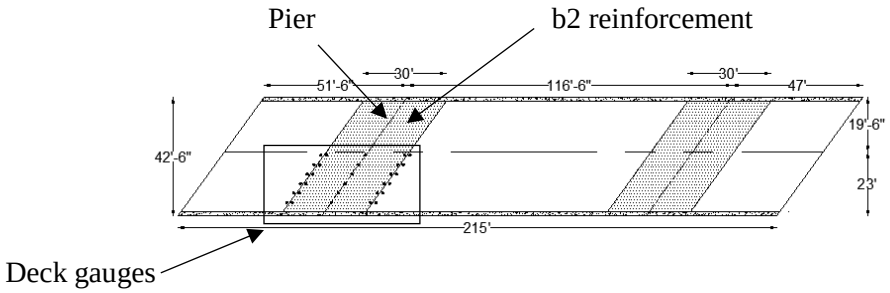

Figure A.4.1. Bridge 4 plan view

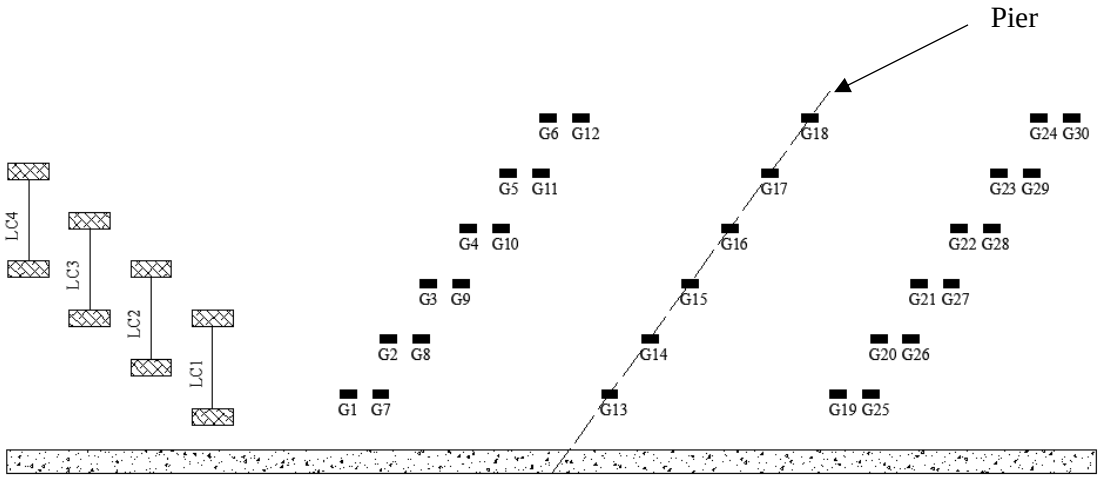

Figure A.4.2. Bridge 4 deck gauge instrumentation plan

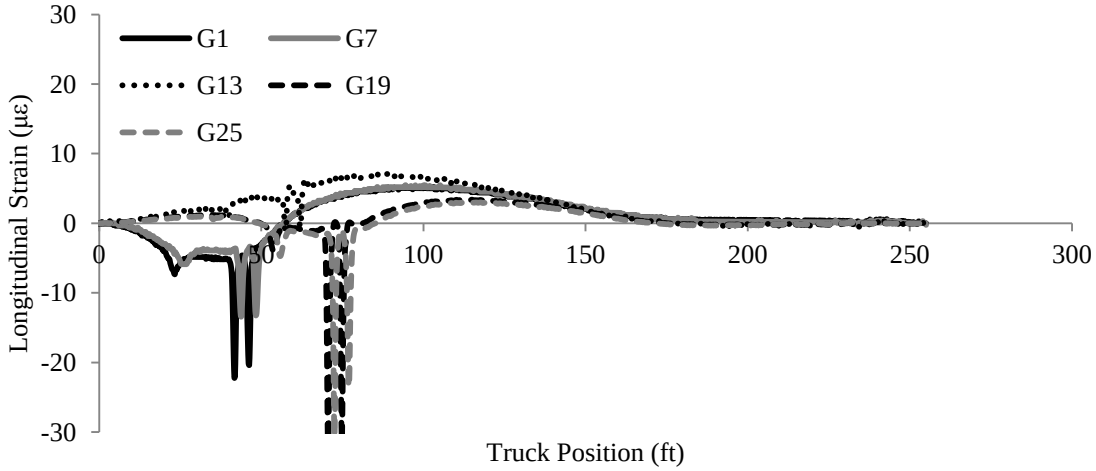

Figure A.4.3. Bridge 4 typical deck gauge longitudinal strain variations close to the wheel path (LC1)

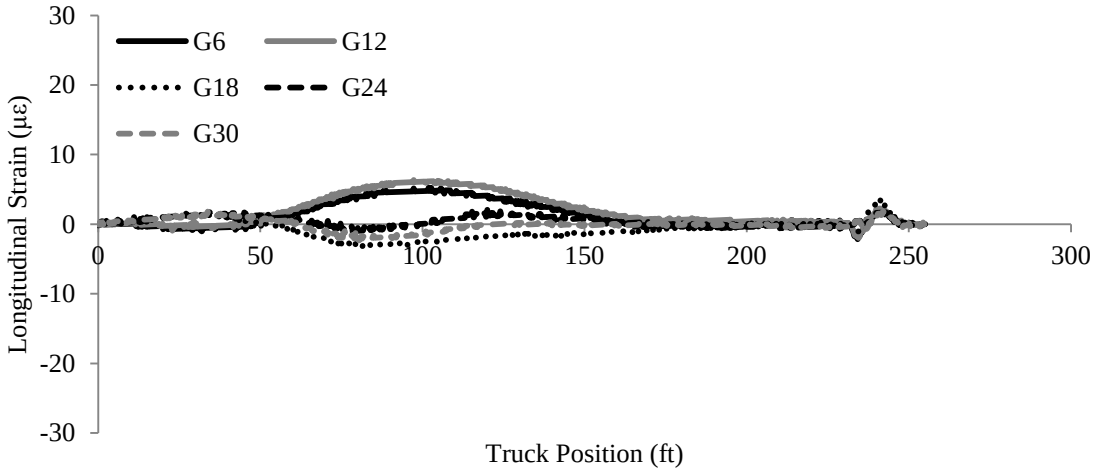

Figure A.4.4. Bridge 4 typical deck gauge longitudinal strain variations away from the wheel path (LC1)

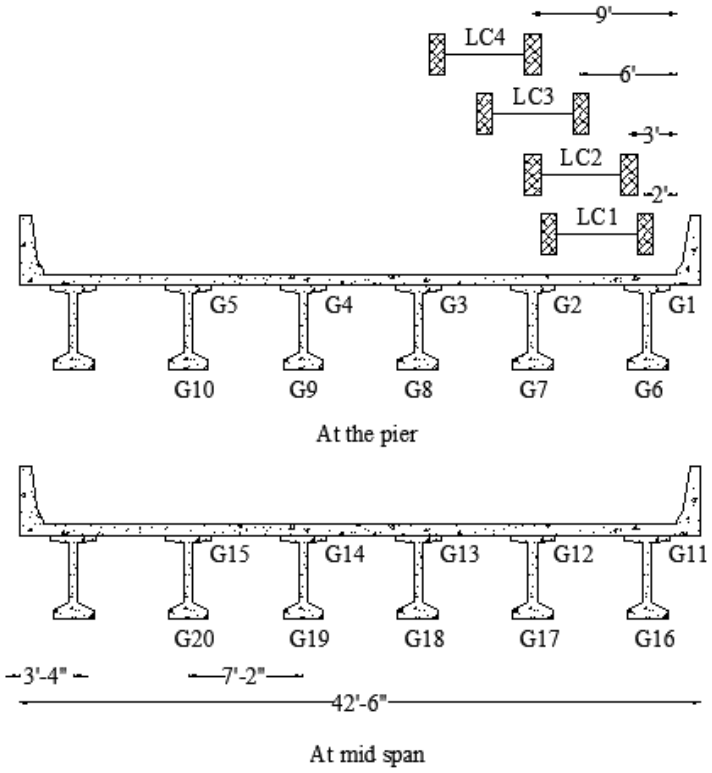

Figure A.4.5. Bridge 4 girder gauge instrumentation plan

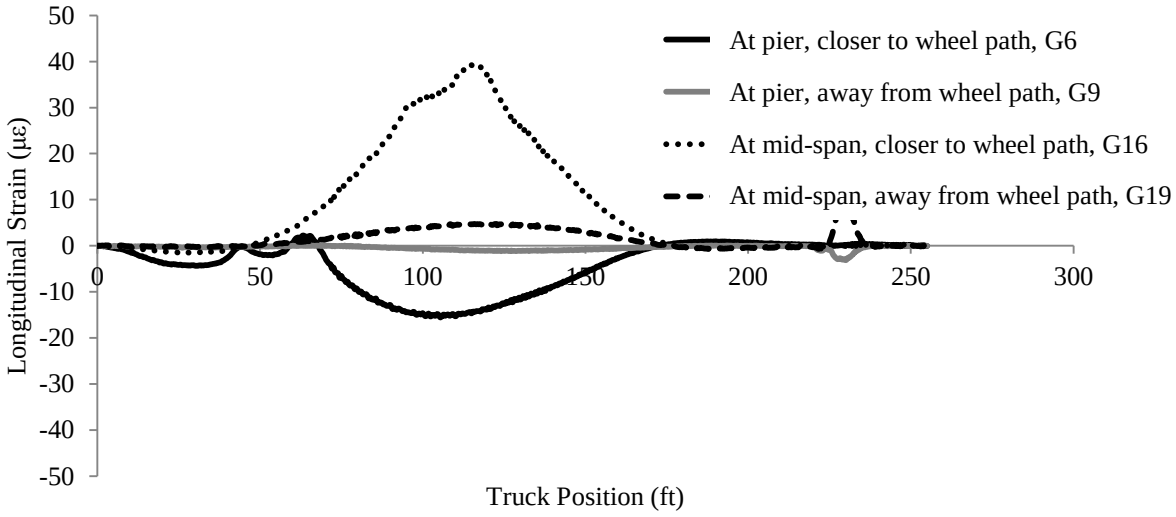

Figure A.4.6. Bridge 4 typical girder gauge strain variations (LC1)

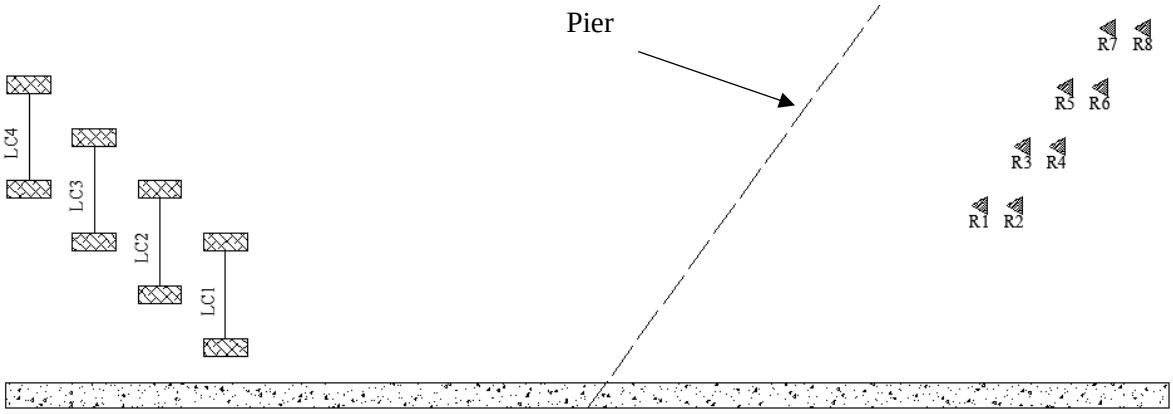

Figure A.4.7. Bridge 4 rosette instrumentation plan

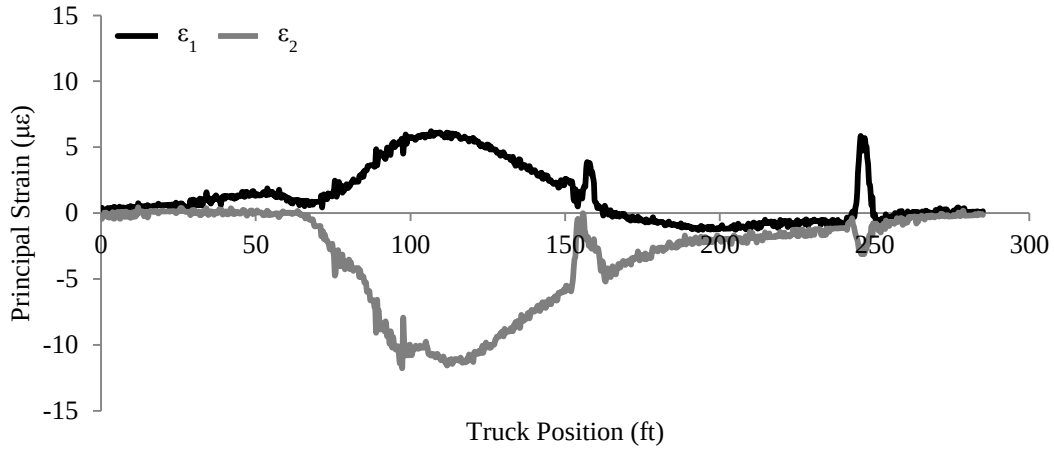

Figure A.4.8. Bridge 4 typical principal strain variations of rosettes (R8) close to wheel path (LC4)

Figure A.4.9. Bridge 4 typical principal strain variations of rosettes (R8) away from wheel path (LC1)

A.5 Bridge 5: On US 20 over Big Whiskey Creek

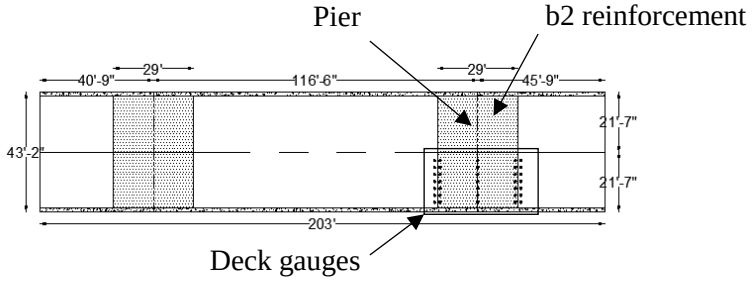

Figure A.5.1. Bridge 5 plan view

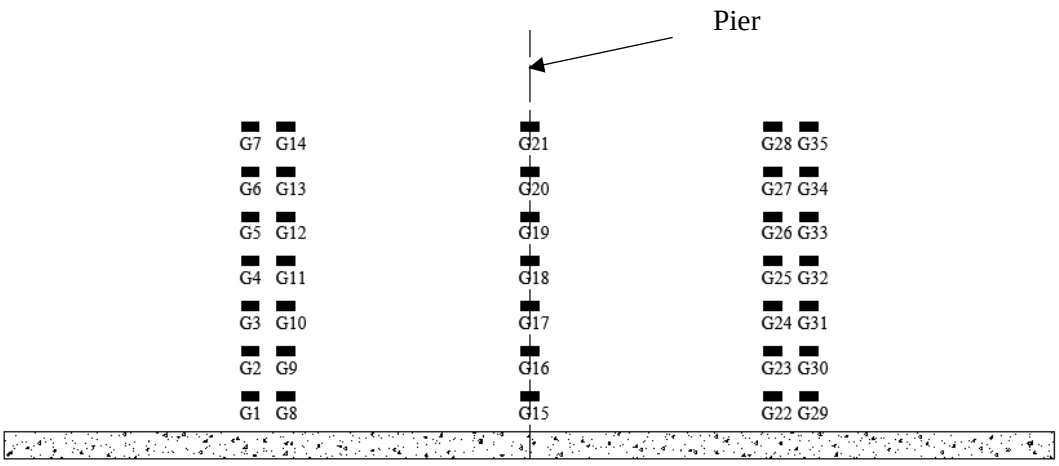

Figure A.5.2. Bridge 5 deck gauge instrumentation plan

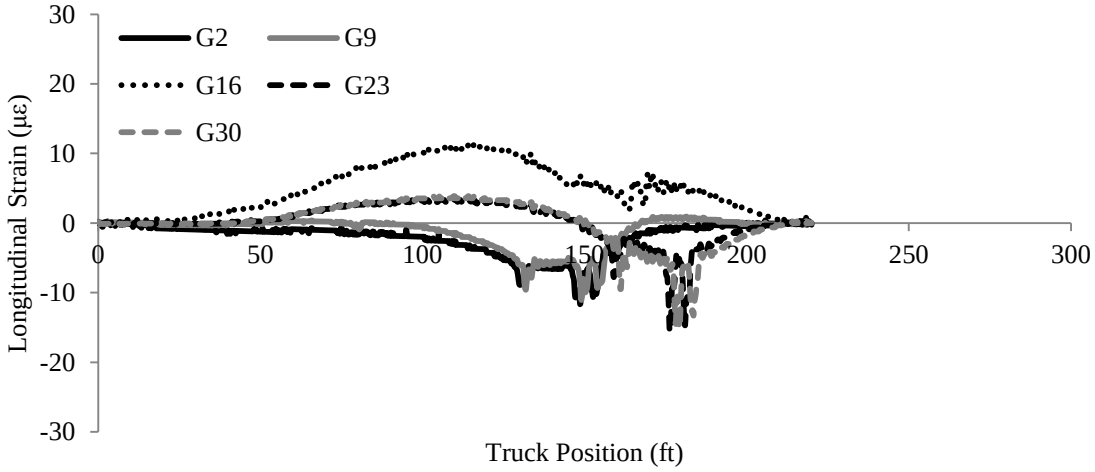

Figure A.5.3. Bridge 5 typical deck gauge longitudinal strain variations close to the wheel path (LC1)

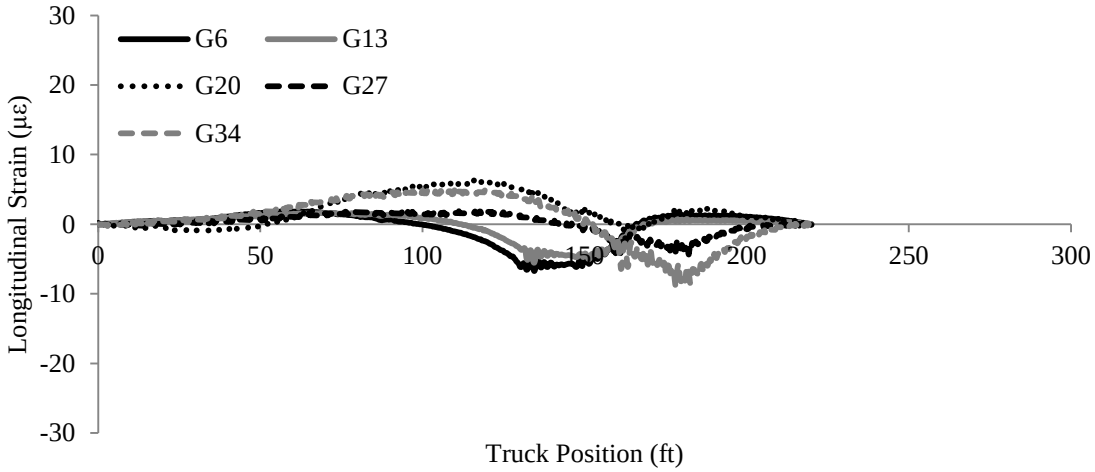

Figure A.5.4. Bridge 5 typical deck gauge longitudinal strain variations away from the wheel path

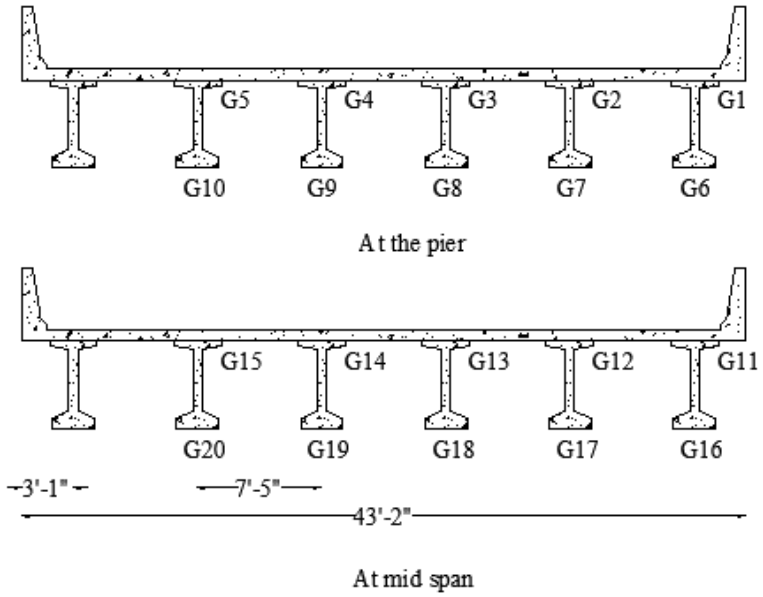

Figure A.5.5. Bridge 5 girder gauge instrumentation plan

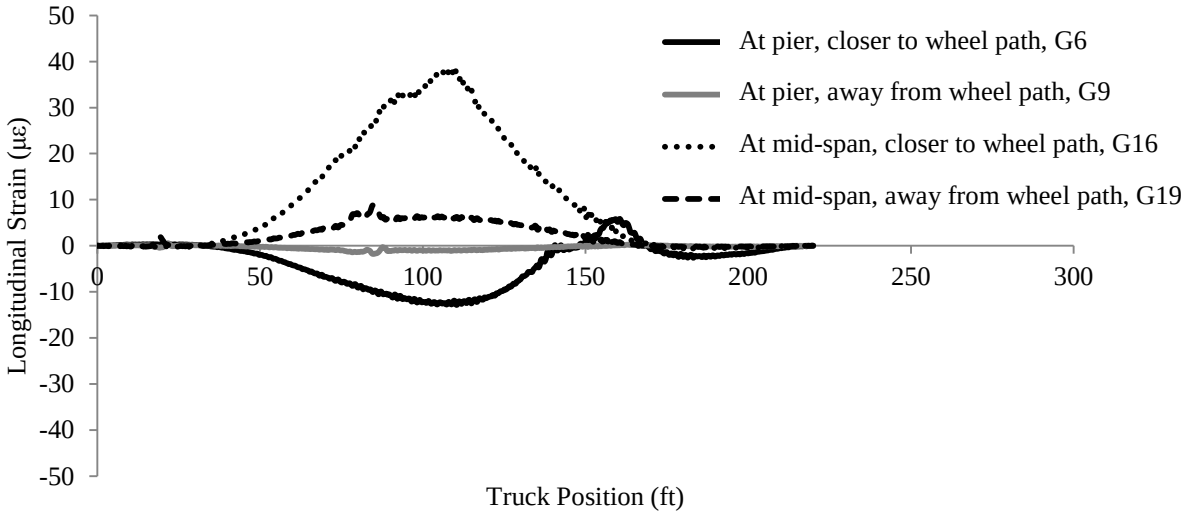

Figure A.5.6. Bridge 5 typical girder gauge strain variations (LC1)

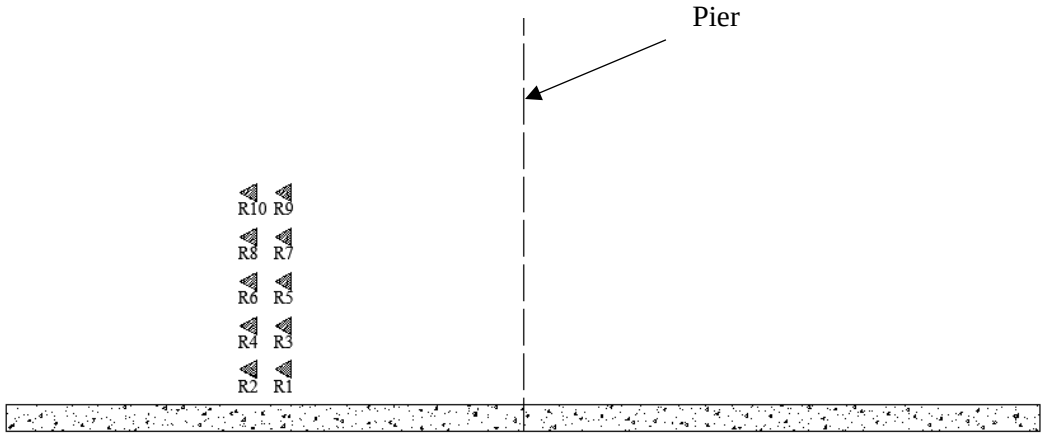

Figure A.5.7. Bridge 5 rosette instrumentation plan

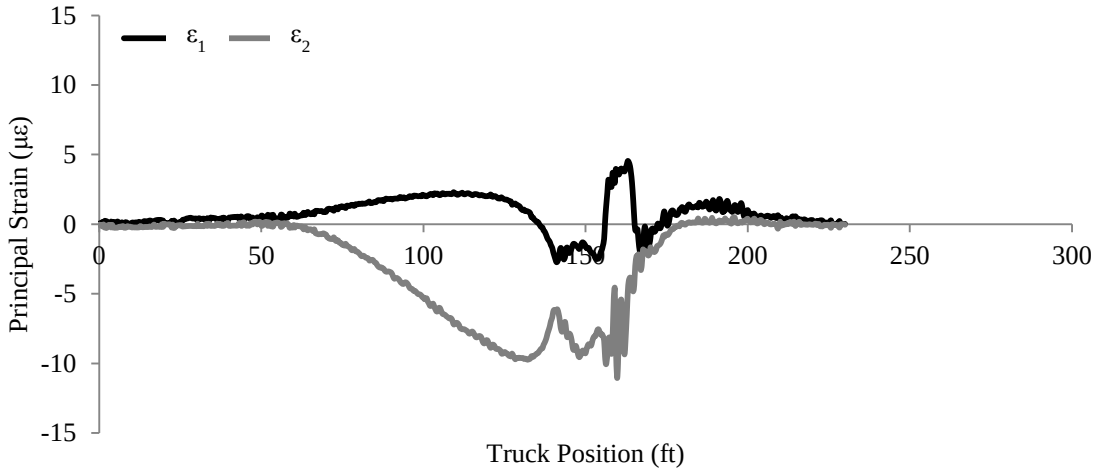

Figure A.5.8. Bridge 5 typical principal strain variations of rosettes (R9) close to wheel path (LC4)

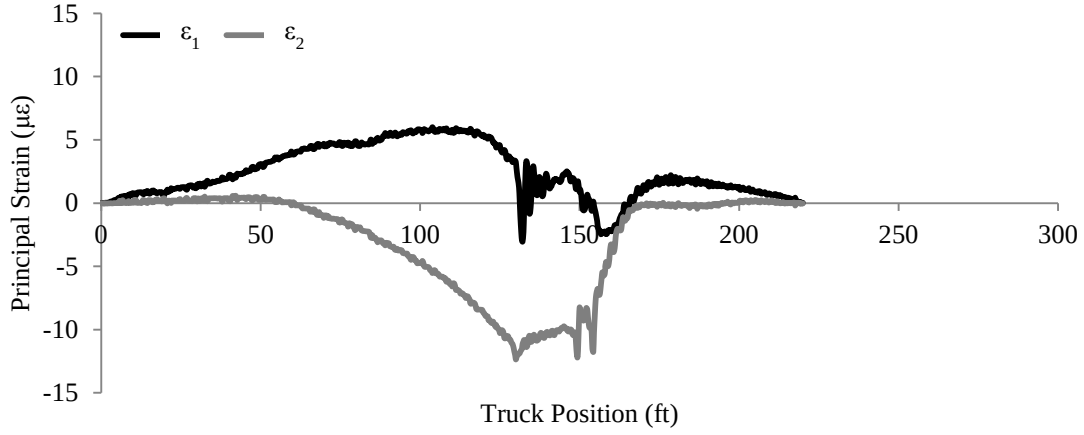

Figure A.5.9. Bridge 5 typical principal strain variations of rosettes (R9) away from wheel path (LC1)